Chapter 3

Mesoscale Processes and Severe Convective Weather

RICHARD H. JOHNSON

Department of Atmospheric Science, Colorado State University, Fort Collins, Colorado

BRIAN E. MAPES

CIRES/CDC, University of Colorado, Boulder, Colorado

REVIEW PANEL: David B. Parsons (Chair), K. Emanuel, J. M. Fritsch, M. Weisman, D.-L. Zhang

3.1. Introduction

Severe convective weather events—tornadoes, hailstorms, high winds, flash floods—are inherently mesoscale phenomena. While the large-scale flow establishes environmental conditions favorable for severe weather, processes on the mesoscale initiate such storms, affect their evolution, and influence their environment. A rich variety of mesocale processes are involved in severe weather, ranging from environmental preconditioning to storm initiation to feedback of convection on the environment. In the space available, it is not possible to treat all of these processes in detail. Rather, we will introduce several general classifications of mesoscale processes relating to severe weather and give illustrative examples. Although processes on the mesoscale are often intimately linked with those on smaller and larger scales, we will exclude from discussion those that obviously lie outside the mesoscale domain (e.g., baroclinic waves on the synoptic scale or charge separation in clouds on the microscale).

a. Definition of mesoscale

There are several definitions of "mesoscale," and even "scale," in common currency. Some use fixed geometrical scales (Fujita 1963, 1981; Ogura 1963; Orlanski 1975) while others are based on dynamical considerations (Ooyama 1982; Emanuel 1986; Doswell 1987).

Ooyama (1982) defines mesoscale flows as those having a horizontal scale between the scale height H of the atmosphere and the Rossby radius of deformation $\lambda_R \approx NH/f$, where N is the Brunt–Väisälä frequency and f the Coriolis parameter.[1] By this definition, mesoscale phenomena occur on horizontal scales between ten and several hundred kilometers. This range generally encompasses motions for which both ageostrophic advections and Coriolis effects are important (Emanuel 1986). In general, we apply such a definition here; however, strict application is difficult since so many mesoscale phenomena are "multiscale." For example, a ~100-km-long gust front can be less than ~1 km across. The triggering of a storm by the collision of gust fronts can actually occur on a ~100-m scale (the microscale). Nevertheless, we will treat this overall process (and others similar to it) as mesoscale since gust fronts are generally regarded as mesoscale phenomena.

b. Scope of paper

The range of mesoscale processes associated with severe weather is enormous. Therefore, to provide focus, we present a division of mesoscale processes according to whether they help to generate severe weather (termed *preconditioning* and *triggering*) or arise from the convection itself. Moreover, we will draw a distinction between preconditioning and triggering, much in the same way as Newton (1963) has done. Newton distinguished factors that precondition (destabilize) the environment, for example, an approaching upper-level trough, differential horizontal advection, low-level jets, from those that release the instability, such as rapid lifting by fronts, cold domes from thunderstorms, drylines, and topography (although slow quasigeostrophic lifting was also suggested as a possibility).

A list of common mesoscale preconditioning processes is provided in Table 3.1. In most instances, these mechanisms serve to gradually destabilize the environment and modify the wind shear profile, thereby setting the stage for severe weather. However,

[1] Ooyama (1982) notes that if the relative rotation and vorticity are increased in an area, f should be replaced by the geometric mean of the absolute vorticity and absolute angular speed.

C. A. Doswell III (ed.), *Severe Convective Storms*

TABLE 3.1. Mesoscale preconditioning processes for severe weather.

Local	Advective	Dynamical
Boundary layer processes • deepening the mixed layer • deepening the moist layer • convergence along dryline • nocturnal inversion, low-level jet formation Terrain effects • creation of convergence zones • development of slope flows • modification of hodograph Surface effects • evaporation, heating • surface, discontinuities —soil moisture —roughness	Differential advection • creation of capping inversion • destabilization • formation of deep, dry PBL (leading to microbursts) Convergence lines • fronts • drylines • sea/land/lake breezes • mountain/valley breezes Moisture advection • increase CAPE, lower LFC • local cumulus moistening	Secondary circulations • geostrophic adjustment • jets Gravity currents, waves • cold pool lifting • localized reduction of CIN • modification of vertical shear Mesoscale instabilities Boundary layer processes • horizontal convective rolls • inertial oscillation (low-level jets)

if the destabilization occurs rapidly enough, some of these processes may actually trigger convection, thus blurring the distinction between preconditioning and triggering.

The mesoscale processes in Table 3.1 have been subdivided into local, advective, and dynamical. Local preconditioning processes include boundary layer mixing and interactions of the atmosphere with geographically fixed features such as topography or gradients of surface properties. Advective processes involve the physical transport of air masses. Advection acts as an important preconditioning process in the prestorm environment (e.g., differential advection of cold air over warm, or the development and convergence of humid air masses). Mesoscale dynamical processes are harder to observe, as they often involve rapidly evolving motions in clear regions of the atmosphere. Events in one location can affect events in another location through the propagation of gravity waves that may travel faster than the wind at any level. Much of the unsaturated fluid dynamics of the atmosphere for which horizontal advection and rotation processes are secondary can be described as gravity wave processes, not just the rare cases of coherent propagating phenomena with a single, well-defined frequency and wavelength. These processes are important both in prestorm environments and inside severe storms. In the former situation, they can include secondary circulations associated with geostrophic adjustment, upper-level jets, and low-level jets. In addition, the atmosphere can be subject to mesoscale dynamical instabilities that may cause convective preconditioning. In this case, there is no "upstream precursor" for a weather development, as there is for the advective phenomena discussed above. Discussion of individual phenomena listed in Table 3.1 is given in section 3.3.

Specific processes involved in triggering convection are identified in Table 3.2. As mentioned earlier, some triggering and preconditioning processes are the same. For example, some cold fronts trigger convection everywhere along their leading edge, whereas others precondition the atmosphere by providing mesoscale lifting and moisture convergence. However, in general, the lifting required for triggering is much stronger than that for preconditioning, particularly

TABLE 3.2. Mesoscale triggering processes for severe weather.

Local	Advective	Dynamical
Boundary layer circulations • thermals Terrain effects • orographic lifting • thermal forcing • obstacle effects Surface effects • sensible/latent heat flux discontinuities	Convergence lines • cold fronts • gust fronts • sea/lake breezes • drylines Boundary intersections • triple point • colliding fronts, sea breezes	Gravity currents, waves Boundary layer horizontal convective rolls

Combined lifting processes:
thermals along fronts
fronts intersecting terrain
boundary layer rolls intersecting fronts, sea breezes, drylines
gravity waves interacting with fronts, drylines

when convective inhibition (CIN) is present. Probably the most common triggering mechanisms are advective in nature: convergence lines (gust fronts, cold fronts, sea/lake breezes, drylines) or boundary intersections (e.g., triple points, colliding gust fronts). Mesoscale dynamical processes are less common, but there are some instances where gravity waves or boundary layer rolls trigger convection. Superpositions of triggering processes are particularly effective at initiating storms (e.g., thermals along fronts, fronts intersecting terrain, rolls intersecting boundaries, etc.). These processes will be discussed in detail in section 3.4.

Once initiated, severe storms generate mesoscale phenomena that impact storm evolution as well as the growth of neighboring storms (Table 3.3). On the local scale, radiation and microphysics are two such processes. Microphysical effects acting on the mesoscale are key in downdraft and cold pool production, generation of microbursts and other high-wind events, generation of midlevel convergence due to melting, and lightning production.

Advective effects include particle advection, fall, and phase changes, which influence downdraft development and upscale growth of convection. Cold pool advective processes lead to cell regeneration and mesoscale convective system (MCS) evolution. Momentum transport and sloping flows are important factors in severe surface winds. Vortex tilting/stretching can generate vertical vorticity, leading to supercell development or MCS mesovortices.

Severe storms have a number of important dynamical effects. Convectively generated gravity waves influence storm evolution and the development of neighboring storms. Mesoscale pressure fields produced by buoyancy and dynamic effects (e.g., shear/updraft interactions) impact supercell evolution and propagation. Baroclinic vorticity generation at gust fronts may play a role in tornadogenesis. These processes are discussed in detail in section 3.5.

3.2. Instability of the atmosphere to mesoscale convection: General considerations

a. Elementary deep convective instability (buoyancy only)

Severe convective weather owes its existence to the buoyant ascent of cloudy air whose source is in the lowest layers of the troposphere. This convective ascent occurs in regions with a temperature and humidity stratification that is typically stable toward small-amplitude vertical displacements, but unstable toward large-amplitude upward displacements of low-level air. Here we review some definitions, measures, and indices of deep convective instability, as tools for considering the effects of mesoscale processes on storm potential and organization.

Buoyancy is defined as the acceleration of gravity times the fractional density difference between a parcel of air and its environment. The density of air + water mixtures at a given pressure level depends on temperature, humidity, and condensed water content. If thermodynamic equilibrium (or a specific disequilibrium) among water phases is assumed, the latter two quantites can be calculated from the total water content.

The density of the parcel and its environment depend quite strongly on the definitions of "parcel" and "environment." Defining these from sounding data can be difficult, because air properties vary considerably within the distances and time intervals between soundings. More problematically, convection modifies its own environment in several ways. Section 3.5 will highlight some of these mechanisms, in light of the products and indices introduced here.

1) PARCELS, SOUNDINGS, AND DEEP CONVECTIVE INSTABILITY

Parcel-oriented sounding diagnostics are useful conceptual and forecasting tools for convective weather situations. Regions of absolute stability can be identi-

TABLE 3.3. Storm-generated mesoscale effects.

Local	Advective	Dynamical
Radiation	Particle advection, fall, and phase changes	Gravity currents, waves
Microphysics	• downdraft generation	• impact on cell/MCS growth
• downdraft, cold pool production	• upscale growth	• influence on neighboring convection
• microburst generation	Cold pool processes	Mesoscale pressure fields
• melting-generated midlevel convergence	• cell regeneration	• buoyancy contribution
• lightning production	• MCS evolution	• dynamic contribution (storm splitting, propagation)
	Momentum transport/sloping flows	• surface mesohighs/wake lows
	• severe surface winds	Baroclinic vorticity generation
	Vortex tilting/stretching	• horizontal vorticity at gust front
	• vertical vorticity generation (supercells, MCS mesovortices)	Vortex breakdown
		• mesocyclone
		• tornado

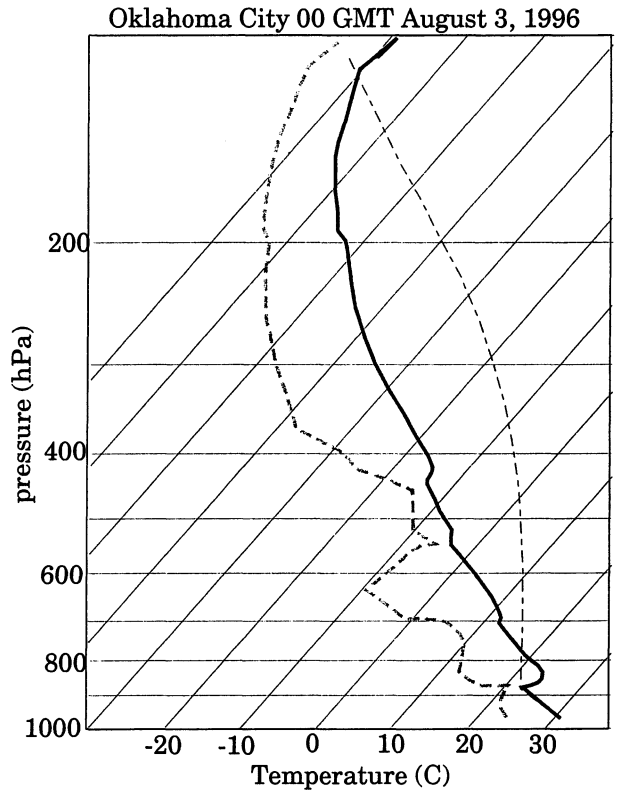

FIG. 3.1. Skew T–log$p$ of Oklahoma City sounding for 0000 UTC 2 August 1996. The temperature of a pseudoadiabatically ascending parcel from the surface (970 mb) is indicated. This parcel temperature is much warmer than the prevailing midtropospheric temperature, indicating a tremendous amount of potential buoyancy. However, this air experiences some negative buoyancy in the capping inversion layer, from 790 to 890 mb, which prevents the atmosphere from simply overturning everywhere.

fied, while relative values of some indices may delineate relative risks of various types of severe weather. Choosing the parcel, environment, and processes is an ambiguous exercise, best illustrated with an analysis of a particular severe storm sounding. Consider the unstable sounding of Fig. 3.1.

A more thorough diagram indicating the possible instability of this sounding is shown in Fig. 3.2. Here the buoyancy of every parcel below the 600-mb level is shown, as a function of pressure on a log scale. When total buoyancy (including water vapor and liquid water density effects) is expressed in temperature units (as a cloud virtual temperature T_{cv}), and a log p coordinate is used in the vertical, integrals of the contoured values in the vertical direction are proportional to work done by the buoyancy force. For example, the convective available potential energy (CAPE, units J kg^{-1}) for air originating at the surface is the integral of the positive values of buoyancy along the left-hand edge of Fig. 3.2:

$$\text{CAPE} = \int_{T'_{cv}>0} RT'_{cv}\, d(\ln p), \qquad (3.1)$$

where prime refers to parcel-environment differences.

Likewise, the convective inhibition energy (CIN; Colby 1984) for surface air is the integral of the negative values along the left-hand edge. The integrated CAPE over the entire depth of the unstable layer (ICAPE, units J m^{-2}) is proportional to the volume of the "mountain" delineated by the positive contours in Fig. 3.2. ICAPE is a property of an atmospheric column rather than of an arbitrarily cho-

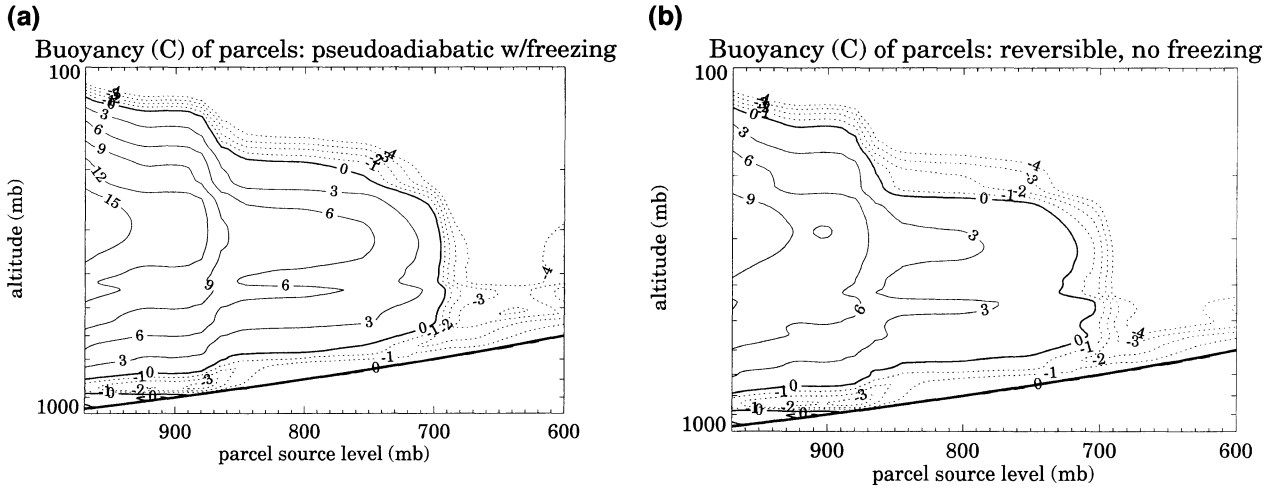

FIG. 3.2. Contours of buoyancy (total density difference, including water vapor and condensate loading effects, but expressed as equivalent degrees Celsius) for all parcels originating between the surface (970 mb) and 600 mb. The altitude scale is logarithmic in pressure, so that area is proportional to work done by the buoyancy force, as on a skew T–log$p$ diagram. Calculations are based on (left panel) pseudoadiabatic ascent of saturated air, with the latent heat of fusion included for vapor that condenses below 0°C; and (right panel) reversible ascent, with no freezing processes. Contours are 0 (heavy), negative (dashed, interval 1°C), and positive (solid, interval 3°C).

sen parcel (Mapes 1993; see also "cumulative CAPE" in Emanuel 1994). Thus, it has the advantage of assessing instability in cases where the CAPE of near-surface air is zero, for example, in the morning (when a convective temperature has to be forecast to compute CAPE) or in frontal overrunning situations.

Figure 3.2 indicates that parcels of air originating anywhere below the 700-mb level can attain positive buoyancy if lifted through the ambient environment for a distance of about 100 mb. The surface air has the highest CAPE, though the entire-mixed layer (below the 880-mb level) has similarly large values. This mixed-layer air has considerable CIN, with negative buoyancies of $-2°$ to $-3°$C over a ~1-km layer. A second, elevated mixed layer between about 700 and 870 mb also makes a significant contribution to ICAPE. This air only experiences negative buoyancy of $-1°$C when lifted through its negative area. Interestingly, the elevated mixed layer serves both as the cap on the extremely unstable air at the surface, and as a possible source layer for convection in its own right. This air is capable of achieving respectable buoyancies of 5°–6°C under pseudoadiabatic ascent, with a smaller CIN than the mixed-layer air.

The CAPE, CIN, and ICAPE indices discussed above are tabulated in Table 3.4 for various assumptions about the precipitation, freezing, and mixing processes in the parcel. The parenthetical values in the entraining cases are for the hypothetical case where the relative humidity of the entrained air is artificially constrained to be no less than 80%.

Large amounts of energy are available to any process that can muster enough energy to overcome the much smaller CIN. If a convective structure can harness just a tiny fraction of the available energy toward overcoming CIN, it can become extremely vigorous. In essence, the mean state is set to amplify convective and mesoscale variability, rendering the prediction problem quite difficult.

Severe convection depends not only on the availability of large CAPE but also on convective initiation processes (overcoming CIN). For example, Graziano and Carlson (1987) note that for a given value of buoyancy, the probability of severe convection increases with increasing lid strength (up to some cutoff value), although the total probability of convection diminishes. In some instances, the actual form convection takes is influenced by details of the initiation process. For example, Fritsch and Rodgers (1981) report on a large hail-bearing storm in Colorado that had radically different structure and movement from other storms in the same large-scale environment, presumably due to a gust front that propagated southward along a north–south barrier. This situation is not uncommon and points to a continuing problem of predicting the form of convection, even though 12–24-h forecasts of the large-scale environment have become quite good.

TABLE 3.4. Instability indices for the sounding of Fig. 3.1 under various assumptions about the parcel process. The last three entries are for an entraining parcel, which continuously mixes with 10%, 20%, or 40% of its original mass per 100 mb traveled.

Parcel processes	$CAPE_{970}$ (J kg^{-1})	CIN_{970} (J kg^{-1})	ICAPE (10^6 J m^{-2})
Pseudoadiabatic + freezing	5986	25	8.14
Pseudoadiabatic	4909	25	6.32
Reversible	3847	34	4.67
Reversible, 10%/100 mb (RH > 80)	2131 (2375)	41 (38)	2.94 (3.46)
Reversible, 20%/100 mb (RH > 80)	1496 (1827)	48 (42)	2.27 (3.00)
Reversible, 40%/100 mb (RH > 80)	993 (1363)	59 (48)	1.68 (2.68)

2) DRY AIR ALOFT

The existence of dry air aloft, for example, from subsynoptic-scale dry intrusions (Carr and Millard 1985), can enhance the evaporation of precipitation and hence the strength of downdrafts and cold outflows from convection. Elevated dry layers, especially with a large storm-relative wind velocity, might enhance the severity and longevity of squall lines, bow echoes, and microbursts by producing vigorous downdraft circulations. Johns and Doswell (1992) note that forecasters consider that the presence of at least some dry air in the downdraft entrainment region is necessary for both bow echo-induced damaging winds and supercell tornado development.

A diagram similar to Fig. 3.2, but with downdraft potential buoyancy contoured below the line of unit slope, may be seen in Emanuel (1994). The downdraft buoyancy can be integrated over pressure to yield DCAPE, a measure of maximum possible kinetic energy production by downdrafts. However, in nature, the thermodynamics of evaporatively driven downdrafts lies much farther from equilibrium among water phases than does updraft thermodynamics. For example, a very dry layer aloft will have a very large potential negative buoyancy, under the assumption that it is brought to saturation isobarically (to its wet-bulb temperature), and then maintained at saturation while it descends. However, this process is unlikely to be realized in this ideal configuration in the real atmosphere. As a result, DCAPE is a difficult quantity to interpret (also see Gilmore and Wicker 1998). In addition, this potentially dense quality of dry air is realized not only as a force to accelerate energetic downdrafts but also as a drag on updrafts that entrain the dry air (Table 3.4). Without a specific idea of the form of convection one expects—highly entraining small cells versus lines, quasi-steady versus intermittent, sloped versus upright, etc.—the overall effects of dry air aloft cannot be easily foreseen.

b. Effects of wind shear

Wind shear significantly influences what form convection is likely to take. Wind shear can be incorporated into indices that may be better predictors of severe weather than buoyant instability alone (Miller 1972; Moncrieff and Green 1972; Moncrieff and Miller 1976; Weisman and Klemp 1982). In an effort to classify the mode of convection, Weisman and Klemp (1982) introduced a bulk Richardson number R similar to the one proposed by Moncrieff and Green (1972) that combines the effects of buoyant energy and shear:

$$R = \frac{\text{CAPE}}{\frac{1}{2}\bar{u}^2}, \tag{3.2}$$

where $\bar{u}$ is defined as the difference between the density-weighted mean wind speed taken over the lowest 6 km and an average surface wind speed taken over the lowest 500 m. Numerical modeling results for storms having CAPEs in the range ~1000–3500 $m^2 s^{-2}$ and calculations of R for a series of documented storms led Weisman and Klemp (1982, 1984, 1986) to conclude that multicell storm growth occurs most readily for $R > 30$ and supercell storm growth for $10 < R < 40$.

However, when applying these or other parameters to real situations, there is inherently scatter. Part of the reason lies in the difficulty in obtaining a representative environmental sounding. Additionally, there is the problem of knowing how much CAPE will actually be realized for a particular storm owing to uncertainties about parcel properties at cloud base or dilution by entrainment, water loading, and ice loading. While it has been well established that strong, deep shear layers are supportive of supercellular convection (e.g., Weisman and Klemp 1986), mesoscale terrain effects, outflow boundaries, or other mesoscale phenomena can modify the mean shear profile and create mesoscale variability in severe-storm potential. Last, there is considerable natural variability in storm evolution owing to the history of convection itself, mesoscale forcing mechanisms, and the impact of neighboring cells.

All of these factors not only serve to make forecasting difficult but also suggest that slight changes in environmental conditions—say, by perturbations on the mesoscale—can dramatically affect storm development. For example, local orography or low-level jets can modify the storm environmental hodograph, thereby yielding different storm types in a region having the same synoptic-scale flow. Similarly, mesoscale processes can locally weaken CIN, allowing storms to develop in some locations and not others.

Some types of severe storms (e.g., hailstorms, tornadoes) occur in moderate-to-strong shear environments, whereas others (e.g., microbursts, flash floods) often occur with weak-to-moderate midtropospheric shear. Damaging microburst winds are more dependent on the thermodynamic profile than shear, as in the case of dry microbursts where deep dry adiabatic layers lead to intense downdrafts (Wakimoto 1985). While flash floods also typically have weak shear throughout the cloud depth (Maddox et al. 1980a), they often occur in the presence of strong low-level flow, which can contribute to repeated storm formation and motion over the same area (Chappell 1986). Since it is the low-level flow that provides the lifting, flash floods are particularly sensitive to mesoscale effects such as topography or outflow boundaries, which may determine the areas of maximum ascent.

Mesoscale organization of convection is also sensitive to wind shear, but the relationships are complex. For example, when CAPE and shear are large, bow echoes can form (e.g., Weisman 1993). Fujita (1978) defined the bow echo as a bowed convective line (25–150 km long in the cases he presented) with a cyclonic circulation at the northern end and an anticyclonic circulation at the southern end. Bow echoes may occur in isolation or as multiple features (e.g., line echo wave patterns) along squall lines. A phenomenon often related to bow echoes is the *derecho* (Johns and Hirt 1987). Derechos are convective systems that produce straight-line wind gusts > 26 m s^{-1} within a concentrated area with a major axis of at least 400 km. Several wind events are common, frequently only a few hours apart. Some have lasted 18 h or longer. Several studies have shown that many derechos are associated with bow echo structure (Przybylinski and DeCaire 1985; Johns and Hirt 1987; Johns 1993; Przybylinski 1995), but not all. For other combinations of CAPE and shear, other types of mesoscale organization can occur, for example, squall lines, mesoscale convective complexes (MCCs; Maddox 1980). However, the occurrence of these phenomena is also related to the existence of synoptic or mesoscale features such as jets, fronts, and convergence lines.

3.3. Mesoscale mechanisms for environment preconditioning

Before severe storms can develop, synoptic and/or mesoscale processes must act to provide adequate moisture and instability for convection to initiate. Once initiated, the interaction of convection with shear produces a pattern of storm evolution that can lead to severe weather. In this section, we consider processes that produce the instability and shear, specifically, those that occur on the mesoscale. As a framework for discussion, we will consider preconditioning processes according to whether they act locally, or are advective or dynamic in nature, as outlined in Table 3.1.

a. Local processes

1) VERTICAL MIXING IN THE BOUNDARY LAYER

Daytime heating of the convective boundary layer (CBL) is probably the most common preconditioning process for convection over land. Typically, once the nocturnal inversion is burned off, clouds can form as boundary layer thermals reach their LCL. The rate at which this occurs depends on the morning inversion depth, sky cover, and surface wetness. Entrainment at the CBL top acts to dry out the boundary layer and reduce the potential for deep convection, but if moisture is sufficient, clouds can still form. If there is a strong capping inversion, the growth of clouds may be restricted or even suppressed. However, moderate capping inversions can enhance the potential for deep convection by allowing shallow cumulus to be suppressed, but then later in the day, as the inversion has been weakened by heating, a lifting mechanism can release the instability quickly (e.g., Carlson et al. 1983).

To illustrate how daytime CBL heating and cumulus cloud development ensue, a time series of reflectivity, CBL height, and cloud base derived from a 915-MHz wind profiler in Illinois on 16 August 1995 is shown in Fig. 3.3 (Angevine et al. 1998). The series of virtual temperature soundings shows a fairly well-defined convective boundary layer developing through the morning hours, with a weak capping inversion above. During the course of the day, the water vapor mixing ratio increases as the CBL deepens, presumably due to surface evaporation and advection. Winds in the CBL (not shown) were 6–8 m s^{-1} from the south, with southwesterly winds above. The top of the CBL is marked by the peak in reflectivity, which is a result of strong gradients of temperature and humidity. The boundary layer top can be seen rising from approximately 500 m AGL at 0900 CST to about 1000 m at 1300 CST. Fluctuations in the entrainment zone atop the CBL during the morning are due to up- and downdrafts associated with thermals or CBL rolls (to be discussed later).

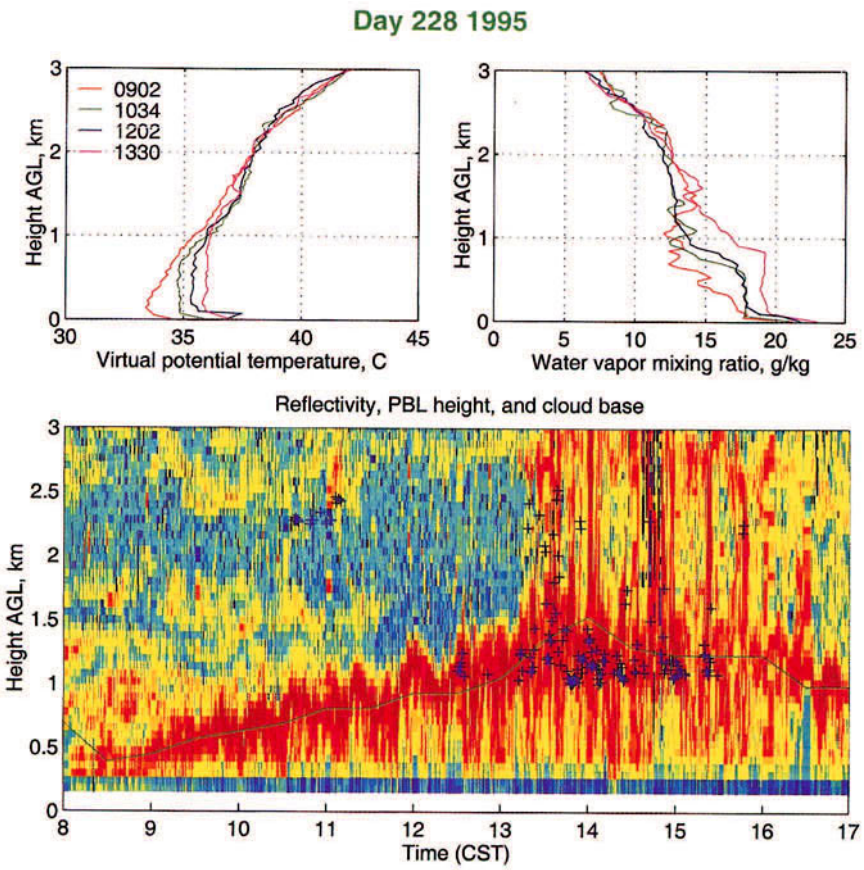

FIG. 3.3. Boundary layer evolution on 16 August 1995. Virtual potential temperature and water vapor mixing ratio from four soundings at the times shown are plotted in the upper panels. The lower panel shows the profiler reflectivity (arbitrary scale) in pseudocolor. The solid green line is the automatically determined boundary layer height, and the blue crosses are cloud-base heights detected by the ceilometer. From Angevine et al. (1998).

Cloud development was apparently triggered by these perturbations once the CBL became deep enough for the LCL of CBL air to be reached (cloud bases shown by crosses).

The upward mixing of moisture in the CBL, acting in combination with low-level convergence, can precondition the atmosphere for deep convection (e.g., Wilson et al. 1992). Vertical mixing can also lead to enhanced convergence along drylines. For example, to the west of drylines, westerly momentum is efficiently transported down to the surface in the deep, dry CBL there, whereas vertical mixing on the moist east side is weaker, thereby enhancing convergence along the dryline axis (Danielsen 1974; Ogura and Chen 1977; McCarthy and Koch 1982). The vertical structures of water vapor mixing ratio, wind, potential, and virtual potential temperature across the dryline of 24 May 1989 (Fig. 3.4) is illustrative of this process (Ziegler and Hane 1983).

2) TERRAIN EFFECTS

Surface relief, whether it be small hills, ridges, escarpments, or mountain ranges, can have profound effects on convection. An excellent review of this topic is given by Banta (1990). He identified three classifications of topographic effects on convection: mechanical lifting to the level of free convection (LFC), thermally generated circulations, and aerodynamic effects (e.g., blocking, flow deflection, gravity waves). The first is directly related to triggering, so examples of these will be given later.

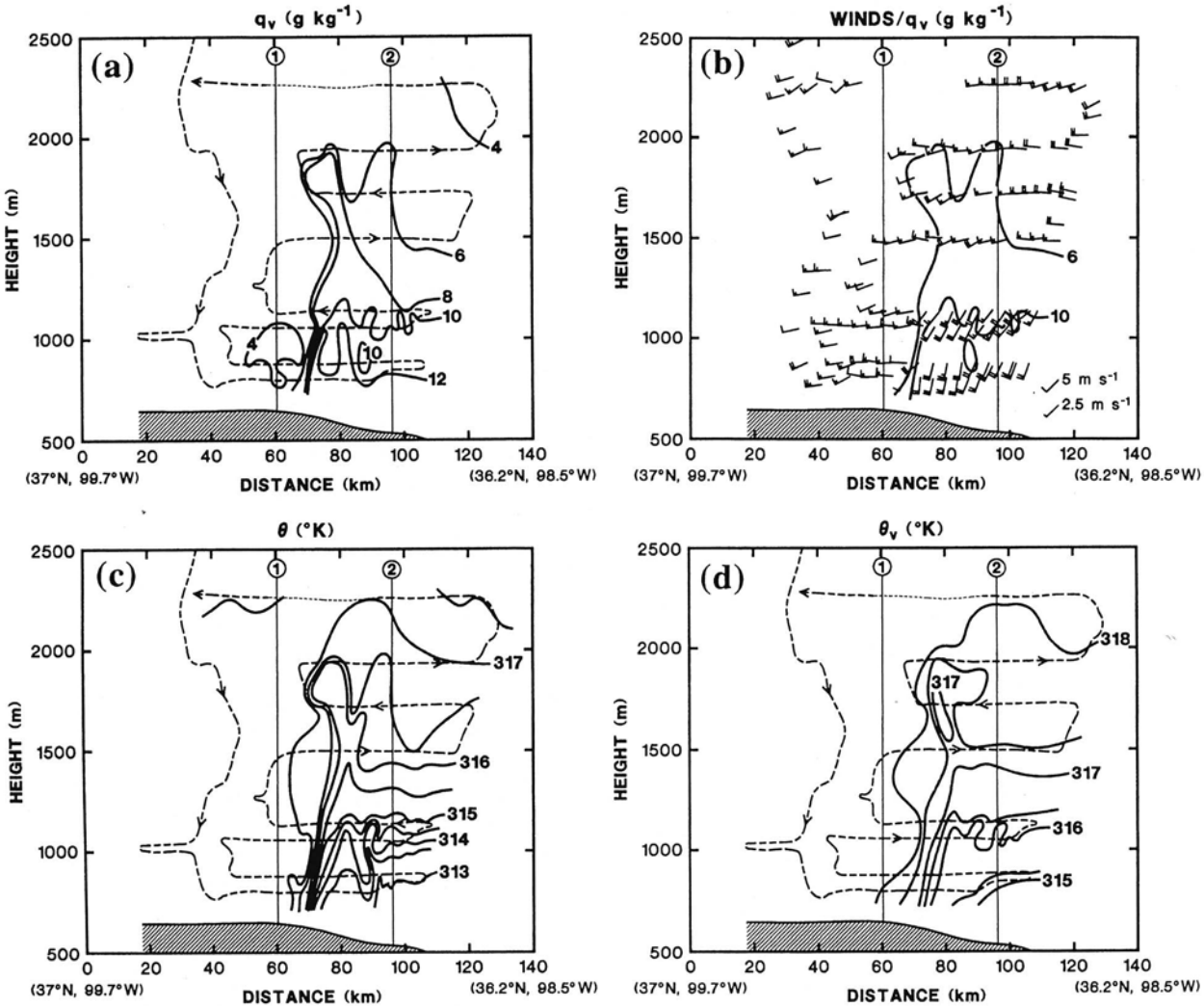

FIG. 3.4. Subjective analyses of P-3 measurements during series of vertically stepped aircraft passes through dryline; (a) q_v (g kg^{-1}); (b) horizontal, ground-relative wind vectors (full barb equals 5 m s^{-1}); (c) θ (K); (d) θ_v (K). Dashed curve in (a), (c), and (d) represents the P-3 flight track. The vertical lines are the locations of M-CLASS soundings projected onto the cross section. The hatching denotes terrain elevation subjectively smoothed as determined from the radar altimeter on the P-3. From Ziegler and Hane (1993).

Thermally generated flows such as upslope and upvalley wind systems can play a prominent role in the initiation and development of hailstorms, tornadoes, flash floods, and high winds associated with dry microbursts. Large mountain barriers like the Rocky Mountains, Tibetan Plateau, Andes, and so forth, generate large-scale, diurnally varying circulation features that are instrumental in establishing the thermodynamic and wind profiles conducive to these types of severe weather. On the mesoscale, smaller topographic features generate thermally forced flows that provide focus areas for convective initiation. As an example, consider the vector-mean surface flow over the plains of northeastern Colorado at 1100 LST for July 1981 (Toth and Johnson 1985) superimposed upon the radar climatology for the summers of 1971 and 1972 (Wetzel 1973; Fig. 3.5). This figure indicates that the preferred regions for convective development coincide in most instances with zones of maximum confluence (and convergence) during the late morning along the two prominent east–west ridges north and south of Denver, Colorado: the Cheyenne Ridge and the Palmer Lake Divide, respectively. That such ridges are a focal point for intense hailstorms was documented in the 1973 National Hail Research Experiment (e.g., Browning et al. 1976). The specific conditions that favor hail or other severe weather occurrence on a particular day consist of the superposition of flows on both the synoptic scale and the mesoscale. For example, Modahl (1979) finds that on hail days in northeastern Colorado the afternoon easterly (upslope) component of the flow is much stronger than on no-hail days,

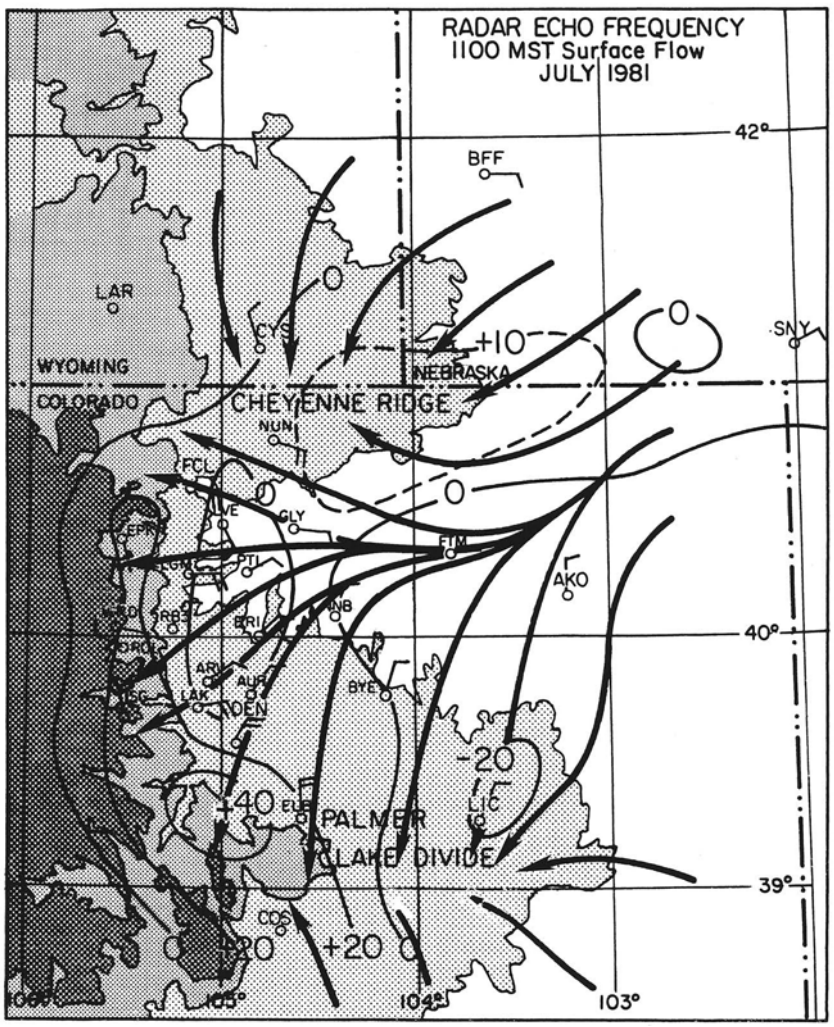

FIG. 3.5. Radar echo frequency (0900–2100 MST), as determined by Limon (LIC), CO, WSR-57 radar, given as percent deviation from azimuthally averaged mean at each radius from Limon (reproduced from Wetzel 1973). Surface streamlines and vector-averaged winds (one full barb = 1 m s^{-1}) are shown for 1100 MST. Dashed line is intermediate contour. From Toth and Johnson (1985).

which leads to enhanced moisture and wind shear favorable for severe storms. However, viewed in a larger-scale context, this finding is consistent with the well-known, favorable Front Range severe weather synoptic pattern characterized by an east–west-oriented front to the south of the threat area and surface high over the northern Great Plains (Doswell 1980).

Flash flood environments are another example of preconditioning by mechanically or thermally forced upslope flows, particularly in the western United States where the time of onset of heavy rains is in the afternoon (Maddox et al. 1980a). Striking examples are the Black Hills and Rapid City, South Dakota, flood of 1972 (Maddox et al. 1978); the Big Thompson River, Colorado, flood of 1976 (Maddox et al. 1978; Caracena et al. 1979); the Johnstown, Pennsylvania flood of 1977 (Bosart and Sanders 1981; Zhang and Fritsch 1986); and the many floods throughout Asia on the windward slopes of mountain ranges during the summer monsoon (Ramage 1971). But there are also cases of floods associated with more subtle topographic features, such as the Balcones Escarpment of Texas, which played a role in the Texas Hill Country flash floods of 1978 (Caracena and Fritsch 1983). Typically, these floods occur in association with low-level jets, weak flow at midlevels, moderate-to-large CAPE, and a low-level inversion (Maddox et al. 1978). The precise locations of the storms producing the flash floods are often determined by complex triggering processes involving interaction of outflow boundaries with terrain, direct orographic lift, and other mesoscale features.

Thermally induced topographic flows also influence the development of dry microbursts (Wakimoto 1985) and their associated high surface winds, which are a common occurrence during the summer along the Front Range of the Rocky Mountains. Typical morning and evening soundings for dry microburst days over the High Plains are shown in Fig. 3.6 (Wakimoto 1985). Characteristic of these soundings is a nearly dry adiabatic lapse rate from just above the surface to near 500 mb, the approximate level of cloud base. Wakimoto (1985) notes that it is a deep dry adiabatic layer that, following precipitation sublimation and evaporation, permits extreme downward vertical velocities to be attained (Brown et al. 1982; Proctor 1989). The mountains play an important role in the microburst process in at least two ways: 1) by providing a deep dry adiabatic layer whose upper portions are in part composed of mixed layers advected from the mountains to the west (Carlson et al. 1983; Wilczak and Christian 1990), and 2) by generating the showers that are the sources of the initial downdrafts.

Flow deflection and blocking by terrain often influence the location and development of convection. Details of flow deflection and blocking are often

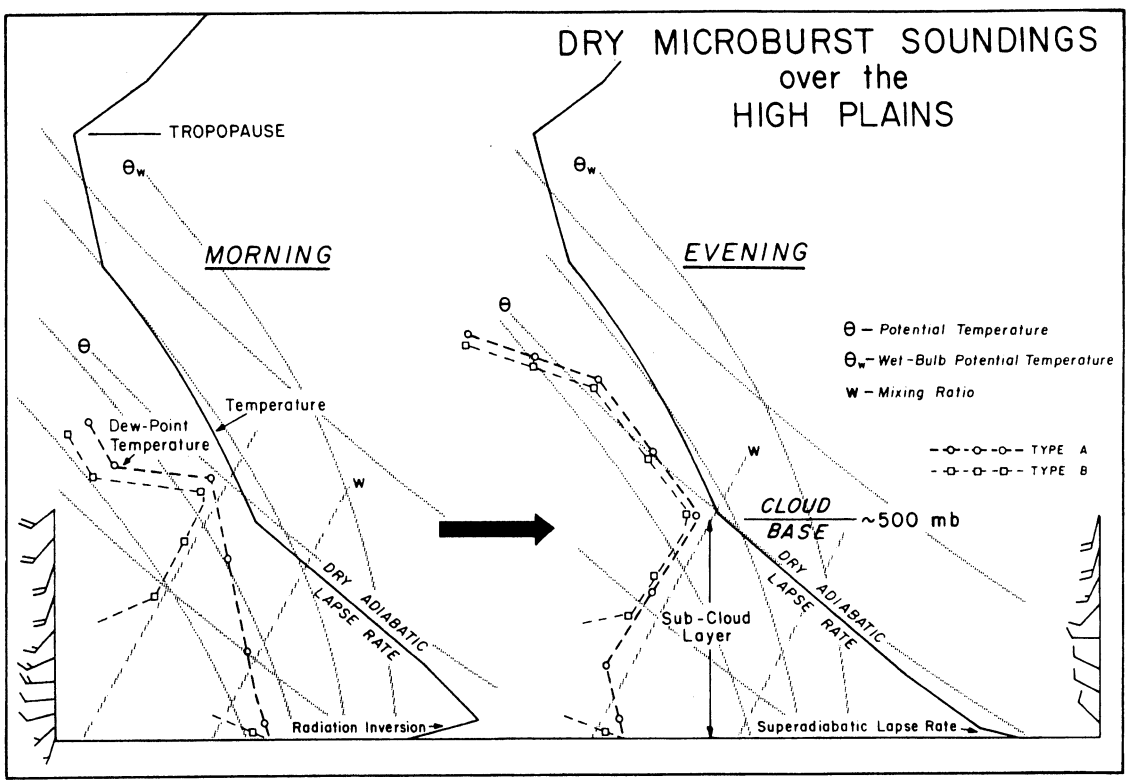

FIG. 3.6. Model of the characteristics of the morning and evening soundings favorable for dry-microburst activity over the High Plains. From Wakimoto (1985).

complex, but they generally depend upon the incident flow speed U and stratification represented by Brunt-Väisälä frequency N through the Froude number $F = U/NH$, where H is the height of the barrier (e.g., Carruthers and Hunt 1990). When $F \lesssim 1$, for example, in stably stratified situations, the flow is typically blocked and goes around a barrier, whereas when $F > 1$, the flow can go over the barrier, except when a very stable layer exists just above it (Fritsch et al. 1992).[2] There are countless examples of these effects worldwide, the most notable of which are in the vicinity of isolated mountains or hills, mountain ranges, and mountainous islands. Banta (1990) provides an extensive review of effects of flow deflection and blocking on convection in the United States and other parts of the world.

Perturbations to the flow downstream of both large-scale and small-scale barriers can affect the occurrence of severe convective weather. A prominent example of the former situation is the southwest vortex to the lee of the Tibetan Plateau, where low-level shear lines and midlevel vortices frequently develop that are often linked to the production of heavy rains (Tao and Ding 1981). The southwest vortex was partly responsible for the 1981 Sichuan flood, which claimed more than 1000 lives (Kuo et al. 1984). In a modeling study, Kuo et al. (1988) showed that the formation of the southwest vortex actually represents a coupling between large- and smaller-scale topographic effects. The Tibetan Plateau is instrumental in setting up a large-scale latitudinal temperature gradient that drives the moist, southwest monsoon flow (e.g., Yanai et al. 1992). This monsoon flow then impinges upon the mesoscale Yun-Gui Plateau that extends from the southeastern corner of the main Tibetan Plateau, and the low-level flow is blocked. The flow then descends into the Sichuan basin on the lee side of the mesoscale plateau, creating cyclonic relative vorticity over the basin by vortex stretching. Kuo et al. (1988) found that latent heat release intensified the southwest vortex and that the interaction between convection and the vortex was crucial for the production of heavy rainfall.

There are also instances where mesoscale topographic features generate downstream eddies and convergence zones that are the sites for severe weather such as hailstorms and tornadoes. Such a convergence zone often exists to the lee of the Olympic Mountains in Washington State (Mass 1981; Mass and Dempsey 1985), although the weather is typically not severe. Another well-known example of this phenomenon is the *Denver cyclone*, which occurs downstream (for south-to-southeasterly flow) of the Palmer Lake Divide on the eastern plains of Colorado (Szoke et al. 1984; Blanchard and Howard 1986; Brady and Szoke 1989). One case of the Denver cyclone is shown in Fig. 3.7 (from Wilczak and Christian 1990). A strong, surface cyclonic circulation center exists just east of the Denver metropolitan area at 0000 UTC 26 June 1987. Wilczak and Christian found that in the late afternoon, as the surface heat flux began to decrease, flow at the vortex center that had earlier been divergent became convergent (Fig. 3.7). The vortex contracted, vorticity increased rapidly, and shortly thereafter intense thunderstorms (up to 60–70 dBZ, producing 4.5-cm diameter hail) developed along the convergence zone on the east side of the vortex center. Although no tornadoes were observed, several small cyclonic vortices developed along the convergence zone. The size and azimuthal shears of these vortices were similar to those of tornado-associated misocyclones observed on other Denver cyclone days (Wakimoto and Wilson 1989). Brady and Szoke (1989) and Wakimoto and Wilson (1989) have proposed that such shear-induced low-level misocyclones, when positioned underneath strong cumulus updrafts, can, through vortex stretching, generate nonsupercell tornadoes (Fig. 3.8). These findings are supported by other studies that have shown that the Denver cyclone and its associated convergence zone are active sites for nonsupercell tornadoes (Szoke et al. 1984; Szoke and Brady 1989). Because the Denver cyclone is a topographically quasi-locked feature, it appears to produce a local maximum in tornado frequency just east and

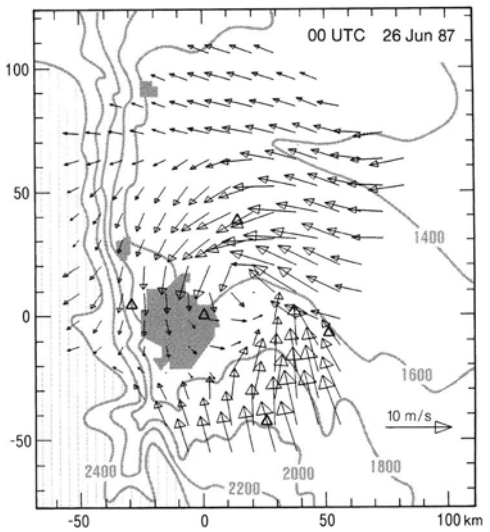

FIG. 3.7. Winds at 0000 UTC 26 June 1987 in eastern Colorado. Terrain contours (plotted every 200 m) and cities are shown in light gray. Elevations above 2400 m are hatched. Triangles and the diamond indicate the locations of the 5 CLASS sites and the BAO tower, respectively, and the origin is Stapleton International Airport where the CP3 radar, the wind profiler, and the Denver CLASS sounding site were located. Axes coordinates are kilometers from CP3. From Wilczak and Christian (1990).

[2] More precisely, flow blocking characteristics depend upon two vertical scales: the height H of the barrier and the depth h of the fluid or stable layer (Simpson 1987). The condition described here is for $h \lesssim H$.

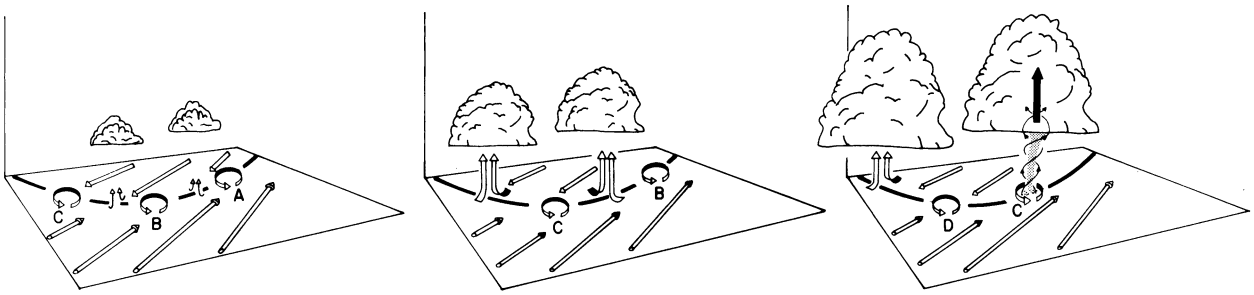

FIG. 3.8. Schematic model of the life cycle of the nonsupercell tornado. The black line is the radar detectable convergence boundary. Low-level vortices are labeled with letters. From Wakimoto and Wilson (1989).

northeast of the Denver metropolitan area (Golden 1978; Wakimoto and Wilson 1989).

Lee vortex phenomena such as the Denver cyclone have been attributed to a variety of mechanisms, operating singly or in combination: tilting of frictionally created horizontal vorticity (Thorpe et al. 1993), baroclinic vorticity tilting (Smolarkiewicz and Rotunno 1989), potential vorticity generation by surface friction or wave breaking (Smith 1989), horizontal variations in the Reynolds stress divergence over sloping terrain (Wilczak and Glendening 1988; Dempsey and Rotunno 1988; Davis 1997), mountain waves (Smith 1982), and Coriolis turning of the decelerated (subgeostrophic) southeasterly flow as it approaches the Continental Divide (Crook et al. 1990a).

Flow deflection by orography can also affect severe weather development by modifying the environmental wind profile. An example of such a situation pertains to hailstorms in Switzerland (Houze et al. 1993). In their study of eight years of data, Houze et al. (1993) found that hailstorms are nearly equally divided between left- and right-moving storms. They obtain realistic numerical simulations of the storms by using observed thermodynamic and wind profiles, while assuming a flat lower boundary. While this finding suggests that the basic characteristics of the storms are not directly a function of flow over complex terrain, the fact that the same thermodynamic sounding and wind hodograph can support a multiplicity of storm structures (left-moving, right-moving, supercell; see Weisman and Klemp 1982, 1984, 1986), indicates that, through modification of the wind profile, local orography may actually determine which type of storm would be favored at a specific time and place.

In another example, Carbone (1982) found the low-level horizontal shear in a prefrontal jet in the Central Valley of California (Fig. 3.9a) to be instrumental in tornado formation along the front. Radar reflectivity and velocity signatures of the tornado are shown in Figs. 3.9c and 3.9d. The prefrontal jet in this case may have been enhanced by barrier winds upstream of the Sierra Nevada, as indicated in aircraft observations (Fig. 3.9b) of yet another case by Parish (1982). Flow deflection by topography has also been observed to generate bulges in drylines (Atkins et al. 1998). In their case, a river valley along the Caprock Escarpment in the Texas panhandle contributed to the bulge, at which point there was enhanced convergence and density contrast across the dryline. Such bulges may become favored locations for severe storm development.

Topographically generated gravity or mountain waves can also affect deep convection. Booker (1963) found that mountain wave activity can affect the distribution of summertime convective rainfall in the mountains of Pennsylvania. Thunderstorm echoes were observed to dissipate in the subsiding air immediately downwind of a mountain barrier only to reform in (presumed) rising air several kilometers farther downwind. Tripoli and Cotton (1989a,b) found support for this concept in a numerical modeling study of convective development to the lee of the Rocky Mountains. On a typical afternoon with westerly flow, convection develops on the west and east slopes of the barrier (Fig. 3.10). The cells on the east slope arise from convergence between mountain wave flow and the developing upslope flow. Several hours later, the west-slope storms merge with those in the east and an explosive growth of convection takes place. The overall convective system then propagates eastward, experiencing an initial weakening owing to the strong change in topographic slope from the Rockies to the plains, but then rebounding in intensity as midlevel warming and growth to larger scales occurs (Fig. 3.11). Pulsing of the intensity of the storm on a timescale of several hours occurs due to oppositely propagating transient gravity wave circulations, but further intensification occurs at sunset as destabilization of the upper-anvil cloud inhibits gravity wave propagation into the stratosphere. The trapping of gravity waves in the upper troposphere contributes to continued growth to larger scales and eventually a quasi-balanced system that moves out onto the plains.

3) SURFACE EFFECTS

Two aspects of surface properties can affect environmental preconditioning: 1) the actual state of the

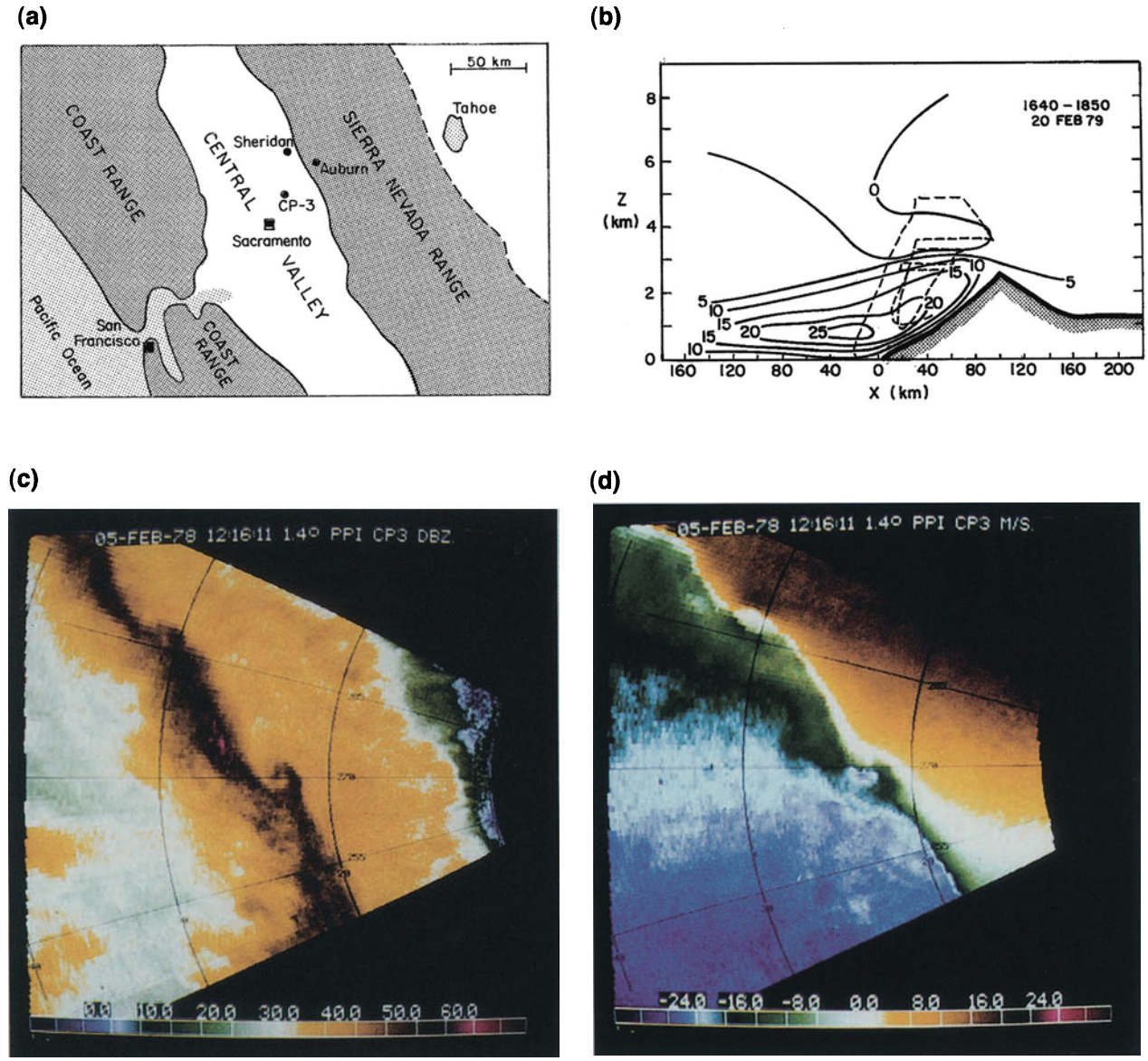

FIG. 3.9. (a) Map of northern California. Three Doppler radar sites are indicated by black dots. Sierra Crest is shown by dashed line and corresponds to 2.0–2.5 km height (above MSL). Central Valley is near sea level. (b) Mountain-parallel wind components (m s^{-1}) derived from rawinsonde and aircraft data for 20 February 1979. Flight track shown by dashed line; flight time listed at top. (c) Radar reflectivity and (d) velocity data from CP-3 radar two minutes prior to tornado damage on ground on 5 February 1978. Range marks are at 10-km intervals. Note two vortex signatures along the line 13 km apart. Panels (a), (c), and (d) are from Carbone (1982). Panel (b) is from Parish (1982).

surface (e.g., dry vs wet soil) and 2) heterogeneities in surface conditions (e.g., dry land adjacent to wet land). In the first instance, soil moisture is one of the most important factors since it affects the partitioning between latent and sensible heat fluxes. As noted by Segal et al. (1995), wet surfaces under clear-sky conditions are generally more conducive to deep convection than dry surfaces. When the surface is wet, large latent heat fluxes can increase the CBL specific humidity in the afternoon, thereby enhancing CAPE. If the capping inversion is weak or absent, convection can readily break out. However, in cases of stronger capping inversions, dry surfaces may be more conducive to deep convection even if there is less moisture since the larger sensible heat flux in those cases can erode the capping layer (e.g., McGinley 1986). Prolonged evaporation and transpiration from vegetation can in some instances lead to a "pooling" of higher moisture in convergence zones (Segal et al. 1989; Chang and Wetzel 1991). The enhanced moisture can provide additional fuel for severe storms, as reported in the derecho study by Johns and Hirt (1985).

Land surface heterogeneities in roughness, wetness, albedo, vegetation cover, snow cover, urbanization,

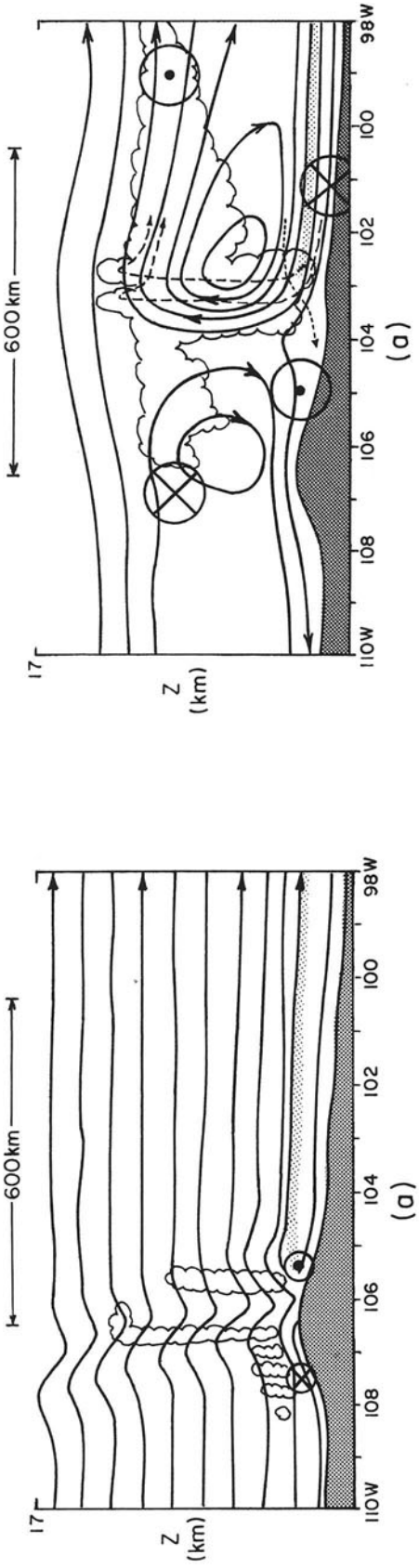

FIG. 3.10. Conceptual model showing flow field and position of convective elements at the time when deep convection forms over the Rocky Mountains. The stippled line represents the position of the plains inversion. Regions of cloud are indicated. (a) depicts the flow field with ground-relative mesoβ-scale streamlines. Circles depict flow perturbation normal to plane. (b) depicts the pressure and temperature response. Pressure centers are depicted by solid closed contours and temperature by dashed contours. The length scale of 600 km ($2 \times$ the Rossby radius) is indicated. From Tripoli and Cotton (1989a).

FIG. 3.11. As in Fig. 3.10 except for mature stage. From Tripoli and Cotton (1989b).

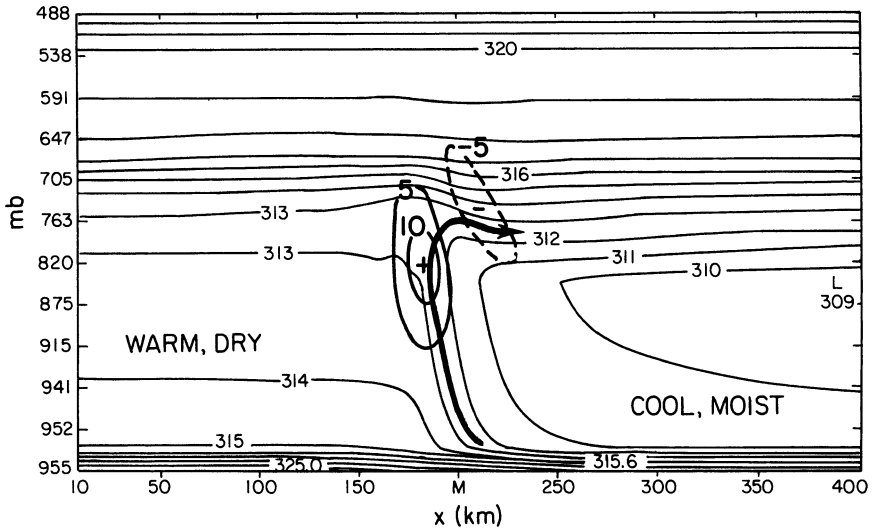

FIG. 3.12. Distributions of potential temperature (K, light solid), vertical motion (cm s^{-1}, heavy solid and dashed), and circulation (arrow) within a developing dryline at 8 h. From Sun and Ogura (1979).

and other factors can produce mesoscale circulations that may lead to convection (e.g., Anthes 1984; Ookouchi et al. 1984; Pielke and Segal 1986; Yan and Anthes 1988; Segal and Arritt 1992). Lanicci et al. (1987) showed that regional variations in soil moisture over the Texas–Oklahoma–Mexico area impact the structure and evolution of the elevated mixed layer (lid), the dryline, easterly ageostrophic flow over east Texas and the Gulf of Mexico, the potential instability of air under the lid, and the location and intensity of precipitation. Collins and Avissar (1994) identified those land surface characteristics that are most important in redistributing energy into turbulent sensible and latent heat fluxes, namely, land surface wetness, surface roughness, albedo, and, when vegetation covers the ground, leaf area index and plant stomatal conductance. Mesoscale circulations induced by surface moisture variability (whether a result of wetness or vegetation heterogeneity) appear to have a marked impact on the atmosphere on timescales ranging from hours (affecting cloud formation, e.g., Rabin et al. 1990) to weeks (contributing to heavy rains such as the 1993 Midwest floods, e.g., Paegle et al. 1996) to seasons (affecting the development of drought conditions, as in the Sahel, e.g., Charney 1975).

To illustrate the possible effects of moisture discontinuities on convection, consider the hypothetical dryline simulations of Sun and Ogura (1979). Since dry surfaces exhibit a much larger diurnal variation of temperature than wet surfaces, the daily march of the temperature contrast across a wet–dry boundary can resemble that across a dryline. Sun and Ogura used a two-dimensional model of the planetary boundary layer to simulate the diurnal variation in temperature across a dryline by specifying the cross-line gradient in surface potential temperature. The potential temperature and vertical velocity after about eight hours, starting from a weak westerly flow and horizontally uniform atmospheric conditions, are shown in Fig. 3.12. As a result of greater vertical mixing due to the warm surface conditions on the left (to the west) than on the right, a deeper mixed layer develops on the left[3] and a horizontal temperature gradient develops in the middle of the domain (the dryline). An up–down vertical motion couplet develops near the top of the mixed layer at the dryline position. The air flow (schematically shown in Fig. 3.12) indicates that the potential for convection to develop along the dryline is enhanced as moist air is drawn westward and upward to the top of the mixed layer. This type of circulation is referred to as an *inland sea breeze* by Ogura and Chen (1977). Sun and Ogura (1979) hypothesized that the localized lifting along the dryline by this mechanism may have accounted for the initiation of the 8 June 1966 squall line. While the results of Sun and Ogura are useful in illustrating circulations that can develop in association with moisture contrasts, additional processes normally occur in real dryline situations, for example, differential vertical mixing of momentum, along-dryline variability, and so forth.

In addition to moisture and vegetation gradients, other factors contribute to mesoscale variability of severe weather and cloudiness. Some studies have suggested an increase of rain, thunderstorms, and hailstorms within or downwind of urban areas due to increased cloud buoyancy, mechanical or thermodynamic effects that produce confluence zones, and en-

[3] The somewhat exaggerated superadiabatic layers may be an artifact of the turbulence parameterization scheme used.

hancement of the coalescence process due to giant nuclei from industrial activity (e.g., Changnon et al. 1976).

b. Advective processes

1) MOISTURE ADVECTION

Direct advection of moisture into a region can increase CAPE and lower the LFC, thereby increasing the potential for deep convection. Strong moisture advection is essential for extreme-precipitation events since rainout far exceeds local evaporation. In such cases low-level jets provide the required moisture transport, for example, for the development of MCCs (Maddox 1983), widespread floods such as the 1993 Mississippi Valley flood (Paegle et al. 1996; Arritt et al. 1997), and localized flash floods (Caracena et al. 1979). Moisture advection on the cloud scale may also be important for local moistening promoting new cloud growth. For example, Perry and Hobbs (1996) find significant humidity enhancements on the downshear and cross-shear sides of cumulus clouds.

2) DIFFERENTIAL ADVECTION

Much of the environmental preconditioning for severe weather arises from differential advection on the synoptic scale, for example, in destabilizing the atmosphere (Newton 1963), in providing the vertical wind shear (Ludlam 1963), or in establishing capping inversions (Carlson and Ludlam 1968). There are a number of examples of similar processes that occur on the mesoscale.

- Low-level jets with high-θ_e air overrunning fronts and cold pools leading to long-lived bow echoes (Johns 1984) and MCCs or mesoscale vorticity centers (MVCs; Maddox 1983; Fritsch et al. 1994).
- The flow of moist boundary layer air out from beneath an inversion or lid (a process called *underrunning*) due to ageostrophic circulations about a mesoscale jet streak leading to intense convection (Carlson et al. 1983).
- Transport of clouds and moisture aloft downstream of mountain barriers producing conditions conducive to dry microbursts (Wakimoto 1985; Wilczak and Christian 1990).
- Differential advection associated with jet streak circulations and boundary layer heating changing markedly over very short periods of time and acting to destabilize relatively small regions immediately prior to convective outbreaks (Kocin et al. 1986).

3) CONVERGENCE LINES

Convergence lines can serve as both preconditioning and triggering mechanisms. For example, lifting by a convergence line may in some cases be adequate to generate convection all along it; however, in other cases, enhanced lifting—say, by collisions or intersections with other boundaries—may be required to lift air to the LFC. The latter subject will be treated in section 3.4d.

Although cold fronts are synoptic scale in the along-front dimension, cross-front circulations are of mesoscale dimension. Localized convergence and lifting at the front destabilize the environment and reduce CIN, thereby making the atmosphere susceptible to deep convection. In some cases, convergence can be so strong that deep or severe convection can occur even in the absence of CAPE (Browning and Harrold 1970; Carbone 1982). In such instances, the front serves as a convective trigger, but in some aspects may still be a preconditioning mechanism. For example, in the case of a strong California cold front (Carbone 1982), the surface frontal zone provided strong cyclonic horizontal shear, which led to perturbations (and eventually tornadoes) along the front. These perturbations arose apparently from a horizontal shearing instability. Lifting can also occur out ahead of fronts, leading to prefrontal squall line formation as a result of cold fronts aloft (Browning and Monk 1982; Locatelli et al. 1995, 1997), jet streak secondary circulations (Browning and Pardoe 1973; Shapiro 1982), or prefrontal wind shifts associated with lee troughs (Hutchinson and Bluestein 1998).

Stationary or warm fronts can also be instrumental in preconditioning the environment for severe weather. Nocturnal MCC development to the north of quasi-stationary surface fronts has been attributed to low-level warm advection (Maddox and Doswell 1982) and to destabilization by diurnally modulated low-level jets, mesoscale ascent produced by the fronts, and convergence near the terminus of jets (Trier and Parsons 1993). Quasi-stationary east–west fronts have also been implicated in bow echo and derecho development (Johns 1984; Johns and Hirt 1987).

Precipitation-driven convective downdrafts, with their associated cold, spreading gravity currents or "gust fronts," probably represent the most common mechanism for generating localized surface convergence in regions where convection already exists. Results from the Thunderstorm Project clearly showed that the spreading cold air was instrumental in generating new convective elements in squall-line or multicell-type storms (Byers and Braham 1949; Newton and Newton 1959). Satellite observations provide convincing evidence that thunderstorm outflows contribute to remote effects of thunderstorms, with new cell growth at distances up to several hundred km from preexisting cells (e.g., Purdom 1973; Gurka 1976; Purdom 1982). On smaller scales, downdraft outflows in supercells (the forward-flank and rear-flank downdrafts described by Lemon and Doswell 1979) have been hypothesized to play varying roles in tornadogenesis (Barnes 1978;

Lemon and Doswell 1979; Klemp and Rotunno 1983; Brandes 1984a,b; Rotunno and Klemp 1985; Klemp 1987). Although lifting at the leading edge of gust fronts can directly trigger new convection, there are many situations where it can be considered a preconditioning mechanism, with convection initiation occurring as a result of collisions or intersections with other low-level perturbations to the flow (e.g., other gust fronts, cold fronts, drylines, terrain features, horizontal convective rolls in the CBL). The localized enhancement of vertical wind shear and convergence along preexisting boundaries can lead to increases in the occurrence of severe weather there (Maddox et al. 1980b).

Drylines also provide a focus for convection through localized convergence (Fujita 1958; Rhea 1966). The two most likely mechanisms contributing to the convergence are 1) solenoidally forced, frontogenetic circulations (Ogura and Chen 1977; Sun and Ogura 1979; Parsons et al. 1991; Ziegler and Hane 1993) and 2) vertical momentum mixing (Ogura and Chen 1977; McCarthy and Koch 1982). However, storms typically do not form everywhere along drylines. Therefore, mechanisms in addition to the above are required to trigger convection.

Low-level convergence also occurs at the leading edge of sea and land breezes. Summer sea breezes often produce vigorous afternoon showers over land as a result of zones of convergence between the synoptic-scale and onshore flow, for example, over Florida (Byers and Rodebush 1948; Gentry and Moore 1954; Atlas 1960; Pielke 1974) or the Texas coast (Hsu 1969). Even lake breezes can contribute to the formation of severe thunderstorms and tornadoes (Lyons and Chandik 1971; King and Sills 1998).

Land breezes are also known to produce nocturnal thunderstorms offshore (e.g., Neumann 1951; Preston-Whyte 1970; Williams and Houze 1987) and contribute to the formation of MCCs in low-latitude locations such as the southern South China Sea off the north coast of Borneo (Houze et al. 1981) and the Gulf of Panama (Danielsen 1982; Velasco and Fritsch 1987).

A number of observational studies indicate that land breezes and their associated cloud lines may contribute to waterspout formation at coastal locations. Wakimoto and Lew (1993) documented the development of a waterspout from a relatively small cumulus cloud (photograph in Fig. 3.13a) that occurred in the early morning along a line of cumuli just off the east coast of Florida. A satellite image taken just after the waterspout occurrence (Fig. 3.13b), when the parent cloud moved ashore, shows several offshore cloud bands. Some of these bands could be shoreward-propagating remnants of land-breeze convergence zones or, as Wakimoto and Lew suggest, mesoscale frontal zones produced by small variations in SST. While it is not known if the other bands produced waterspouts, the tendency of waterspouts to form along cloud lines has been well documented (e.g., Dinwiddie 1959; Golden 1973; Simpson et al. 1986). In fact, Golden (1974) argues that less than 5% of waterspouts develop from isolated cumulus. Considering the findings of Wakimoto and Wilson (1989) that surface convergence zones (and associated small-scale vorticity centers) are important for nonsupercell tornadoes, it may be that the offshore cloud lines are a reflection of similar convergence/vorticity zones that provide a low-level vorticity source upon which stretching by cumulus growth can act.

In some cases, the low-level lifting provided by sea, land, or lake breezes is adequate by itself to generate convection along the boundary. However, as in the case of fronts, drylines, and convective outflows, the actual triggering of convection is more often controlled by the intersection of such fronts with other phenomena that accentuate the lift.

Mountain/valley breezes are also important for preparing the atmosphere for a number of types of severe weather. For example, the preference for afternoon onset of flash floods in the western United States (Maddox et al. 1980a) indicates the importance of upslope flow in providing convergence and lifting to prepare the atmosphere for such storms. Schmid and Lehre (1998) found drainage flows in the Swiss Alps to be an important factor in providing a wind profile conducive to severe storms in eastern Switzerland.

c. Dynamical processes

1) SECONDARY CIRCULATIONS

Upper-level wind maxima (jet streaks) and low-level jets have long been associated with severe convective weather. In the case of upper-level jets, transverse ageostrophic circulations about the jet axis are argued to help initiate some severe storms (Uccellini and Johnson 1979; Bluestein and Thomas 1984). An example of such circulations within an idealized straight jet streak (which propagates more slowly than the maximum wind in the jet itself) is shown in Fig. 3.14. In the entrance region of the jet, wind speeds are subgeostrophic, resulting in a cross-stream ageostrophic component of the flow toward the cyclonic side of the jet (Fig. 3.14a). This component is the upper branch of a thermally direct circulation cell (Fig. 3.14b). In the exit region, winds are supergeostrophic and the transverse circulations are reversed. These circulations arise from geostrophic confluence and diffluence forcing, but can be modulated in many situations by the effects of horizontal shearing deformation (Shapiro 1981; Keyser and Shapiro 1986), flow curvature (Beebe and Bates 1955; Shapiro and Kennedy 1981; Moore and VanKnowe 1992), and transience (Ziv and Paldor 1999). The pattern of vertical motion induced by the confluence/diffluence forcing supports the concept that clouds and precipita-

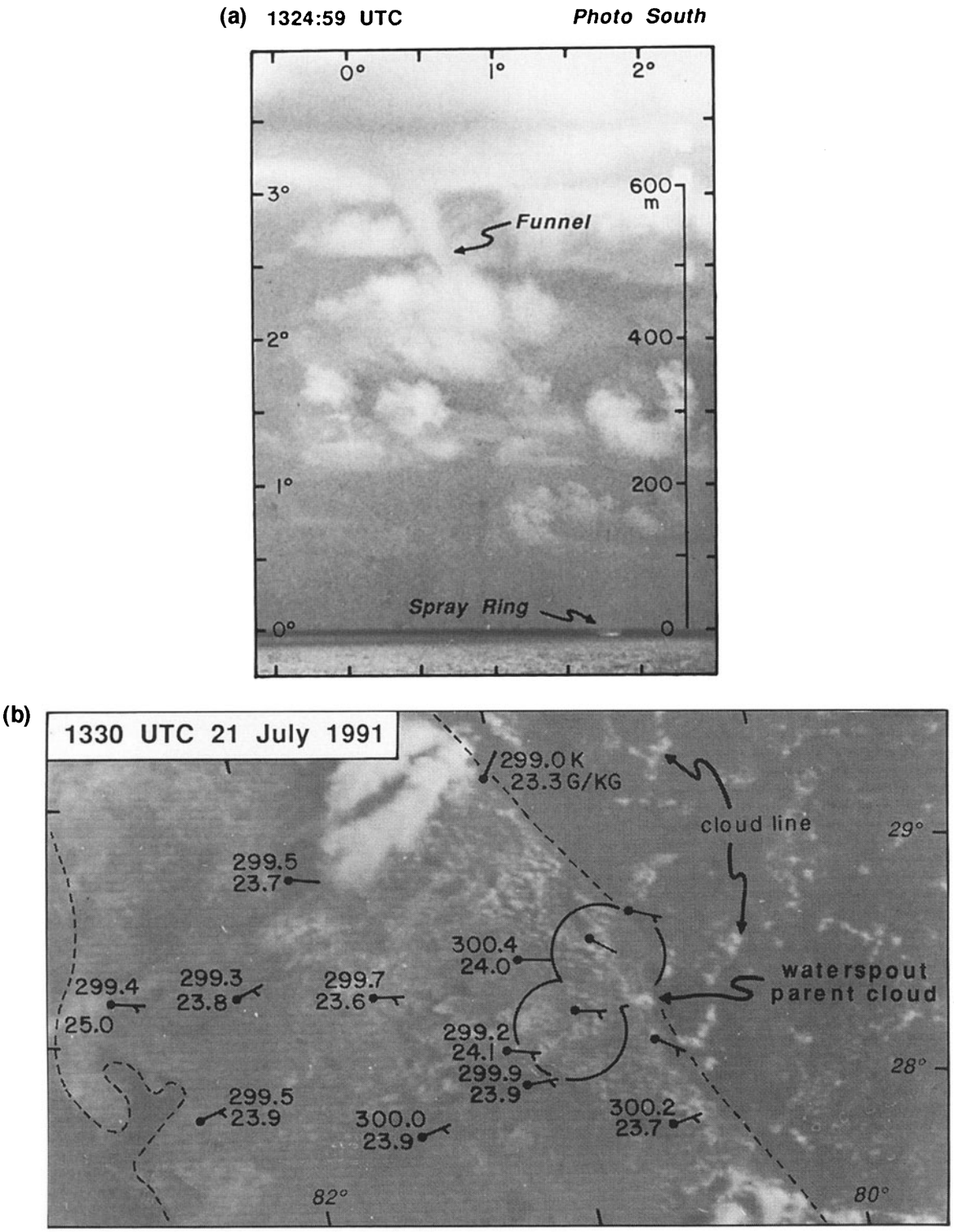

FIG. 3.13. (a) Photograph of cloud base and the waterspout taken from the Photo-South site at 1324:59 UTC. The height scale is valid at the distance of the waterspout. Azimuth and elevation angle grids from the photo sites are also indicated in the figure. (b) Visual satellite image at 1330 UTC on 21 July 1991. Potential temperature, mixing ratio, wind speed, and direction for select PAM stations are shown in the figure. Wind vectors are drawn with one barb and half-barb representing 5 and 2.5 m s^{-1}, respectively. The dual-Doppler lobes for the CP-3 and CP-4 baseline are also indicated in the figure. From Wakimoto and Lew (1993).

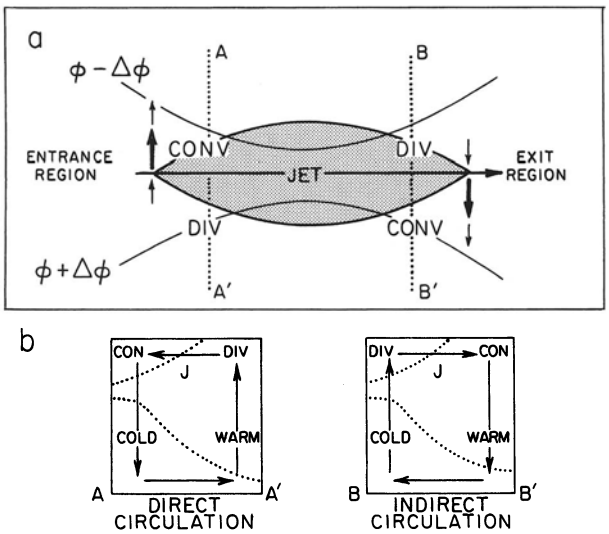

FIG. 3.14. (a) Schematic of transverse ageostrophic wind components and patterns of divergence (DIV) and convergence (CON) associated with the entrance and exit regions of a straight jet streak. ϕ refers to geopotential height. (b) Vertical cross section illustrates vertical motions and direct and indirect circulations in the entrance region (line A–A′) and exit region (line B–B′) of a jet streak. Cross sections include two representative isentropes (dotted), upper-level jet (J) location, upper-level divergence, and horizontal ageostrophic wind components within the plane of each cross section. Adapted from Uccellini (1990).

tion should be most prevalent in the right entrance and left exit region of straight jet streaks, a pattern that is often observed (e.g., Namias and Clapp 1949; Uccellini and Johnson 1979).

Low-level jets (LLJs) have also been linked with the generation of severe weather, presumably through enhancement of moisture and temperature advection, localized increase in low-level convergence, and an increase in the vertical wind shear (Means 1952; Bonner 1966; Wallace 1975; Maddox 1983; Trier and Parsons 1993). Such jets are most common at night, which has led to a theory for their development based on nocturnal boundary layer decoupling (Blackadar 1957). Recent observations (Mitchell et al. 1995; Arritt et al. 1997; Whiteman et al. 1997) support Blackadar's (1957) inertial oscillation theory for the LLJ, but other factors are probably also involved. In particular, diurnal oscillations associated with sloping terrain over the plains appear to contribute to a nocturnal maximum in the LLJ (Holton 1967; Paegle 1978; McNider and Pielke 1981).

The coupling between upper- and lower-level jets has been studied by Uccellini and Johnson (1979), Kocin et al. (1986), and others. They find that the mass adjustment associated with the upper-level jet ageostrophic flow forces an isallobaric wind that represents a return branch of the indirect circulation in the jet exit region (Fig. 3.14b). This return branch is argued to be an important factor in the development of LLJs in active synoptic situations. The LLJ is shown to be enhanced by diabatic heating (e.g., CBL heating or convection).

These processes have been studied in detail by Sortais et al. (1993) using data from the FRONTS-87 experiment. They found a coupling between the indirect circulation in the exit region of an upper-level jet and a low-level jet, and a cold front and its diabatic heating (Fig. 3.15). The lower branch of the upper-level jet transverse ageostrophic circulation came into phase with the low-level jet, which advected warm, moist air toward the ascending branch where deep convection occurred. In addition, mesoscale transverse ageostrophic circulations associated with the LLJ assisted in the formation of convection ahead of the cold front.

Other cases have been documented where secondary circulations (producing rising motion) ahead of fronts (Shapiro 1982) have interacted with boundary layer horizontal convective rolls (Trier et al. 1991) or drylines (Nieman and Wakimoto 1999) to generate severe convection.

2) GRAVITY CURRENTS, WAVES, BORES, AND SOLITARY WAVES

Many convergence-producing phenomena leading to convection possess the characteristics of density or gravity currents: fronts (Shapiro 1985), gust fronts (Charba 1974), sea and land breezes (Simpson 1969; Wakimoto and Atkins 1994), and drylines (Schaefer 1974b; Parsons et al. 1991). The movement of these features is described fairly well by gravity current theory (Simpson 1987), although in the case of drylines, vertical mixing may significantly affect dryline propagation (Schaefer 1974a).

Thunderstorm initiation depends sensitively on the vertical structure (depth) as well as strength of lifting by gravity currents. Lower-tropospheric wind shear plays a significant role in determining the depth and uprightness of lift at the leading edge of gravity currents (Droegemeier and Wilhelmson 1985; Rotunno et al. 1988; Crook 1996). Specifically, the role of the low-level shear in lifting at the leading edge of a thunderstorm cold pool is illustrated in Fig. 3.16 (from Rotunno et al. 1988). Horizontal vorticity produced by horizontal buoyancy gradients in a cloud updraft (Fig. 3.16a), when combined with the negative vorticity of an underlying cold pool in a no-shear environment, can cause the updraft to lean upshear (Fig. 3.16b). When shear exists in the absence of a cold pool, the updraft leans downshear (Fig. 3.16c). When the vorticity of the cold pool and shear are in balance, the updraft is erect (Fig. 3.16d). Rotunno et al. define this as an *optimal state* where the full CAPE can be realized without being inhibited by the cold pool or shear. Such situations should be characterized by a narrow leading convective line, such as the cases

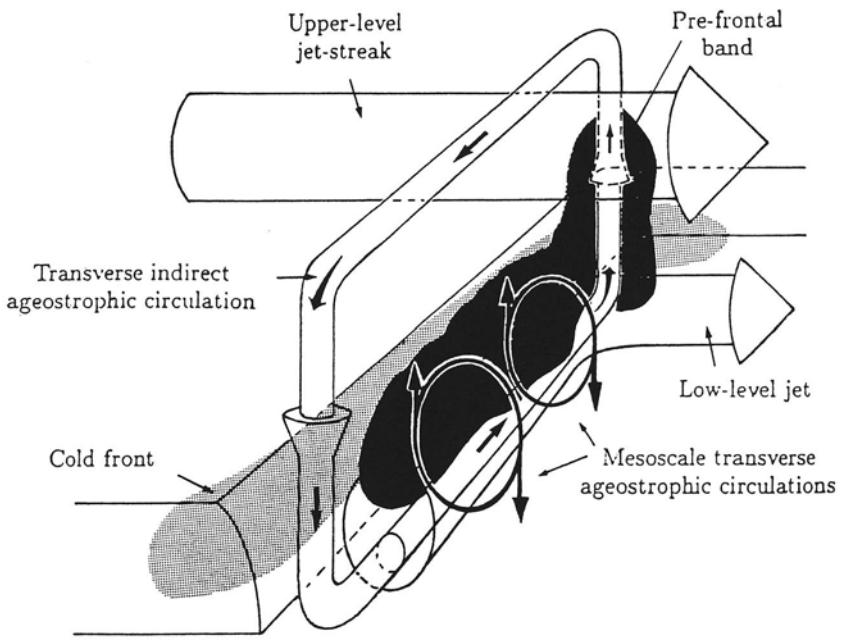

FIG. 3.15. Conceptual model showing the structure and orientation of the ageostrophic circulations associated with low- and upper-level jets in the vicinity of a cold front. From Sortais et al. (1993).

studied by Smull and Houze (1987), Ogura and Liou (1980), and Carbone (1982).

There are a number of boundary layer phenomena resembling or often associated with gravity currents—gravity waves, internal undular bores, and solitary waves—that at times are linked with the initiation of severe convective weather. Disturbances of this type often occur in connection with surface-based stable layers, such as nocturnal inversions, thunderstorm outflows, or marine inversions. Gravity waves represent a periodic oscillation of the upper surface of the stable layer. They may be generated by an impulsive forcing such as a downdraft impinging upon a stable layer, in which case there is no change in the mean depth as the oscillations pass by, or by a gravity current (e.g., a thunderstorm outflow) intruding on the stable layer, in which case an *undular bore* can be generated. A bore consists of an increase in depth of a fluid advancing with a series of waves on its surface that typically separate from the gravity current and move ahead of it. Figure 3.17 (from Simpson 1987) illustrates the production of such a disturbance by this process. Whether or not an undular bore develops depends upon the density current speed U normalized by $(g'h)^{1/2}$ (the internal Froude number F, where g' is the reduced gravity $g\Delta\rho/\rho$, $\Delta\rho$ being the density difference between the two fluids) and the ratio of the gravity current depth d to the depth of the undisturbed stable layer h (Fig. 3.17, lower diagram). If the gravity current is shallow relative to the stable-layer depth (d/h small) and F is >1, then the flow is *supercritical* and the gravity current moves faster than any disturbance can move forward along the top of the dense layer; the interface between the fluids rises smoothly over the head as the gravity current advances. If d/h is small and $F < 1$, the flow is *subcritical* and the only distur-

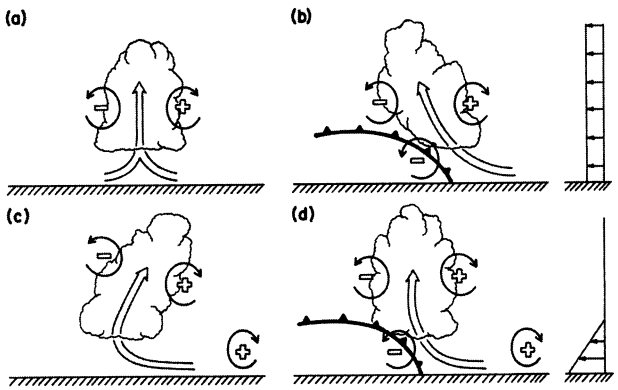

FIG. 3.16. Schematic diagram showing how a buoyant updraft may be influenced by wind shear and/or a cold pool. (a) With no shear and no cold pool, the axis of the updraft produced by the thermally created, symmetric vorticity distribution is vertical. (b) With a cold pool, the distribution is biased by the negative vorticity of the underlying cold pool and causes the updraft to tilt upshear. (c) With shear, the distribution is biased toward positive vorticity and this causes the updraft to lean back over the cold pool. (d) With both a cold pool and shear, the two effects may negate each other, and allow an erect updraft. From Rotunno et al. (1988).

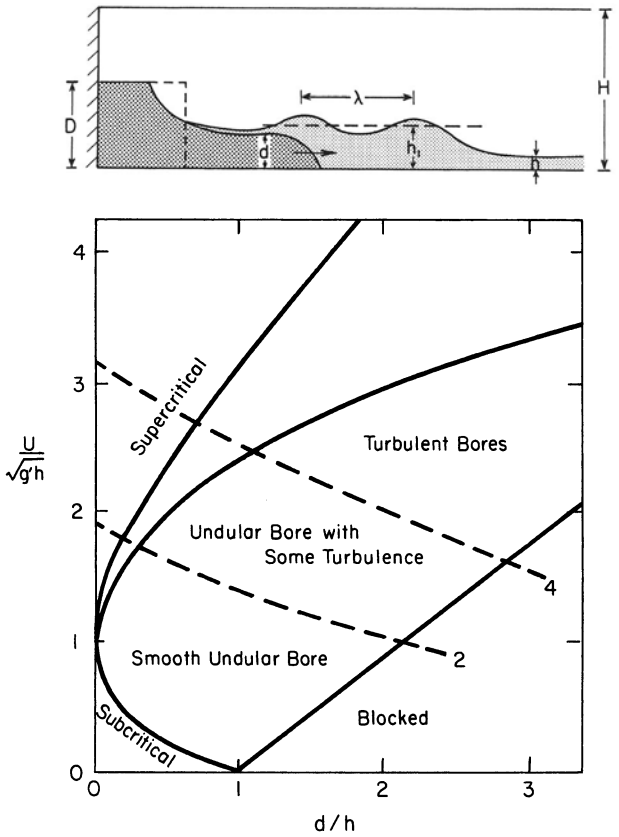

FIG. 3.17. (Upper) Depiction of internal bore generated by gravity current in the laboratory. (Lower) Flow regime diagram for gravity current of depth d impinging on a stable layer of depth h. Ordinate is internal Froude number $U/(g'h)^{0.5}$, where U is speed of the gravity current and abscissa is d/h. Dashed lines refer to undular bore magnitude (h_1/h). D is the depth of the reservoir containing denser fluid (a dense salt solution) on the left (dark shading) that is released into the less-dense fluid (water) on the right (light shading) by opening a gate (vertical dashed line). Redrafted from Simpson (1987).

bance is a small depression in the layer that moves along above the advancing gravity current head. Undular bores typically occur if the density current depth is comparable to or greater than the stable-layer depth and if F is not too small (otherwise the gravity current will be blocked or rise on top of the stable layer).

Probably the most dramatic atmospheric example of an undular bore is the morning glory of northeastern Australia (Clarke 1972; Smith 1988; Christie 1992). The morning glory is characterized by a spectacular low-level roll cloud or series of roll clouds often extending over several hundred kilometers in length. Although the precise mechanisms for its origin are uncertain, it is thought to develop as a result of colliding sea breezes over the Cape York peninsula (Clarke 1984). There have been numerous studies based on surface, tower, and Doppler radar data of similar atmospheric bore-like phenomena associated with thunderstorm outflows (Pothecary 1954; Shreffler and Binkowski 1981; Doviak and Ge 1984; Haase and Smith 1984; Carbone et al. 1990; Fulton et al. 1990). In some of these cases, the bores were observed to evolve into solitary waves as the density current weakened and slowed down. Undular bores or solitary waves may also be the explanation for the surface pressure jumps and oscillations reported in papers by Tepper (1950, 1951), Curry and Murty (1974), Uccellini (1975), and Balachandran (1980), particularly since many of the cases occurred at night, but these authors did not describe them as such. The gravity waves in these cases were argued to have originated by convection or cold fronts and evidence was presented for them initiating thunderstorms downstream by lifting air to the LFC.

However, there are problems in extending the laboratory two-fluid analog of Fig. 3.17 to the atmosphere, since atmospheric stratification above bores or solitary waves should allow energy to radiate vertically and limit the amplitude of the disturbances (Lindzen and Tung 1976). But Lindzen and Tung showed that a stable layer capped by an unstable layer can, depending on flow conditions, reflect wave energy and form a duct that allows wave propagation over great distances with little loss of amplitude. Similar trapping has been found to occur when there is a curvature in the wind profile (or a wind reversal) aloft (Crook 1986), a jet in the lower layer that opposes the wave motion, or an inversion at a certain height above the stable layer (Crook 1988). For "morning glories," all of the above three trapping conditions appear to be met (Crook 1988), whereas low-level opposing flow appears to be the trapping mechanism in several Midwest borelike disturbances (Shreffler and Binkowski 1981; Fulton et al. 1990). On the other hand, Karyampudi et al. (1995) found curvature in the wind profile of the low-level jet to be important in sustaining a prefrontal bore that developed downstream of the Rocky Mountains and played a role in the generation of severe weather over Kansas and Nebraska.

A unique set of observations of a mesoscale ducted gravity wave was obtained in the FRONTS-84 field experiment (Ralph et al. 1993). Surface, wind profiler, and rawinsonde data were used to determine the vertical structure of such a wave ducted between the ground and a critical level (where the phase velocity of the wave matches the wave-parallel background wind speed) (Fig. 3.18). The vertical velocity is a maximum (and the horizontal perturbation velocities are zero) at the antinode of the oscillation, which corresponds to the top of the layer of strong static stability, and which is at an altitude of one-quarter of a vertical wavelength. The temperature and vertical velocity perturbations at midlevels are in quadrature, and the horizontal velocity perturbations are in phase with the pressure perturbations at the surface, which allows detection of such waves in surface data (Koch and Golus 1988). Ralph et al. (1993) could not determine whether the wave was initiated by convection or induced convection. However, Koch et al. (1988)

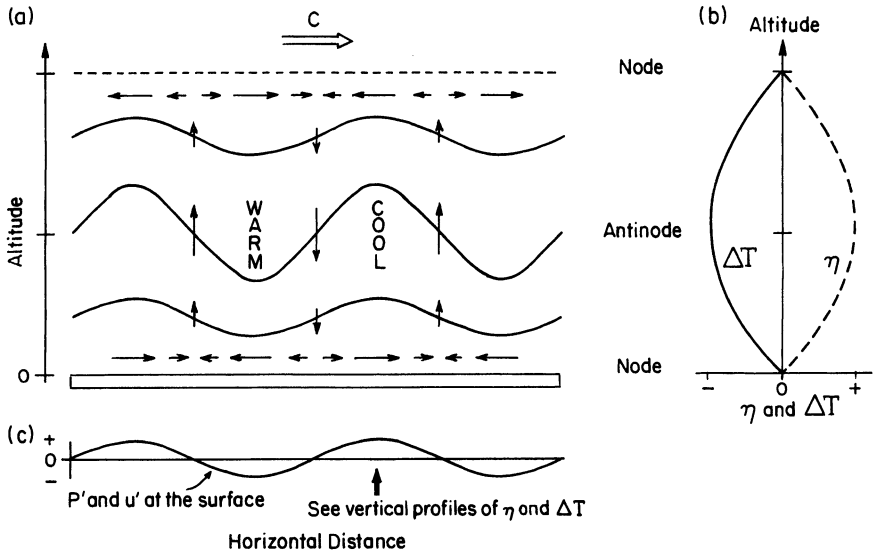

FIG. 3.18. Schematic representation of a ducted mesoscale gravity wave with one-half of a vertical wavelength contained between the ground and a critical level. (a) Horizontal cross section perpendicular to wave phase lines, showing wave-induced vertical and horizontal motions (arrows), streamlines or isentropes (solid lines), the ground (shaded), the critical level (dashed), and the direction of wave motion (labeled C). Regions of cool and warm air created by the vertical displacements are also shown. (b) Vertical profiles of vertical displacement (η) and temperature change (ΔT) for the phase of the wave marked in (c). (c) Wave-induced surface pressure perturbations (P') and wave-parallel wind perturbations (u') drawn for the same wave segment shown in (a). Notice that u' and P' are in phase, and that they lag behind the phase of the vertical motion within the duct by 90°. From Ralph et al. (1993).

argued for a close linkage between the waves and convection, and found deep convection and precipitation near the pressure maximum and low pressure ahead of and behind the squall line. The coupling of convection with gravity waves was argued by Koch et al. (1988) to be in qualitative agreement with predictions from wave-CISK (Lindzen 1974; Raymond 1975), where it is proposed that the gravity wave provides moisture convergence into the storm and the heating/cooling distributions from the storm in turn provide the energy to drive the wave disturbance.

Sources of convection-affecting mesocale gravity waves might all fit under the umbrella of "geostrophic adjustment processes" associated with (a) wind imbalances, for example, in the right-exit region of a jet streak approaching a ridge (Koch and Dorian 1988; Koch and Golus 1988; Koch et al. 1988, 1993; Koch and Siedlarz 1999) and (b) mass imbalances, for example, as a response to heating (Miller and Sanders 1980; Ulanski and Heymsfield 1986; Crook 1987; and Crook et al. 1990b's 7-h mesoscale oscillation). Mesoscale instability was also cited by Koch and Dorian (1988) as a possible explanation for their gravity waves.

3) MESOSCALE INSTABILITIES

Numerous instability mechanisms have been proposed to explain various mesoscale phenomena. Conditional instability is associated with the development of cumulus clouds, which occurs on small scales, but growth to the mesoscale can occur, especially when wind shear exists. Other instability mechanisms involving latent heat release have been proposed: CISK (conditional instability of the second kind; Charney and Eliassen 1964), wave-CISK (Lindzen 1974), CSI (conditional symmetric instability; Bennetts and Hoskins 1979), and others. Some instabilities do not require the release of latent heat: inertial instability, (dry) symmetric instability and Kelvin–Helmholtz instability (although the latter is typically associated with submesoscale phenomena, e.g., billow clouds).

On the synoptic scale, the condition for inertial instability ($\zeta + f < 0$) is rather rare, although it can occur on the anticyclonic side of strong upper-level jets (Knox 1997). One example of such a situation is found in Ciesielski et al. (1989), where the instability appeared to be manifested by a series of disturbances in the cirrus canopy on the anticyclonic side of the jet axis. On smaller scales, inertial instability can develop within the upper-level outflow jets of MCSs and severe storms (Maddox 1983; Blanchard et al. 1998).

When horizontal shears become very large, even if $\zeta + f$ is everywhere positive, a hydrodynamic instability can arise, sometimes called *Rayleigh* or *shearing instability*. From linear theory, disturbances that develop have a wavelength approximately 7.5 times the

width of the shear zone (Miles and Howard 1964). This instability has been used to explain the formation of small-scale vortices—the precursors to dust devils—along low-level shear zones (Barcilon and Drazin 1972). Other possible examples of mesoscale phenomena arising from this instability are vortices along cold fronts (Carbone 1982, 1983) or along outflow boundaries (Mueller and Carbone 1987; Wakimoto and Wilson 1989) that may be subsequently related to tornadogenesis. Lee and Wilhelmson (1997) successfully simulated the development of vortices (misocyclones) arising from shearing instability (caused by an outflow boundary advancing into boundary parallel flow) and found updraft maxima to develop adjacent to the misocyclones, which may provide an explanation for the colocation of cumulus updrafts and surface vortices illustrated in Fig. 3.8 (from Wakimoto and Wilson 1989).

The concept of CSI considers an atmosphere stable with respect to vertical (buoyancy) and horizontal (inertial) displacements (hence no CAPE), but unstable with respect to displacement along slant paths (Bennetts and Hoskins 1979; Emanuel 1979; see Schultz and Schumacher 1999 for a review). If CAPE is present and the LFC is reached by a displacement, then it seems logical that conditional gravitational instability (CGI) should be realized as opposed to CSI since the former has the fastest growth rate. However, a coupling between convective and mesoscale motions has been hypothesized to occur in environments of weak symmetric stability where CGI exists (Emanuel 1980; Xu 1986; Jascourt et al. 1988; Seman 1994). Emanuel (1980) showed that if the secondary circulations are hydrostatic and isentropic, the amount of work done by subsidence in the environment of upward fluid displacements decreases as the symmetric stability is reduced, at some point becoming less than the kinetic energy generated by the convective updraft. When this point is reached, the mesoscale circulation in the environment enhances the convection.

This idea has been extended by Seman (1994) to the nonlinear, nonhydrostatic case with CAPE, where vertical momentum transports in deep convection are found to produce inertial instability aloft (strictly speaking, negative isentropic absolute vorticity, the condition for CSI, is generated aloft). It is suggested that the instability enhances horizontal mass transport in the outflow branch, which ventilates the upper levels of the system, thereby promoting further convection. Blanchard et al. (1998) have provided some observational evidence that supports this positive feedback process, which they and Seman (1994) argue leads to the upscale growth of convection. Such coupled convective–mesoscale motions may have occurred in the early stages of the development of parallel, deep convective bands of precipitation over the south-central United States (Jascourt et al. 1988). Satellite and conventional data analysis suggested that a layer of weak symmetric stability modified the atmosphere's response to free convective instability, contributing to highly organized banded convective structure.

Zhang and Cho (1992) have shown that in the stratiform region of a squall line,[4] moist potential vorticity (MPV; potential vorticity defined using θ_e) can become negative as a result of modification of the stability and absolute vorticity fields by upward and rearward transport in the front-to-rear flow. The resulting symmetric instability considerably enhances the vertical motion and precipitation rate in the stratiform clouds. They also suggest that the generation of negative MPV contributes to inertial instability aloft that enhances the anticyclonic outflow at upper levels.

CSI has been argued by Colman (1990) to also play a possible role in the development of elevated thunderstorms in frontal overrunning situations. The cases studied exhibited negligible CAPE, yet strong thunderstorms occurred. He found that the storms developed in a strongly baroclinic environment and, in general, were aligned along the geostrophic shear. These observations are consistent with the theory of moist symmetric instability (Emanuel 1979, 1983). However, frontogenetical forcing in a symmetrically neutral environment was also suggested as a possible initiation mechanism (Emanuel 1985). In addition, it may be that while coarse sounding data indicate negligible CAPE in overrunning situations, significant CAPE may exist on smaller scales not sampled by the sounding network.

Mesoscale cloud bands have also been attributed to parallel instability, an instability of the Ekman boundary flow (Lilly 1966; Raymond 1978). CSI and parallel instability are analogous in the sense that both instabilities arise in vertically sheared flows; however, the shear in the case of CSI depends on the thermal wind (i.e., horizontal temperature gradient and the earth's rotation), whereas in the case of parallel instability the shear is due to the Ekman wind profile (i.e., boundary layer friction and the earth's rotation). Raymond developed a theory for parallel instability within the shear layer below a low-level jet and applied this idea to the development of three powerful squall lines and the massive tornado outbreak of 3 April 1974. The rolls connected with this instability (wavelength ~100 km) were hypothesized to concentrate low-level vorticity into narrow shear lines that generated banded cloud structure prior to the onset of deep convection.

The wave-CISK approach to the problem of thunderstorm generation considers the storm as a forced

[4] Here we use conventional terminology "stratiform" for the trailing light-rain region of a squall line, even though this region may contain some embedded convective elements aloft and it owes its existence largely to hydrometeor transport from the leading convective line (Houze 1997).

gravity wave and uses linear theory to predict the modes of maximum growth rate (Lindzen 1974; Raymond 1975, 1976). Wave-CISK as applied to severe storms has been reviewed by Lilly (1979). Ooyama (1982) has argued against the usage of the term "wave-CISK" for squall lines, etc., since CISK generally refers to a process introduced by Charney and Eliassen (1964) to explain hurricane genesis as a cooperative instability involving deep convection and large-scale moisture convergence. Raymond (1987) recommends that a more appropriate terminology for the wave-CISK-type process is *forced gravity wave mechanism.* This concept has been used by a number of authors to explain the development and propagation of squall lines, but results are highly parameterization dependent. According to Raymond (1987), "In spite of the difficulties with existing forced gravity wave models, the *idea* that gravity waves interact constructively with convection to produce propagating convective systems remains an attractive one. However, a more accurate treatment of convection is needed before the idea can be seriously tested against observation."

4) ORGANIZED BOUNDARY LAYER CIRCULATIONS

When the atmospheric boundary layer is heated from below, organized circulations often develop having a vertical scale equivalent to the depth h of the boundary layer and horizontal scales ~1 to 50 times h. For winds ~5–10 m s^{-1} or greater, boundary layer plumes or thermals tend to become approximately aligned with the wind, where they constitute the updraft portions of horizontal rolls or helical circulations (LeMone 1973). Rolls are generally thought to be formed by the along-roll wind shear and thermal instability (Kuo 1963; Asai 1970) or wind-shear curvature (Kuettner 1971), which are argued to organize convection into wind-parallel bands. Linear theory of inflection-point or convective instability predicts roll circulations with aspect (width to depth) ratios of 2–4 (Brown 1980). However, rolls with aspect ratios much larger than these (up to 15) have been observed, which are attributed by Etling and Brown (1993) to vortex pairing or merger and interactions with gravity waves in the free troposphere (Balaji and Clark 1988). When adequate moisture is available, the visible evidence of the rolls is cloud streets, where the individual clouds are initiated by periodic along-roll vertical velocity maxima (Kuettner 1959; Christian and Wakimoto 1989). There are instances over the ocean where complex, but organized, patterns of boundary layer circulations (e.g., lines, hexagonal cells, etc.) develop whose horizontal dimension is much greater than h (~30–50 km) and whose boundaries are foci for showers and thunderstorms (e.g., Agee 1984).

3.4. Triggering of convection

Convective-triggering mechanisms can operate in isolation (e.g., storms along a gust front) or in combination (e.g., gust fronts colliding with each other or with topography). In this section, we first consider these processes in isolation. Then combinations of these processes are treated.

a. Local processes

Buoyancy-driven circulations in the CBL are often sufficient to trigger convection. They can take the form of thermals or, in the case of a flat surface and moderate winds, horizontal convective rolls (HCRs). The growth of many isolated cells arises from thermals. In some cases the growth of cells is restricted by inversions or entrainment. Large numbers of fair-weather cumulus clouds arise simply from overshooting buoyant eddies in the CBL, referred to as *forced cumulus* (Esbensen 1978; Stull 1985). Others achieve sufficient buoyancy from latent heat release to rise to great heights, referred to as *active cumulus.* HCRs often lead to cloud rows or streets (Kuettner 1959), but seldom to severe weather in isolation. However, from a forecasting standpoint, it is important to recognize that HCRs lead to substantial inhomogeneities in the boundary layer moisture field (the updraft portions of HCRs are relatively moist; Weckwerth et al. 1996) so that an individual rawinsonde observation may not properly represent the true convective potential of the boundary layer.

Terrain forcing is a common trigger of convection. Houze (1993) discusses various ways in which this can occur (see his Fig. 12.24). Cloud initiation often arises from leeside convergence (Banta 1990) as the cold pool "burns off" in the morning and upslope flow develops (Fig. 3.19). Such storms do not usually

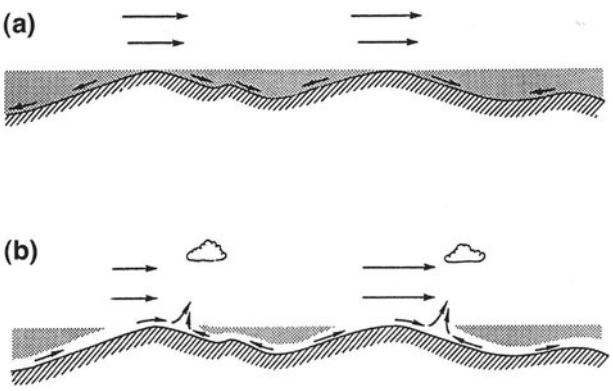

FIG. 3.19. Schematic cross section of (a) the nocturnal inversion layer, or "cold pool" buildup at night, and (b) the appearance of the shallow mixed layer the next morning. The inversion layer is shaded. The convergence zone forms at the uphill edge of the cold pools and leads to cloud initiation. From Banta (1990).

become severe; however, as they propagate downstream, they may develop into severe storms or organize into mesoscale convective systems (e.g., Tripoli and Cotton 1989a,b). Small-scale topographic features such as the "Caprock" escarpment in the Texas panhandle (Newton 1963), the Ozark Mountains (Hagemeyer 1984), and even the small ~100-m high Wichita Mountains in Oklahoma (Bluestein and Woodall 1990; Bluestein and Hutchinson 1996) can contribute directly to the initiation of severe convective weather through localized thermally induced lifting or earlier attainment of the convective temperature. Flow deflection by topography can also trigger severe weather by generating low-level convergence, as demonstrated by Watanabe and Ogura (1987) in a study of a flash flood in western Japan, or by orographic lift, as in the 1997 Fort Collins flood (Petersen et al. 1999).

Surface inhomogeneities in soil moisture or vegetation type can lead to both preconditioning and direct triggering of convection (Anthes 1984). This effect has been demonstrated in observational studies showing cumulus clouds to form first in Oklahoma over harvested wheat where the ground was warmer than adjoining areas dominated by growing vegetation (Rabin et al. 1990) and in Brazil where cumulus clouds developed preferentially over deforested land (Cutrim et al. 1995). This effect has been modeled by Lynn et al. (1998), who found that the total accumulated rainfall from mesoscale circulations generated by adjacent wet/dry patches was a maximum for patch sizes comparable to the radius of deformation (~130 km).

b. Advective processes

Convection often initiates along sharp boundary layer convergence lines of some type. Sometimes these lines are associated with density contrasts, but not always (Wilson and Schreiber 1986). Often they are outflows from previous convection. These convection-initiating convergence lines are typically very narrow, with horizontal dimensions of just a few km; really they are convective scale in the cross-line dimension, almost by definition (Byers and Braham 1949; Purdom 1982; Wilson and Schrieber 1986; Carbone et al. 1990; Lee et al. 1991; Wilson et al. 1992; Kingsmill 1995; Fankhauser et al. 1995). Shallow convergence lines, inadequate to trigger convection, may deepen the moist layer such that subsequent or additional lifting is more effective at initiating convection. These narrow convergence lines are visible as radar echo lines, apparently because insect concentrations are increased (Wilson and Schreiber 1986).

Fankhauser et al. (1995, their Figs. 20 and 21) and Crook and Tuttle (1994) show how initially broad convergence zones rapidly collapse to become fine lines of convergence in a flow model (the same process as in frontal collapse). The implication is that many diagnosed "mesoscale" convergence zones may actually be narrow convective-scale convergence lines, undersampled by sparse wind measurements. Convergence features above the surface can also affect convective development, especially in cases in which the convectively unstable air lies above the surface (e.g., Rochette and Moore 1996).

Several examples of direct triggering of deep convection by cold-frontal lifting were cited earlier (Browning and Harrold 1970; Carbone 1982). In another case, Ogura and Portis (1982) found a direct vertical circulation with moist warm air ascending directly above the surface front that apparently triggered and sustained severe storms. In a numerical modeling study of the Carbone (1982) California squall line, Parsons (1992) found that the intense updrafts (up to 20 m s^{-1}) at the front could be explained in terms of the gravity current–shear interaction concept of Rotunno et al. (1988). Parsons's results are illustrated in Fig. 3.20, which shows the most vigorous updrafts occurring when there is an optimal balance between the horizontal vorticity associated with the low-level wind shear and that associated with the cold air behind the front. An important distinction between the California cold front and the optimal balance for squall lines described by Rotunno et al. (1988) is the absence of CAPE and therefore appreciable buoyancy effects in the approaching flow. Intense upward motion and a narrow band and heavy precipitation were achieved solely by a strong upward-directed pressure force from convergence at the front.

While advective phenomena such as gust fronts, sea/lake breezes, and drylines represent loci for convection, deep convective cells typically do not form everywhere along them. However, intersections of these features can trigger storms. For example, the intersection of a dryline with a front (sometimes referred to as a *triple point* since it separates three different air masses) can lead to convective storm formation in its proximity (e.g., Bluestein 1993). The collision of gust fronts (Mahoney 1988) or sea breezes can lead to vigorous convection along the axes of intersection. Sea breeze collision often occurs over relatively narrow peninsulas or flat islands. A notable example is the daily occurrence of an intense thunderstorm "Hector" over Bathhurst and Melville Islands just north of Darwin, Australia, during the summer monsoon (Keenan et al. 1990, 1993; Simpson et al. 1993).

Whatever contributes to inhomogeneities along fronts, drylines, etc., may serve as a trigger for convection. CBL thermals may be sufficient in some cases. In other cases, horizontal convective rolls may provide the enhanced lift. It is the collision or intersection of these phenomena with each other, or with other features such as terrain or horizontal convective rolls, that provides the most energetic triggering of convection (Wilson and Schreiber 1986). The sub-

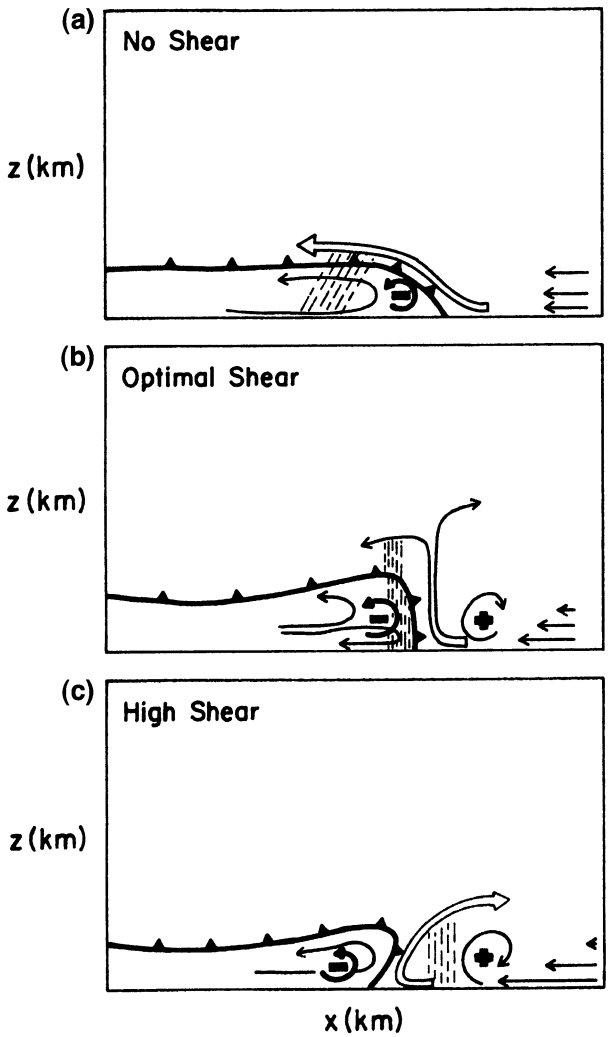

FIG. 3.20. A schematic of the dependence of the circulations at a cold front upon vertical shear. The horizontal vorticity due to the low-level vertical shear ahead of the front and that due to the horizontal gradient of buoyancy associated with the leading edge of the cold air mass are indicated. (a) Low-shear simulations with a sloped updraft and a broad area of precipitation that trails the front. The flow within the cold air mass is in the same sense as in a classical dry gravity current. (b) Optimal vertical shear with a deep and intense vertically oriented updraft and a narrow band of heavy rainfall. (c) Higher-than-optimal vertical shear with an updraft sloping into the warm air. The flow is unsteady due to the effect of precipitation interrupting the inflow and the influence of potential instability created by the overrunning of cold air. The airflow within the cold air mass is different from a classical gravity current due to an initial flow being prescribed within the cold air mass but is without the flow reversal evident in the optimal-shear simulations. From Parsons (1992).

ject of combined lifting processes will be treated in section 3.4d.

c. Dynamical processes

Horizontal convective rolls are thought to represent some form of a dynamical instability (e.g., Brown 1980), but as mentioned before, they generally do not trigger severe storms in isolation from other lifting mechanisms. In some instances, gravity waves have been linked to the triggering of severe convective weather (Uccellini 1975), but more commonly the triggering of convection by them occurs in conjunction with other processes, as described below. In the Tropics, where CIN is relatively weak, gravity waves or bores have been identified as direct triggers for squall lines, for example, morning glory-generated squall lines over northern Australia (Smith and Page 1985; Drosdowsky and Holland 1987).

Certain mesoscale instabilities may be related to the triggering of severe weather. For example, horizontal shearing instabilities have been linked with tornadogenesis (Carbone 1982; Wakimoto and Wilson 1989), although the parent clouds were presumably initiated by other processes. Similar instabilities may have initiated the tornado-like vortices in Hurricane Andrew (Wakimoto and Black 1994; Schubert et al. 1999). A mesoscale instability was implicated in triggering convection in a localized outbreak of severe storms in the Oklahoma–Kansas area (Sanders and Blanchard 1993). A very strong inversion existed in the region of the outbreak. While transverse circulations associated with a jet streak were not adequate to locally break the lid in the area of convection, they did produce an environment within which a shearing instability developed characterized by strong vertical motions on a 200-km scale. It was this oscillation that apparently triggered the convection.

d. Combined lifting processes

The genesis of severe storms can often be traced back to combinations of local, advective, and dynamical lifting processes.

Recent work with radar data has shown that when boundary layer rolls intersect convergence lines, they can locally amplify vertical motion and trigger deep convection. This process is illustrated in Fig. 3.21 (from Wilson et al. 1992). On 17 July 1987, a Denver cyclone was present during the afternoon (1500 MDT or Mountain Daylight Time) in the Denver area (Fig. 3.21a). Note the prominent north–south convergence line just east of Denver (DEN). An enlargement of an area along the convergence zone (thick line) centered near DEN at 1645 MDT is shown in Fig. 3.21b. Several showers were located 5–10 km east of the convergence line at this time. Also indicated are the updraft axes of horizontal rolls (thin lines). The rolls were subjectively identified using "clear-air" reflectivity and velocity data from a multiple-Doppler radar network. The analysis shows a clear correspondence between the roll updrafts and the clouds, suggesting that a superposition of lifting mechanisms—the convergence line and the rolls—contributed to cloud development. The primary effect of the convergence

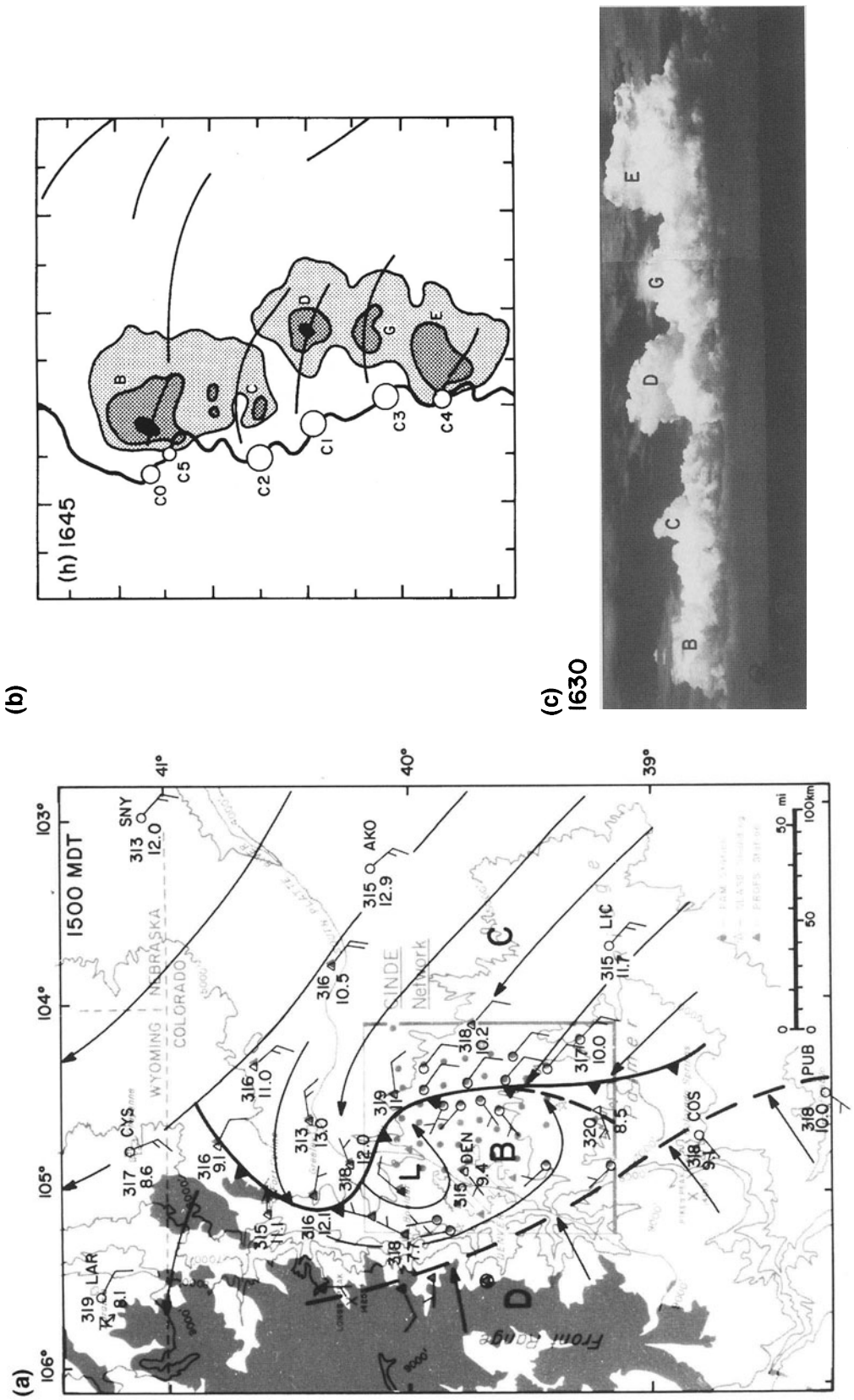

FIG. 3.21. (a) Surface map at 1500 MDT on 17 July 1987. The indicated winds and streamlines are based on NWS, PROFS, and selected PAM stations. A full barb is equivalent to 5 m s^{-1}, and a half-barb, 2.5 m s^{-1}. Potential temperatures and mixing ratios are shown next to the selected stations. The low is the Denver cyclone, and the cold-front type boundary is the Denver convergence line. The letters represent different air masses, and the inner box delineates the CINDE network and boundaries of (b). (b) Relative location of convergence line (heavy solid line), horizontal rolls (light solid lines), misocyclones (labeled open circles beginning with letter C), and precipitation echo at 6.5 km MSL (contours shown are 10, 30, and 50 dBZ_e) at 1645 MDT. (c) Photograph of clouds B, C, D, E, and G in (b). From Wilson et al. (1992).

line was to deepen the moist layer locally and provide a region potentially favorable to deep convection. A photograph of clouds B, C, D, E, and G from Fig. 3.21b is shown in Fig. 3.21c. Also indicated in Fig. 3.21b are positions of small-scale vortices or misocyclones along the convergence line. Wilson et al. (1992) found that these misocyclones formed where the rolls intersected the convergence line and that they were important in the initiation phase of a number of the radar echoes. When misocyclones became colocated with convective updrafts, they produced, in several instances, nonsupercell tornadoes (Wakimoto and Wilson 1989).

The above example illustrates convective triggering associated with the intersection of horizontal rolls and a terrain-induced convergence zone. However, similar triggering has recently been documented in connection with sea breeze front and roll intersections over south Florida (Wakimoto and Atkins 1994; Atkins et al. 1995; Fankhauser et al. 1995; Kingsmill 1995). Atkins et al. found that close to the front the roll axes were tilted upward and lifted by the frontal updrafts, leading to a deeper updraft and an additional impetus for cloud development (Fig. 3.22). Also, the same mechanism for cloud formation has recently been reported to occur along a dryline (Atkins et al. 1998). Based on these results, convective triggering may be rather commonplace as a result of intersections of rolls with a wide variety of convergence zones, for example, fronts, outflow boundaries, and so forth.

Observations suggest that dryline convection tends to be isolated, exhibiting a variety of modes of development (Bluestein and Parker 1993). The inhibiting factor is typically a strong capping inversion, which is broken only by enhanced lifting (Hane et al. 1997). A number of mechanisms have been suggested that could contribute to localized, enhanced lifting along drylines leading to severe storms: mesoscale low pressure areas (Bluestein et al. 1988), intersection of fronts with drylines (Shapiro 1982; Schaefer 1986; Parsons et al. 1991), intersection of boundary layer rolls or cloud lines with drylines (Hane et al. 1997; Atkins et al. 1998), and mesoscale gravity waves interacting with drylines (Koch and McCarthy 1982; McCarthy and Koch 1982).

To illustrate the complexity of processes associated with severe storm initiation along a dryline, consider the dryline of 26 May 1991 investigated by Hane et al. (1997) with aircraft, sounding, and mesonetwork data. In Fig. 3.23 results are shown from aircraft sawtooth traverses of the dryline at 860 mb (~1 km AGL). A cloud line was observed to intersect the dryline near the center of the domain, at which location the first

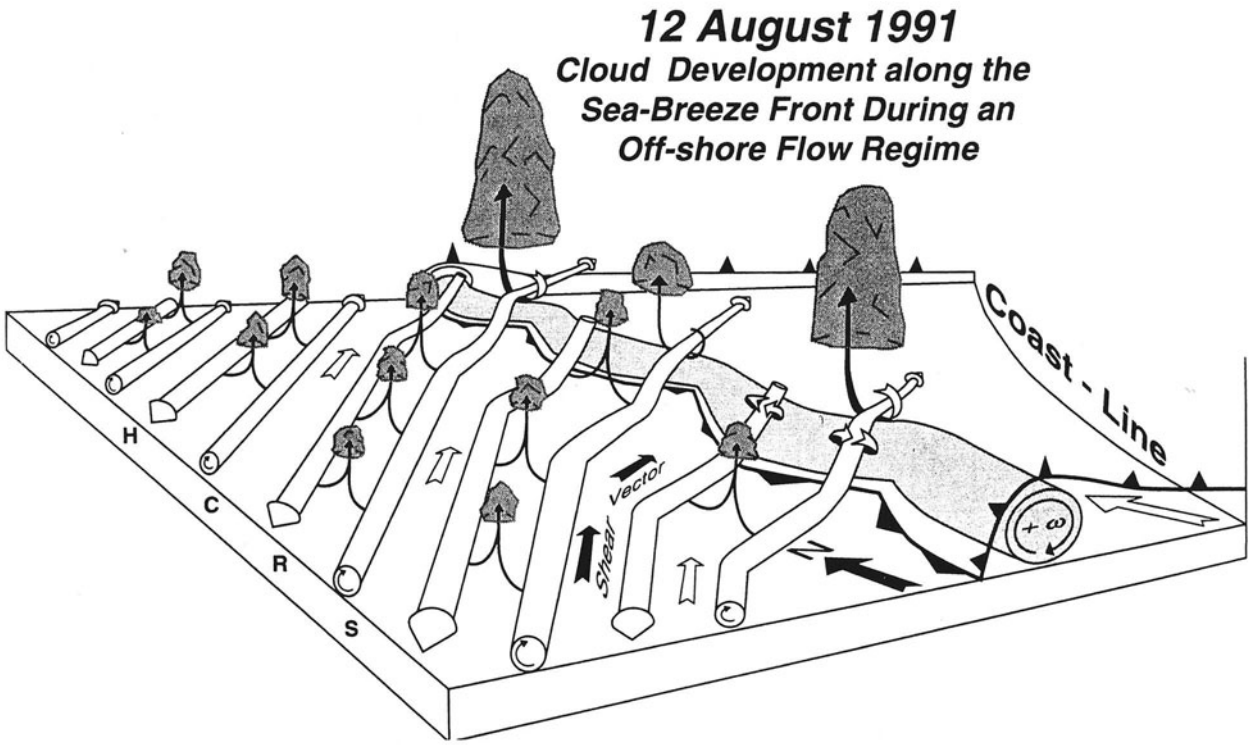

FIG. 3.22. Schematic diagram showing the interaction between the sea-breeze front and horizontal convective rolls (HCRs) and how it relates to cloud development on 12 August 1991. The sea-breeze front is delineated by the heavy, barbed line. The head circulation is lightly shaded. The horizontal vorticity vectors associated with the counterrotating roll circulations are shown. Clouds along the HCRs and at the intersection points along the front are shaded gray. The shear vector (solid, 2D arrow) and low-level winds (white, 2D arrow) are also shown. From Atkins et al. (1995).

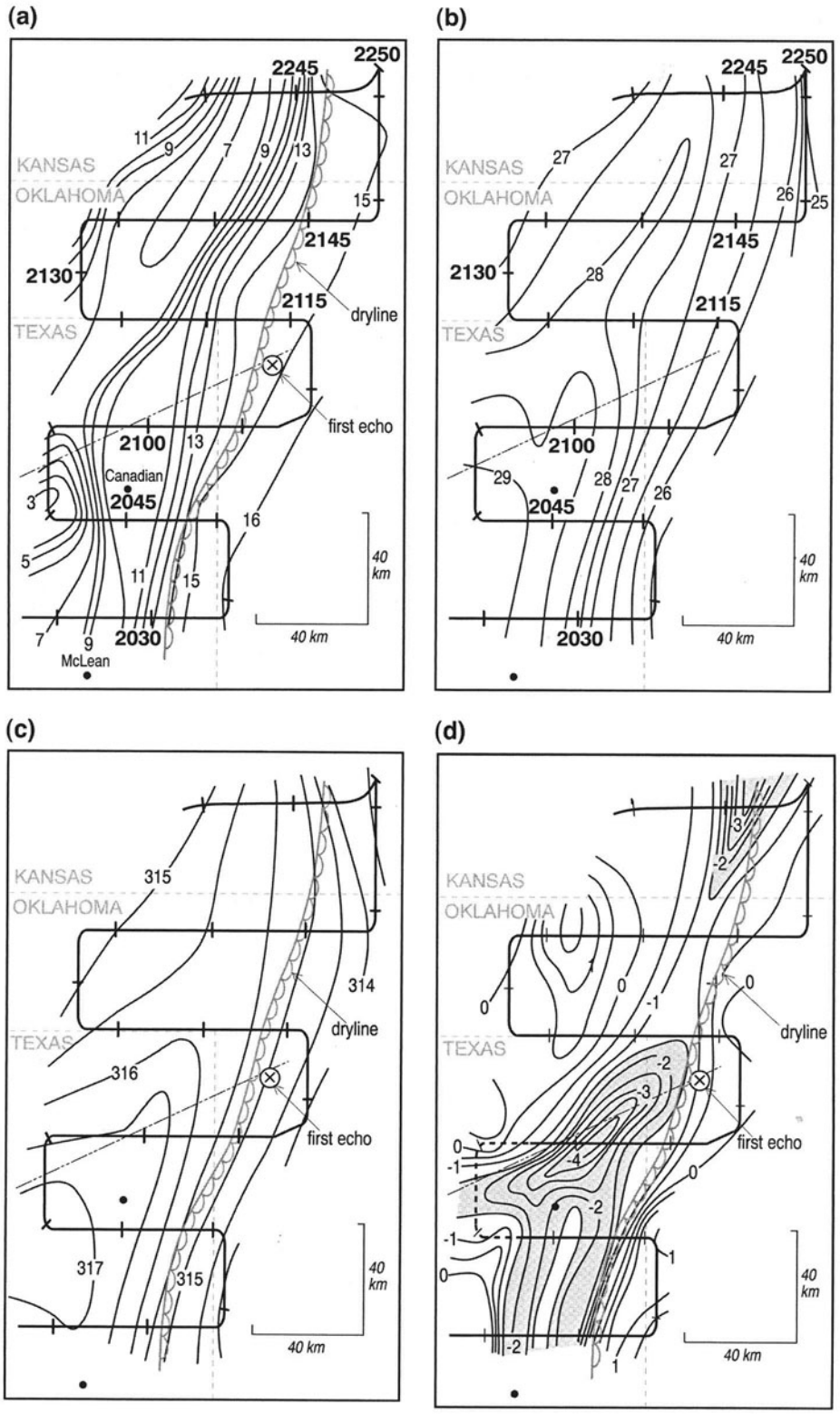

FIG. 3.23. (a) Dewpoint distribution in the dryline region based on aircraft observations (sawtooth pattern) at 860 mb. Dewpoint temperature (°C) shown by solid contours is derived from aircraft measurements along track shown. Dryline is indicated by scalloped line and cloud line by dash-dot-dot line; location of first echo also noted. (b) Temperature field (°C), (c) virtual potential temperature (K), and (d) horizontal divergence (10^{-4} s^{-1}). From Hane et al. (1997).

echo formed (at 2115 UTC), which later became one of several tornadic storms that developed along the dryline on this day. The rather sharp moisture discontinuity across the dryline can be seen in Fig. 3.23a, although the moisture drop is not everywhere uniform behind the line. Temperatures at this altitude were 2°–3°C warmer to the west of the dryline (Fig. 3.23b) as a result of the stronger surface sensible heat fluxes and a deeper mixed layer there. A 1°–2°C gradient in θ_v existed across the dryline (Fig. 3.23c), strongest in the southern part, supporting the existence of a dryline solenoidal circulation (Parsons et al. 1991; Ziegler and Hane 1993; Ziegler et al. 1995). Axes of convergence were detected at flight level both along and just behind the dryline and along the cloud line (Fig. 3.23d). Hane et al. argue that convective clouds developed along the cloud line in dry air and were advected across the dryline zone through a strongly convergent region. They encountered increasing low-level moisture as they moved east-northeastward, and upon reaching the deep moisture east of the dryline, they grew vigorously. A key question, though, is what produced the cloud line in the first place? An explanation for this feature turned out to be elusive, although satellite data suggest that surface vegetative inhomogeneities may have played some role in its generation. This example points to the difficulty in short-term (several hours) forecasting of convection along drylines but some potential for reliable nowcasting (0–30 min) of storm initiation with frequent, high-resolution visible satellite imagery.

There are other examples of combined lifting processes: gust fronts intersecting terrain (e.g., the 1979 Fort Collins hailstorm with softball-sized hail; Fritsch and Rodgers 1981); undular bores interacting with the dryline (e.g., the 14 April 1986 high plains severe weather outbreak; Karyampudi et al. 1995); interactions among gravity currents, bores, drylines, and low-level jets (e.g., the explosive convective development of 26–27 May 1985 in Kansas; Carbone et al. 1990); interactions between gust-front-generated internal gravity waves and Kelvin–Helmholtz waves to produce new convective cells atop a thunderstorm outflow in Alabama (Weckworth and Wakimoto 1992); and a combination of cloud forcing from thermally direct boundary layer circulations and gravity waves (Balaji and Clark 1988). The complexity of such processes represents a serious challenge for short-term forecasting.

3.5. Storm-generated mesoscale processes

Severe storms generate a host of mesoscale effects. Some act to promote storm development, severity, and longevity, for example, cold pool lifting, vortex tilting/stretching, generation of mesoscale pressure fields by dynamic and buoyant effects, vortex breakdown. Others act to weaken storms, for example, rapidly spreading cold pools, cloud shading, changed shear profiles due to gravity waves. A list of such processes is given in Table 3.3. In this section, we discuss these processes according to whether they are local, advective, or dynamical in nature.

a. Local effects

An example of a local process inside an existing cloud system is radiation. Radiative transfer is not local in the vertical direction, but it tends to transfer energy within a single vertical column of the atmosphere, in contrast to the horizontal transports effected by advective and dynamical processes. On the ~1–2-h timescale of most severe storms, cloud–radiative effects are not important in storm evolution. However, they may be important in the development of new storms, for example, from cloud shading of cirrus anvils generating inhomogeneities in boundary layer properties and subsequent convergence zones (McNider et al. 1995; Markowski et al. 1998). Also, on the longer (~6–12 h) timescale of MCSs, cloud–radiative interactions may be important in promoting the longevity of storms by enhancing the mass circulation within them (Gray and Jacobson 1977; Chen and Cotton 1988; Dudhia 1989) or by trapping storm-generated gravity waves in the upper troposphere through cloud-top radiative destabilization (Tripoli and Cotton 1989a,b). They may also increase storm total precipitation through longwave radiative cooling at cloud top and heating at cloud base (Tao et al. 1993).

Likewise, microphysical processes such as phase changes or particle spectrum evolution tend to have local effects, although these effects can later be advected to other regions. Production of the surface cold pool occurs principally through evaporation (e.g., Sawyer 1946) and melting (Atlas et al. 1969). The strength of the cold pool is important to supercell behavior and longevity (Weisman and Klemp 1982), to squall-line intensity and longevity (Thorpe et al. 1982; Rotunno et al. 1988), and to baroclinic vorticity generation in tornadic storms (Klemp 1987). In MCSs, sublimation, evaporation, or both, is important in causing the rear-to-front flow aloft (the *rear-inflow jet* after Smull and Houze 1987) to descend to the lower troposphere (Zhang and Gao 1989; Stensrud et al. 1991; Braun and Houze 1997). In microbursts, particle sizes are important in determining downdraft intensity, with smaller hydrometeors being most conducive to strong downdrafts (Brown et al. 1982; Srivastava 1985, 1987; Proctor 1989). In frontal rainbands, evaporation, sublimation, and melting can have the effect of enhancing the thermal contrast across cold fronts, thereby increasing their intensity and longevity (Parsons et al. 1987; Rutledge 1989; Barth and Parsons 1996).

b. Advective effects

A very common effect of convection on subsequent convection involves the outflow of cold air from convective downdrafts in a density current along the earth's surface. Cold pools are responsible for cell regeneration in multicell storms (Browning et al. 1976). As the cold pool spreads out over a large area and becomes shallow, its lifting may no longer be sufficient to cause air parcels to reach their LFC, and new cell growth will cease. Downdraft outflows are also important in supercells, where forward-flank downdrafts (FFD, produced by the downstream advection and evaporation of condensate) and rear-flank downdrafts (RFD, dynamically induced as strong low-level rotation lowers the pressure locally and draws air from above; Klemp and Rotunno 1983) produce storm-scale "fronts" (Fig. 3.24) that intersect at the main center of supercell rotation (the mesocyclone center; Lemon and Doswell 1979). Tornadoes generally form in the updraft ahead of the RFD (Fig. 3.24). As RFD advances, cold air is ingested into the updraft at the point of occlusion of the "fronts," thereby weakening the mesocyclone. However, as shown by Burgess et al. (1982), on some occasions new mesocyclones may form at the occlusion, leading to a succession of tornadoes with near-parallel tracks (Fig. 3.25).

Advection of condensate is also an important factor in the development of trailing stratiform regions of squall lines. Falling snow particles generated at upper levels in the leading convective line are advected rearward by the storm-relative front-to-rear flow aloft (Fig. 3.26), where they eventually fall out in a secondary band of precipitation (Biggerstaff and Houze 1991). The precipitation in the secondary band is also produced in part by in situ generation of condensate by a mesoscale updraft (e.g., Rutledge and Houze 1987). Houze et al. (1990), in a study of six years of springtime squall lines in Oklahoma, found that nearly

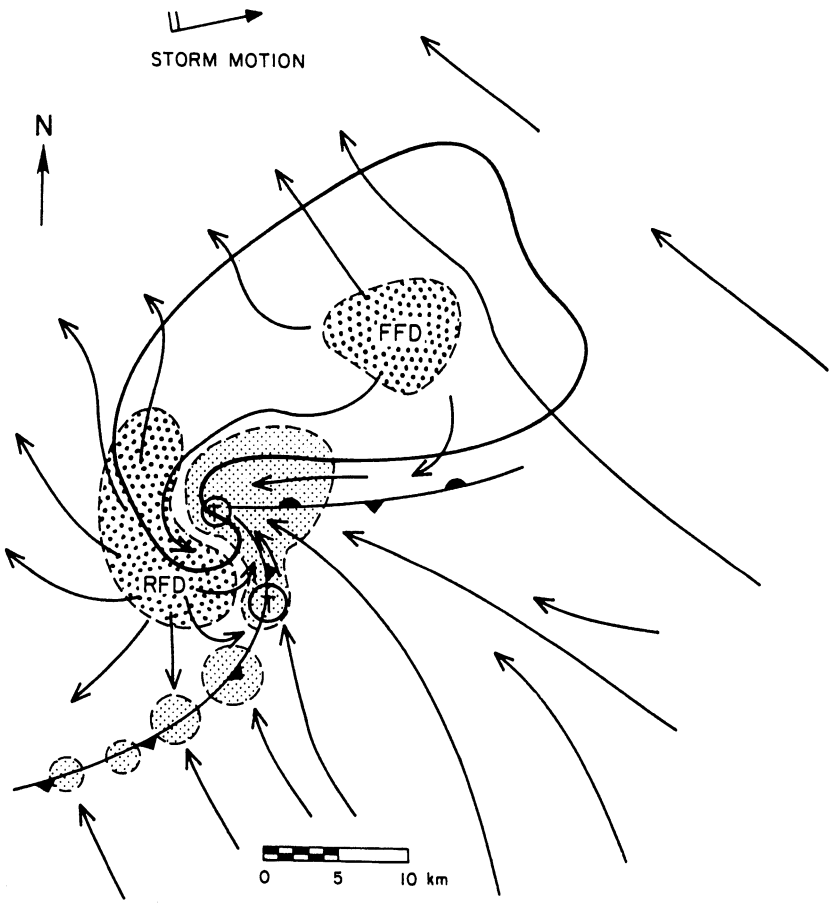

FIG. 3.24. Schematic plan view of a tornadic thunderstorm near the surface. The thick line encompasses the radar echo. The cold-front symbol denotes the boundary between the warm inflow and cold outflow and illustrates the occluding gust front. Low-level position of the updraft is finely stippled, while the forward-flank (FFD) and rear-flank (RFD) downdrafts are coarsely stippled. Storm-relative surface flow is shown along with the likely location of tornadoes (encircled T's). From Lemon and Doswell (1979).

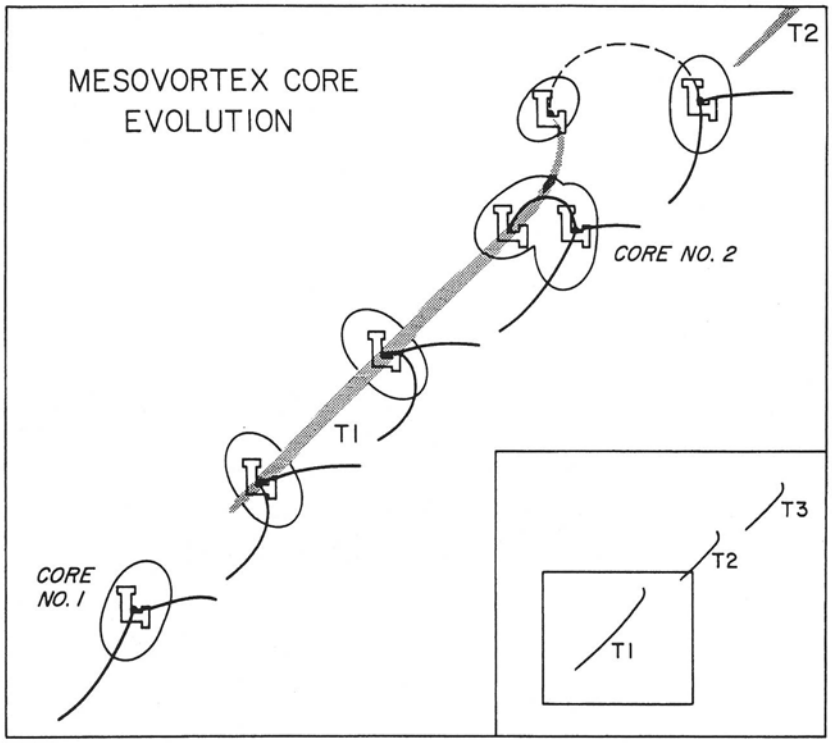

FIG. 3.25. Conceptual model of mesocyclone core evolution. Low-level wind discontinuities (thick lines) and tornado tracks (shaded). Inset shows the tracks of the tornado family and the small square is the expanded region in the figure. From Burgess et al. (1982).

two-thirds of the lines exhibited a leading-line/trailing-stratiform-region structure.

Momentum transport also represents an advective process in severe storms. Newton (1950) has shown that in squall-line systems, vertical transport of horizontal momentum helps to generate convergence at the leading convective line. A similar process may be operating in bow echoes associated with derechos where rear-inflow jets descend to the surface (Weisman 1993; Przybylinski 1995), although extreme surface winds in derechos may also be a direct consequence of downburst winds impacting the surface (Fujita and Caracena 1977) or intense surface pressure gradients that develop within the storm (Schmidt and Cotton 1989).

Another advective effect is vortex tilting, which in vertically sheared environments leads to the development of vertical vorticity couplets in storm updrafts (Rotunno 1981; Davies-Jones 1984; Klemp 1987). This process is illustrated in Fig. 3.27a, where a tube of low-level horizontal vorticity associated with unidirectional shear is tilted vertically, generating positive and negative vorticity centers within the updraft. Later, as the downdraft develops (Fig. 3.27b), the vortex tube is tilted downward, producing two vortex pairs. Given sufficient vertical shear, the storm can split into right- and left-moving cells as a result of dynamical effects, namely, lifting pressure gradients that reinforce new updraft growth on the southern and northern flanks of the central updraft (Schlesinger 1980; Rotunno and Klemp 1982).

Tilting can also produce vertical vorticity in MCSs. An example is the bow echo (Fig. 3.28), which exhibits a vortex couplet (cyclonic on the north end and anticyclonic on the south; Fujita 1978). Bow echoes are often associated with severe surface winds. Weisman (1993) argues that the primary mechanism for the generation of the vortex couplet or "bookend vortices" is tilting of horizontal vorticity associated with the ambient vertical shear by precipitation downdrafts (note cyclonic and anticyclonic eddies at northern and southern ends of the downdraft in Fig. 3.27b). In a numerical modeling study of the bow echo, Weisman (1993) found that the bookend vortex pair associated with the downdraft persisted throughout the storm simulation, while the anticyclonic and cyclonic eddies associated with the updrafts on the northern and southern ends of the line (Fig. 3.27b) did not persist as new, shorter-lived updrafts were generated at the leading gust front.

The development of mesovortices in MCSs such as bow echoes has been studied from a potential vorticity perspective by Davis and Weisman (1994) and Weisman and Davis (1998). They find that, in addition to the mechanism described by Weisman (1993) involving an interaction between the downdraft and the

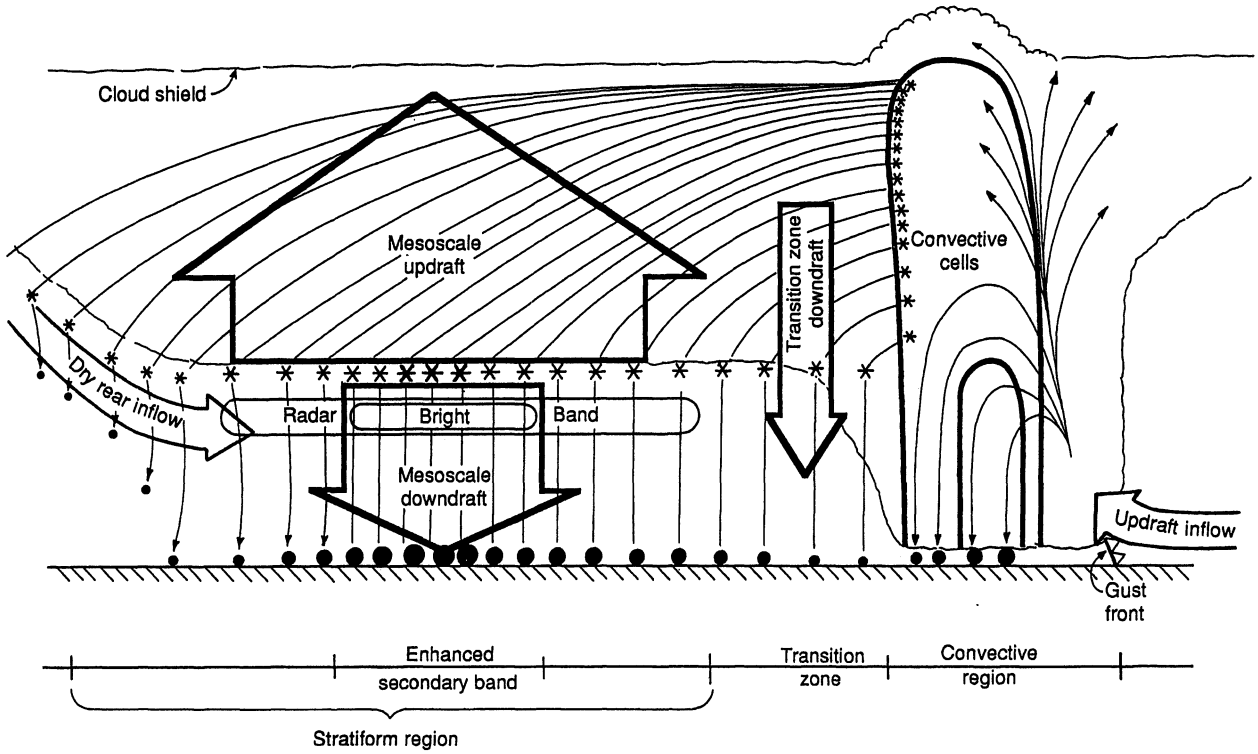

FIG. 3.26. Conceptual model of the two-dimensional hydrometeor trajectories through the stratiform region of a squall line with trailing stratiform precipitation. From Biggerstaff and Houze (1991).

ambient westerly shear (Fig. 3.29b), another tilting mechanism is operative involving perturbation shears associated with the storm itself. Buoyancy forces act to generate front-to-rear (FTR) and rear-to-front (RTF) flow, that is, perturbation shears and a horizontal vortex tube pointed toward the south (Fig. 3.29a). The tilting of this vortex tube by the ascending FTR flow at the leading edge of the storm serves to strengthen the vortex couplet. The numerical simulations by Weisman and Davis (1998) indicate that tilting of perturbation shears generated by the cold pool is important in the production of line-end vortex pairs in environments with weak-to-moderate shear, whereas tilting of ambient vorticity is operative in environments with stronger and deeper shear. The cyclonic circulation at the north end of a bow echo often resembles the mesovortex observed within the trailing stratiform region of mature squall lines (Zhang and Fritsch 1986, 1988; Houze et al. 1989; Skamarock et al. 1994; Loehrer and Johnson 1995); however, the latter are frequently of much larger scale (several hundred km across; Bartels and Maddox 1991). As squall lines mature, Coriolis effects appear to be important in the development of mesovortices on their north ends (Zhang 1992; Skamarock et al. 1994; Weisman and Davis 1998), leading to the eventual evolution of many squall lines to an asymmetric precipitation pattern (Houze et al. 1990; Loehrer and Johnson 1995).

Advective changes also include the effects of the plume of heat and moisture, both vapor and ice, lofted by primary convection. Weisman (1992) argues that the convective/advective warming of the midtroposphere is the primary mechanism for the generation of the midlevel rear-inflow jets in squall lines. Moistening can increase the buoyancy of secondary convection that entrains the air, compared to the buoyancy it would have if it entrained drier unmodified environmental air. For example, Table 3.2 shows the (mostly modest) effects on instability indices if the relative humidity above the 900-mb level is raised to 80%, and this air is entrained by the updraft parcel. Moistening of the environment, particularly at low levels, by the detrainment of moist cloudy air might play a larger role in encouraging the development of deep convection than is indicated by the small continuous entrainment rate calculations of Table 3.2.

c. *Dynamical effects*

Dynamical effects of convection are numerous, occurring on scales ranging from individual cells up to the scale of MCSs and even the synoptic scale. One important process is the generation of mesoscale pressure fields through buoyancy and dynamic effects. On the storm scale, dynamical effects (lifting pressure gradients on the flanks of updrafts) contrib-

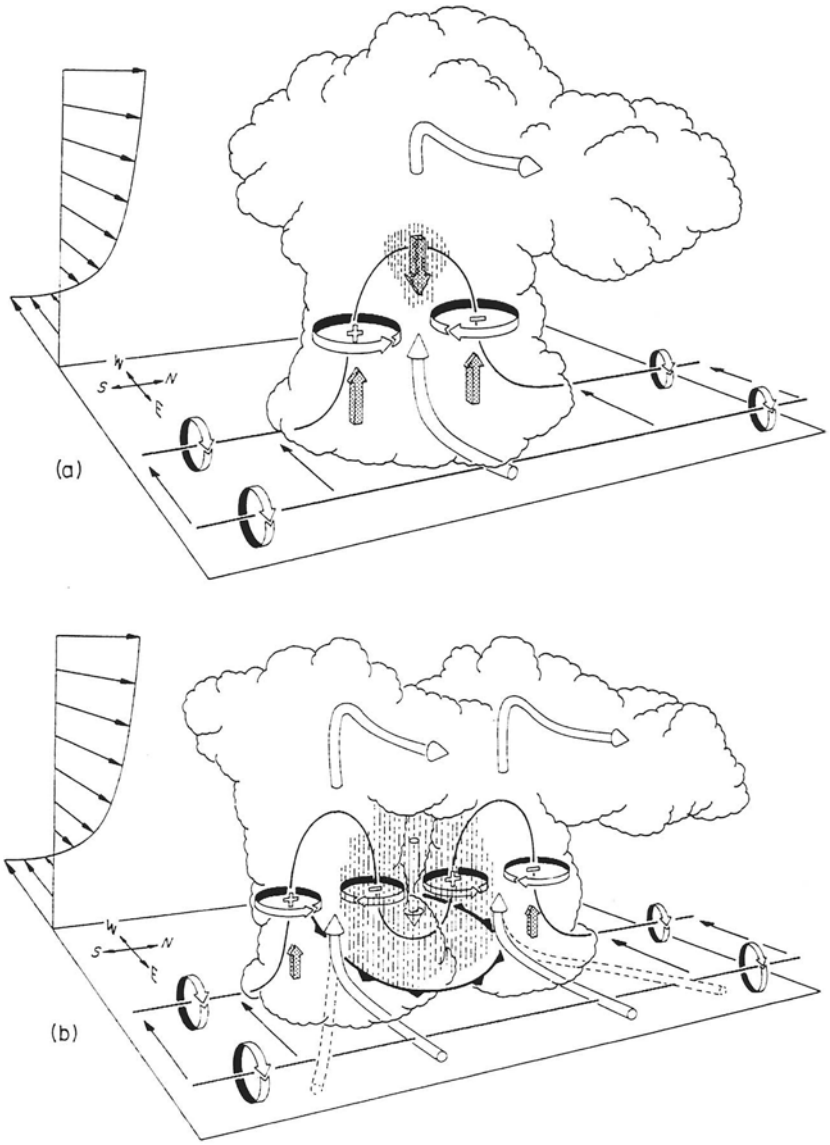

FIG. 3.27. Schematic depicting how a typical vortex tube contained within (westerly) environmental shear is deformed as it interacts with a convective cell (viewed from the southeast). Cylindrical arrows show the direction of cloud-relative airflow, and heavy solid lines represent vortex lines with the sense of rotation indicated by circular arrows. Shaded arrows represent the forcing influences that promote new updraft and downdraft growth. Vertical dashed lines denote regions of precipitation. (a) Initial stage: Vortex tube loops into the vertical as it is swept into the updraft. (b) Splitting stage: Downdraft forming between the splitting updraft cells tilts vortex tubes downward, producing two vortex pairs. The barbed line at the surface marks the boundary of the cold air spreading out beneath the storm. From Klemp (1987); adapted from Rotunno (1981).

ute to the splitting of supercells (Rotunno and Klemp 1982). The lifting arises from the dynamic lowering of pressure at midlevels within vorticity centers of both sign along the flanks of the updraft (Fig. 3.27a). Updraft growth is thereby induced on these flanks, leading to storm splitting. Environments with unidirectional shear yield an equal preference for right- and left-moving storms. However, in the central United States, the shear vector in severe storm situations normally turns clockwise with height (Maddox 1976), which leads to a favoring of right-moving supercells. Rotunno and Klemp (1982) explain this behavior by showing that high (low) pressure perturbations develop when the shear vector points toward

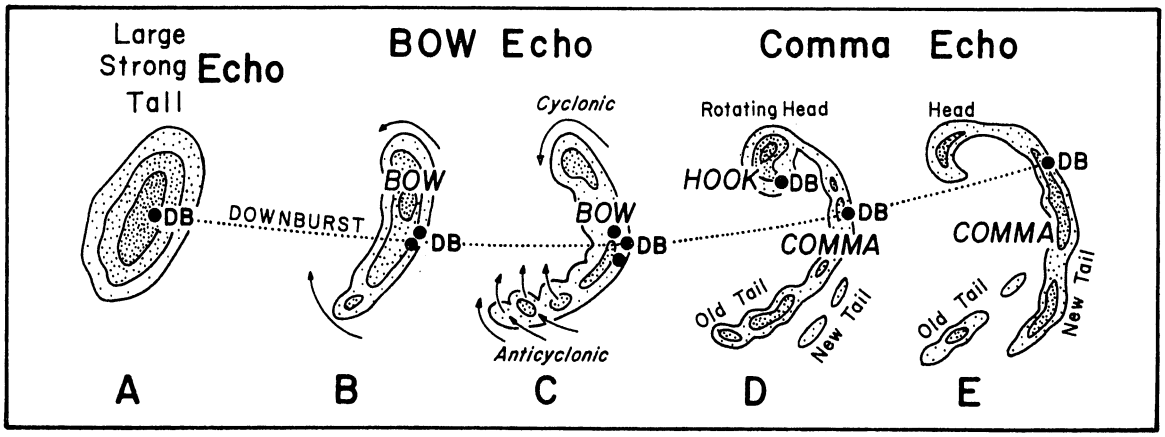

FIG. 3.28. A typical morphology of radar echoes associated with bow echoes accompanied by strong and extensive downbursts. Some bow echoes disintegrate before turning into comma echoes. During the period of strongest downbursts, the echo often takes the shape of a spearhead or a kink pointing toward the direction of motion. From Fujita (1978).

(away from) the updraft. In the case of unidirectional shear (Fig. 3.30a), this leads to an upward-directed pressure gradient on the leading edge of the storm and a downward-directed gradient to the rear. This configuration does not contribute to preferential growth on either of the flanks transverse to the shear. However, when the shear vector turns clockwise with height (Fig. 3.30b), the interaction of the shear with updrafts leads to an upward-directed pressure gradient on the right flank of the storm and a downward-directed gradient on the left, thus favoring new cell growth on the right.

The evolution of supercells to the tornadic phase involves a number of mesoscale dynamical processes that are not completely understood. Among others, they include the ingestion of streamwise vorticity into updrafts (Davies-Jones 1984), baroclinic vorticity generation along supercell forward-flank downdrafts (Klemp and Rotunno 1983; Rotunno and Klemp 1985), and mesocyclone vortex breakdown (Brandes 1978; Wakimoto and Liu 1998). The tornado itself can be subject to vortex breakdown, leading to smaller-scale suction vortices (Rotunno 1984; Davies-Jones 1986). These topics are treated in detail elsewhere in this volume.

Another dynamical process involves cold pool–shear interactions (Fig. 3.16), which influence the generation of new convective cells. It has been argued that continual regeneration is favored if there is an optimal balance between horizontal vorticity generated by the cold pool and that associated with the ambient low-level shear (Fig. 3.16d), yielding deeper, stronger, and more erect updrafts (Thorpe et al. 1982; Rotunno et al. 1988). However, the situation is often complicated by the existence of additional sources of vorticity when storms evolve to larger scales (Lafore and Moncrieff 1989; Weisman 1992). Moreover, the "optimal" state is not a requirement for long-lived

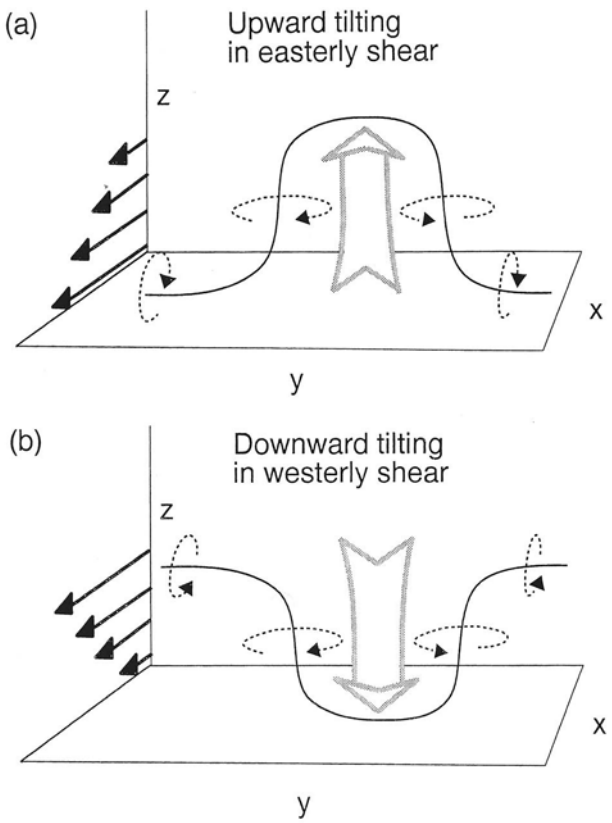

FIG. 3.29. Schematic of vertical vorticity generation through vortex tilting. For easterly shear (a), ascending motion tilts the vortex lines, resulting in cyclonic rotation on the north end and anticyclonic rotation on the south end. Localized descent in westerly shear (b) also produces the same pattern of vertical vorticity through tilting. From Weisman and Davis (1998).

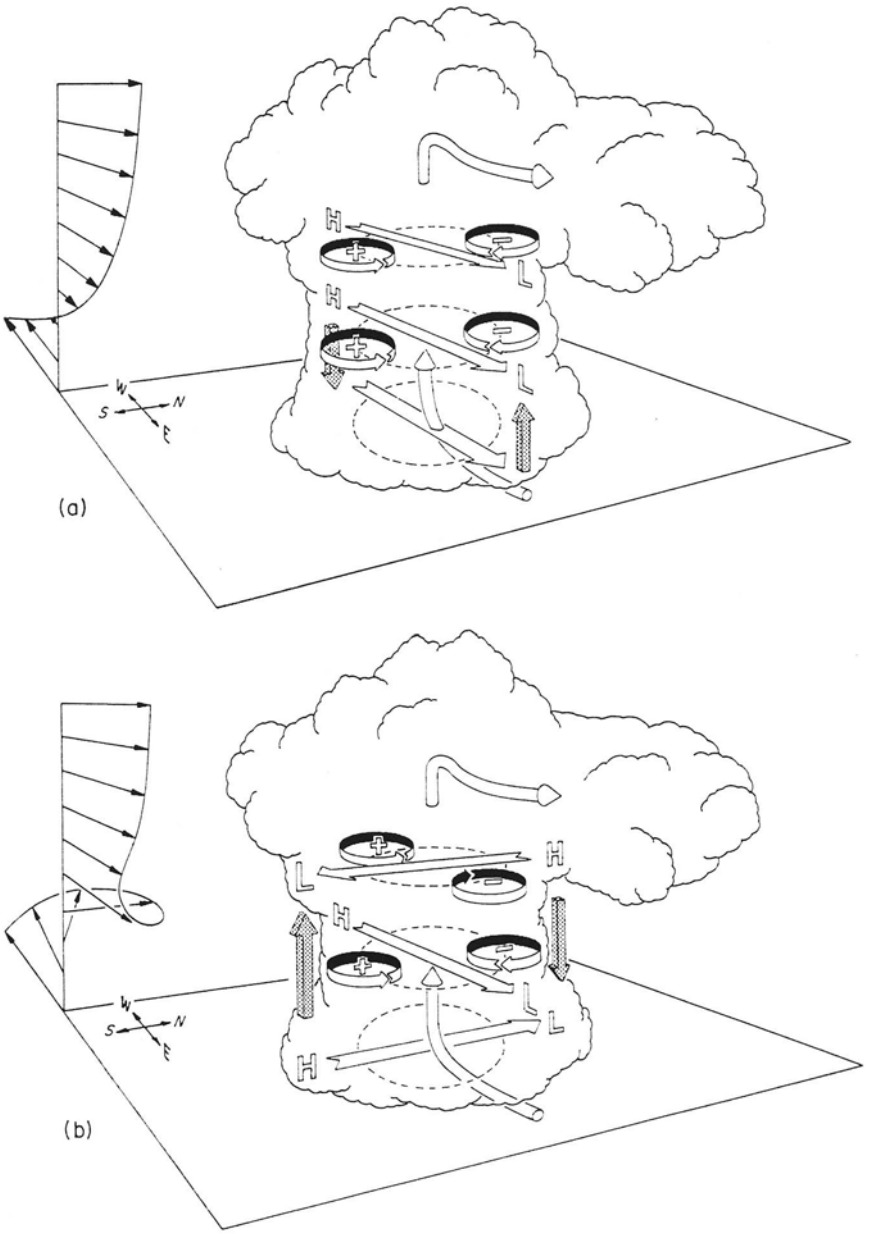

FIG. 3.30. Schematic illustrating the pressure and vertical vorticity perturbations arising as an updraft interacts with an environmental wind shear that (a) does not change direction with height and (b) turns clockwise with height. The high (H) to low (L) horizontal pressure gradients parallel to the shear vectors (flat arrows) are labeled along with the preferred location of cyclonic (+) and anticyclonic (−) vorticity. The shaded arrows depict the orientation of the resulting vertical pressure gradients. From Klemp (1987); adapted from Rotunno and Klemp (1982).

squall lines in all numerical simulations (Fovell and Ogura 1988, 1989; Grady and Verlinde 1997). Fovell and Ogura find the upshear sloping phase (Fig. 3.16b) to possess a quasi-equilibrium state.

Lafore and Moncrieff (1989) and Weisman (1992) propose that mesoscale influences come about through the following sequence of events.

1) An initial updraft leans downshear in response to the ambient vertical shear (Fig. 3.31a).
2) The circulation generated by the storm-induced cold pool balances the ambient shear, and the system becomes upright (Fig. 3.31b).
3) The cold pool overwhelms the ambient shear and the system tilts upshear. A rear-inflow jet (Smull

and Houze 1987) develops as horizontal buoyancy gradients along the rear edge of the buoyant plume aloft and the cold pool near the surface generate horizontal vorticity favoring rear inflow (Fig. 3.31c).

The development of rear-inflow jets can be important in producing intense surface winds (Weisman 1992; Przybylinski 1995). Rear-inflow jets can also influence storm evolution. On the scale of MCSs, buoyancy effects can be used to explain the existence of mesoscale pressure fields and storm circulations. Lafore and Moncrieff (1989) show specifically how a rear-inflow jet develops in response to horizontal and vertical buoyancy gradients aloft (Fig. 3.32). The vertical buoyancy gradient influences the perturbation pressure p' field, which can be seen by taking the divergence of the horizontal momentum equations:

$$\frac{1}{\rho_0}\nabla^2 p' = -\nabla\cdot(\mathbf{v}\cdot\nabla\mathbf{v}) + \frac{\partial B}{\partial z}, \tag{3.3}$$

where $B = g\theta_v'/\bar{\theta}_v$. A positive buoyancy anomaly in the upper troposphere and negative anomaly in the lower troposphere produce a positive $\partial B/\partial z$ in the midtroposphere, thereby creating a mesolow ($\nabla^2 p' > 0$). The horizontal gradient in B aloft (Fig. 3.32) produces a horizontal pressure gradient that contributes to both the rear inflow and the front-to-rear flow in the convective line. This mechanism does not require an extensive stratiform region and, indeed, there is evidence to indicate that rear-inflow jets can form independently of the existence of the stratiform region (Klimowski 1994), although they are enhanced as the stratiform region develops. Equation (3.3) can also be used to explain the common occurrence of mesohighs aloft in MCSs (Fritsch and Maddox 1981; Maddox et al. 1981), since $\partial B/\partial z < 0$ in the upper troposphere.

Another interpretation of rear-inflow jets is that they can form as a gravity wave response to convective heating (Pandya and Durran 1996). The heating function specified by Pandya and Durran represents the heating associated with the sloping front-to-rear ascending and rear-to-front descending branches of a mature squall line, which are produced in large part by advective effects within the squall line. The gravity wave response that is then generated explains the far-field generation of a rear-inflow jet as a response to an "advectively" produced nearer-field component heating described by Weisman (1992) and Lafore and Moncrieff (1989). Additional complications in the interpretation of rear-inflow jets are the roles of processes on large scales—for example, upper-level jets and shortwave troughs—and on the storm scale—for example, mesovortices—in their development (Zhang and Gao 1989; Belair and Zhang 1997).

Convection can also change the ambient density field, and hence convective stability, in distant regions through dynamical effects. These dynamics have received considerable theoretical attention in recent years, and gravity wave motions are a central mechanism. Convection has at least three effects on the gravity wave field. The temporal transience of convection and gust front circulations excites abundant high-frequency waves, essentially by mechanical agitation. In addition, wind blowing across the tops of convective clouds can generate the equivalent of mountain

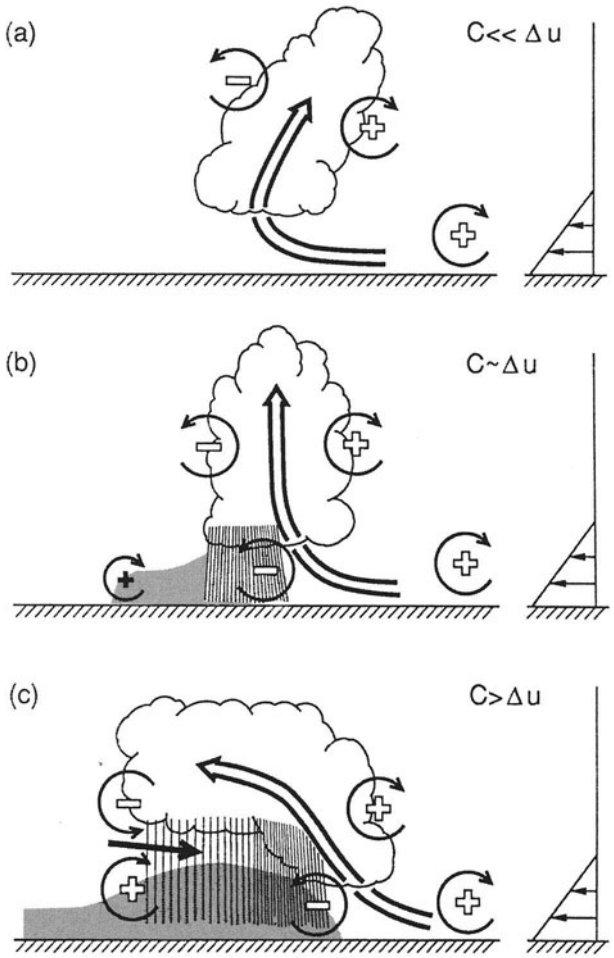

FIG. 3.31. Three stages in the evolution of a convective system. (a) An initial updraft leans downshear in response to the ambient vertical wind shear, which is shown on the right. (b) The circulation generated by the storm-induced cold pool balances the ambient shear, and the system becomes upright. (c) The cold pool circulation overwhelms the ambient shear and the system tilts upshear, producing a rear-inflow jet. The updraft current is denoted by the thick, double-lined flow vector, with the rear-inflow current in (c) denoted by the thick, solid vector. The shading denotes the surface cold pool. The thin, circular arrows depict the most significant sources of horizontal vorticity, which are either associated with the ambient shear or are generated within the convective system. Regions of lighter or heavier rainfall are indicated by the more sparsely or densely packed vertical lines, respectively. The scalloped line denotes the outline of the cloud; C represents the strength of the cold pool, while Δu represents the strength of the ambient low-level vertical wind shear. From Weisman (1992).

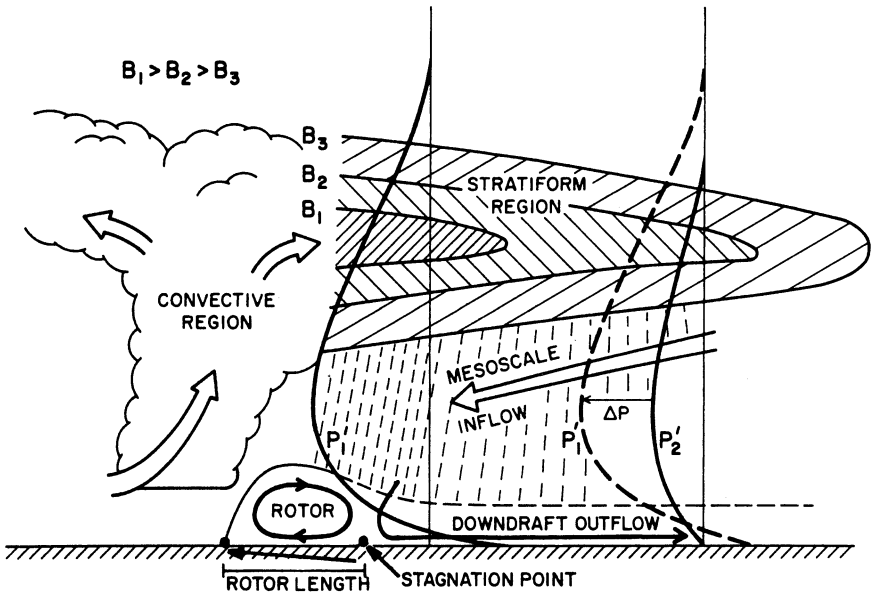

FIG. 3.32. Schema of the relation between buoyancy and the pressure perturbation fields in the mesoscale region of the squall line. Here B_1, B_2, and B_3 represent the perturbation buoyancy fields. From Lafore and Moncrieff (1989).

waves. These waves occur in the troposphere as winds blow across shallow boundary layer cumulus (Hauf 1993), and in the stratosphere above deep convective systems (Fovell et al. 1992). These waves may also be responsible for V-shaped structures in the cloud-top temperature field (Heymsfield and Fulton 1994). Both of these mechanically forced types of waves tend to propagate upward out of the troposphere within a relatively short distance of their source, because they have high frequency. However, for certain configurations of static stability, wind shear, and wavelengths, these oscillatory waves can be trapped or "ducted" and so propagate long distances horizontally without appreciable loss of energy to vertical propagation. Such ducted waves can have important effects on future convective developments, especially if they are generated and trapped at low levels (section 3.3c).

A third gravity wave effect involves the response of the atmosphere to the irreversible, diabatic rearrangement of mass in deep convection (i.e., the net heating associated with precipitation). Because the heating is irreversible, the response includes a very low frequency component that is fairly independent of the details of the convection. This response constitutes the warming caused by convective heating, and it remains in the troposphere for all time, at least in a linear approximation (Bretherton and Smolarkiewicz 1989; Nicholls et al. 1991; Pandya et al. 1993; Bretherton 1993; Mapes 1998). Because this part of the response is less dependent on the details of the convection, we examine it in some detail (but in extreme idealization).

Figure 3.33a illustrates how gravity waves can redistribute heat added to one region of a nonrotating stratified fluid, as by a precipitating cloud. The region of elevated temperature (contours), which contains the heat added to a narrow zone near the origin some time before the time of Fig. 3.33a, propagates continuously to the right. A downwelling wavefront adiabatically warms air at the leading edge, while a trailing wavefront of ascent restores air to its original temperature.

The passage of this structure at a point causes net horizontal displacements of air, toward the origin at low levels and away from the origin aloft. In a rotating fluid, such horizontal displacements generate geostrophic currents, which require thermal perturbations for balance. As a result, heat added to a rotating stratified fluid is exponentially trapped within a Rossby deformation radius given by $R = c/f$, where c is the gravity wave speed and f is the Coriolis parameter. This trapping becomes apparent when the gravity wave structure has traveled for a time f^{-1}. Figure 3.33b shows a situation equivalent to Fig. 3.33a, but with rotation. The warming (contours) is now trapped in a mesoscale region near the origin, with an e-folding distance of $R = c/f \sim 300$ km, while the wavefront structures have become ordinary oscillatory inertio-gravity waves, with no warming between them. In an unbounded atmosphere, these waves would propagate up out of the troposphere.

Figure 3.33 depicts the geostrophic adjustment process in response to localized heating for a single vertical mode with gravity wave speed c, valid only for the case of a special heating profile in a stratified

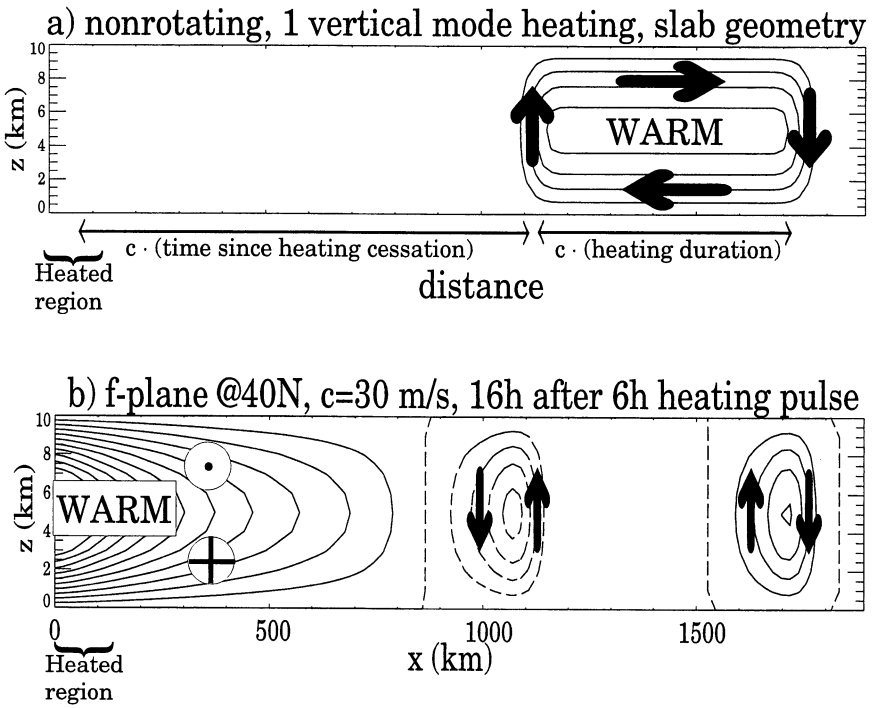

FIG. 3.33. Temperature (contours) and schematically indicated winds (arrows) that occur in a bounded linear stratified fluid in response to a transient slab-symmetric heating at the origin some time ago. (a) In the nonrotating case, the warming propagates away from the heated region as a roll circulation traveling at gravity wave speed, leaving no trace. See Nicholls et al. (1991) for details. (b) In a rotating fluid, the warming is trapped within a Rossby deformation radius of the heated area by geostrophic currents (point: out of page; cross: into page). The high-frequency inertio-gravity waves at x = 1000 and 1700 km in (b) would propagate vertically in an unbounded atmosphere.

fluid bounded above by a lid.[5] In the unbounded atmosphere, tropospheric heating generates gravity waves with a spectrum of values of c (vertical modes). This spectrum of waves separates out in space as the waves dispersively propagate away from the source, with the deepest spectral components traveling faster than shallower components. In a rotating fluid, these different vertical modes have different Rossby radii c/f. This dispersion can have some surprising consequences.

If the mass convergence into a convecting region has its peak value above the surface, then the response of the atmosphere to this convection can include low-level upward displacements, and hence adiabatic cooling, in the near vicinity of the convection. Surprisingly, this cooling can occur even for heating profiles that are positive at all levels (as overall convective system heating profiles tend to be). If these low-level upward displacements are more important to convection than the concomitant upper-level subsidence, then this effect could be destabilizing, rendering convection "gregarious," as hypothesized by Mapes (1993). On the other hand, if the subsidence aloft is strong enough to prevent deep convection, then the result might be merely a burst of cumulus congestus capped by a midlevel inversion, as studied by Stensrud and Maddox (1988) and Johnson et al. (1995). A more complex sequence of events was envisioned for MCSs by McAnelly et al. (1997). They proposed that the initial gravity wave response to an intensifying convective system, involving the gavest vertical mode generated by convective heating, leads to brief MCS weakening, followed by a resurgence of growth due to a second vertical mode associated with condensational heating aloft and evaporative cooling at low levels.

[5] Figure 3.33 shows the special case of a single-mode heating profile in a fluid trapped beneath a reflecting upper boundary. While atmospheric conditions can sometimes reflect gravity waves, in general they propagate vertically, dispersing along sloping ray paths. Since larger horizontal wavenumbers propagate preferentially upward, the tropospheric parts of the solution become spatially smoothed with time (e.g., Appendix 1 of Mapes 1998). The tight spatial gradients in Fig. 3.33 are therefore artifacts of the rigid lid approximation.

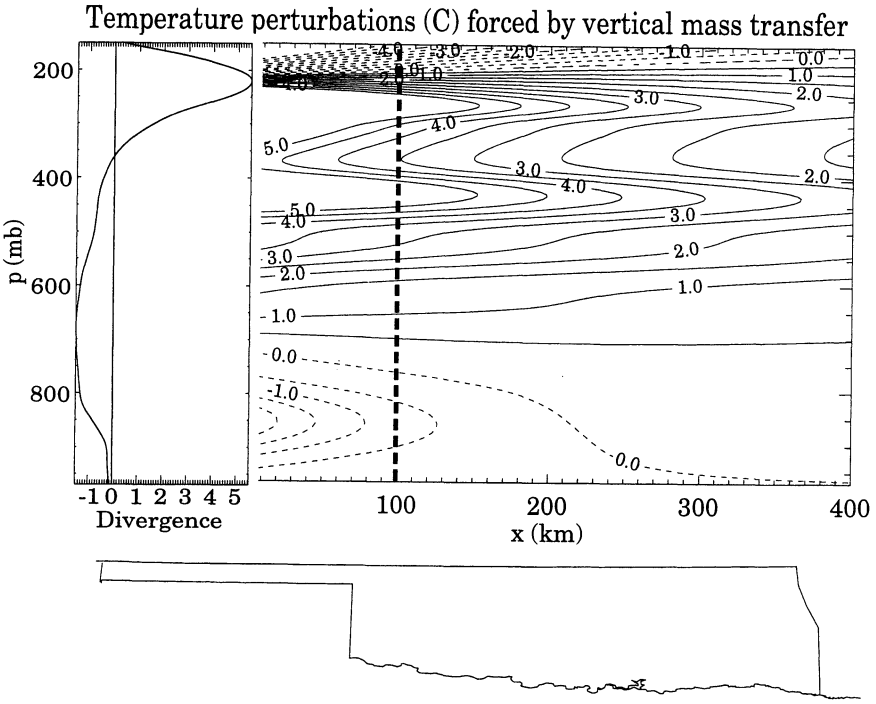

FIG. 3.34. The linear, geostrophically balanced temperature response to a narrow line of heating at the origin, in a uniform resting atmosphere with basic state density stratification taken from the sounding of Fig. 3.1. The heating profile is a cross-isentropic (vertical) mass transfer, characterized by the horizontal wind divergence profile, as plotted here. This profile is adapted from divergence observations around mesoscale convective complexes (Fig. 7 of Maddox 1983; units 10^{-5} s^{-1}). Vertical shear of geostrophic currents balances the temperature gradients. The magnitude of the heating is equivalent to 3 in. of rain in a 100-km-wide zone. The outline of Oklahoma is shown for scale.

Midlatitude organized convection tends to have its maximum convergence near 700 mb (e.g., Fig. 7 of Maddox 1983; data replotted in Fig. 3.34 here). This translates into a net heating profile that is positive at all levels but top-heavy, with its peak in the upper troposphere. The elevated convergence is largely inflow into downdrafts driven by the evaporation of precipitation.

Figure 3.34 shows the geostrophically balanced temperature response to a line of convection-like heating at the origin, in a linear resting atmosphere on an f plane at 45° latitude. The model is forced with the heating profile implied by the composite divergence profile of mature MCCs from Maddox (1983), acting in a static stability profile derived from a smoothed version of Fig. 3.1. The calculation procedure is described and discussed in Mapes and Houze (1995) and Mapes (1998). For each vertical wavelength in the spectrum excited by this heating profile the associated temperature perturbation falls off with distance as $e^{-x/R}$, where $R = c/f$ is the Rossby radius of deformation as discussed above (see chapter 7 of Gill 1982).

At a distance of 100 km from the zone of heating (heavy dashed line), the temperature is ~1°C cooler at low levels, and 5°C or more warmer aloft. Rerunning the parcel instability diagnostics of Table 3.4 with this change to the temperature sounding indicates that the pseudoadiabatic ICAPE including freezing is decreased by 33%, to 5.5 × 10^6 J m^{-2}, by the warming aloft. However, the CIN of surface (970 mb) air has decreased from 24 J kg^{-1} to 10 J kg^{-1}. CIN for air originating at other levels undergoes a similar numerical decrease. Such an alteration to the sounding might actually favor new convective development, if the CIN change outweighs the CAPE change. If the line of heating were not infinitely long, for example, if a circular patch of heating were used, the cool core at low levels would be even more pronounced relative to the deep warming that decreases the CAPE and ICAPE.

The temperature changes shown in Fig. 3.34 are initially caused by adiabatic vertical displacements in gravity wave fronts (as in Fig. 3.33a), and are rendered permanent by the development of geostrophic currents (as in Fig. 3.33b). Although the cooling processes in downdrafts are responsible for the elevated convergence peak, which in turn causes the cool core at low levels in Fig. 3.34, it is worth noting that there is no actual diabatic cooling in this model—only a top-heavy diabatic heating process, representing mesoscale convective complex heating in its totality, with its peak in the upper troposphere. Of course, horizontal

advection by mean storm-relative wind and wind shear can be expected to deform and redistribute the warmed and cooled regions seen in Fig. 3.34, so this calculation is only a rough approximation to the true situation in any real case. Similar calculations of the balanced response to squall line heating events have been calculated using nonlinear potential vorticity methods by Schubert et al. (1989) and Hertenstein and Schubert (1991).

As noted earlier, gravity waves occurring in environments of variable stability can have some interesting effects. Wave ducting or trapping can occur if a near-adiabatic layer exists above a stable layer. Since stable layers are often generated near the ground in thunderstorm outflows, wave trapping conditions may exist within some storms. Schmidt and Cotton (1990) have proposed that such conditions may occur in squall lines and that the interaction of high-amplitude gravity waves with the stable layer can produce severe surface winds. Since derechos often occur along and to the north of stationary frontal boundaries (Johns 1984; Johns and Hirt 1987), this interaction may explain extreme surface winds accompanying these phenomena.

When a stratiform region exists, rear-to-front flow aloft in an MCS typically descends to lower levels as a result of sublimation or evaporation, or both, along the lower boundary of the stratiform cloud (Zhang and Gao 1989; Stensrud et al. 1991; Braun and Houze 1997). Rear-inflow jets can descend all the way to the surface and play a significant role in the triggering of new convection by the gust front circulations with which they eventually link up (Lafore and Moncrieff 1989; Weisman 1992) or in the dissipation of the MCS (Zhang and Gao 1989). Weisman (1992) further elucidates these relationships, noting, in particular, that the degree to which a rear-inflow jet may help trigger new convection depends, among other things, on whether the jet descends to the surface well behind the leading edge of the system or remains elevated to near the leading edge of the system.

Upon encountering trailing stratiform precipitation regions, rear-inflow jets have been observed to descend very rapidly. Just behind the stratiform region, strong warming in the lower troposphere is observed. As a result, strong surface pressure falls are often produced locally in the region of warming, leading to the development of wake lows (Fujita 1955, 1963; Pedgley 1962; Williams 1963; Zipser 1977; Johnson and Hamilton 1988). These features are distinct from presquall mesolows, which occur ahead of squall lines (Hoxit et al. 1976) and are typically of smaller amplitude (1–2 mb). However, both may be a gravity wave response to convective heating and/or cooling in the squall line (e.g., Koch et al. 1988; Koch and Siedlarz 1999).

In support of this idea, Haertel and Johnson (2000) simulated MCS mesohighs and wake lows using a linear dynamical system in which the only forcing was the lower-tropospheric cooling associated with stratiform precipitation. The response consisted entirely of gravity waves, whose amplitudes were enhanced in the direction of the cool source motion. When the moving cool source was defined to have a three-dimensional structure, both a mesohigh and mesolow developed having characteristics of squall-line mesohighs and wake lows (Fig. 3.35). The simulated evolution closely resembles that described by Pedgley (1962), Fujita (1963), and Johnson and Hamilton (1988). When an upper boundary was introduced directly above the cooling, the response approached a steady state in which a mesohigh–mesolow couplet was centered on the cooling. An analytic solution showed that the large-amplitude response to stratiform cooling in squall lines is a unique consequence of the fact that the stratiform region's forward speed of motion typically approaches the gravity wave speed associated with the vertical wavelength of the stratiform cooling. The modeled wake low intensified when the stratiform precipitation terminated (after 4 h in Fig. 3.35), consistent with Fujita's (1963) observations of wake low

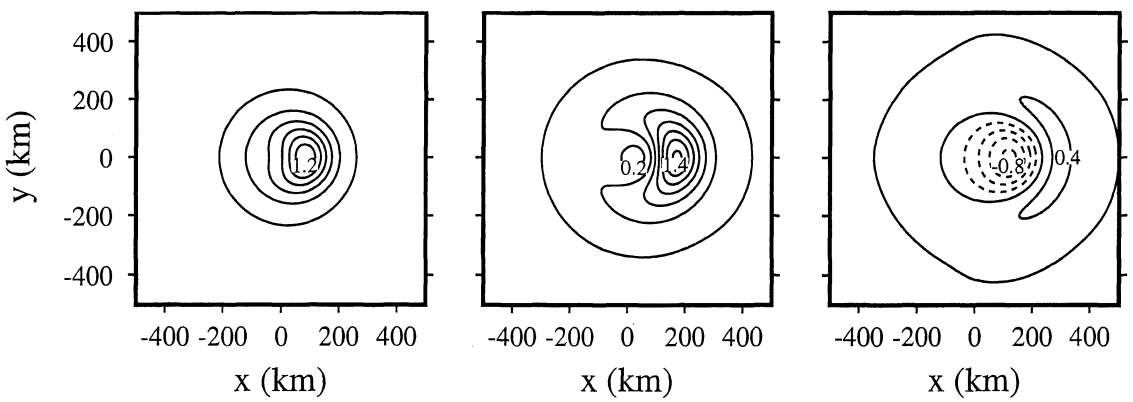

FIG. 3.35. The surface pressure response to a moving, axisymmetric cooling at 2, 4, and 6 h. The forcing is chosen to represent lower-tropospheric cooling associated with the stratiform precipitation region of a squall line (width = 150 km; height = 4 km; lifetime = 4 h). The contour interval is 0.2 mb. From Haertel and Johnson (2000).

intensification during the latter stages of the life cycle of squall lines. These findings are also consistent with observations showing that wake lows tend to occur only when trailing stratiform regions exist.

In rare instances, the rapidly descending flow in an MCS reaches the surface as a hot blast of air, referred to as a *heat burst.* The early work by Williams (1963) actually suggested an association between rear inflow and heat bursts; however, the details of the relationship between the rear-inflow jet and cloud and precipitation structures were limited due to the sparsity of radar and sounding data. Johnson (1983) proposed that heat bursts are a consequence of strong downdrafts penetrating a shallow layer of cool air near the surface. This idea is supported by the modeling study of Proctor (1989) and the observational study of the 23–24 June 1985 heat burst by Johnson et al. (1989). The lower-tropospheric thermodynamic structure in the 23–24 June case closely resembled a dry microburst environment (Wakimoto 1985), except that a shallow, ~500 m deep stable layer existed near the surface. If an evaporating parcel were introduced from cloud base (near 500 mb), then sufficiently cooled, it could descend all the way to the surface if it had enough downward momentum to penetrate the surface stable layer. Johnson et al. (1989) found that on 23–24 June downdrafts of 6–8 m s^{-1} were sufficient to reach the surface. Later dual-Doppler analyses by Johnson and Bartels (1992) and Bernstein and Johnson (1994) confirmed that downdrafts of this magnitude existed.

In some instances, the pressure gradients to the rear of the stratiform region are intense (Bosart and Seimon 1988; Loehrer and Johnson 1995; Johnson et al. 1996). One such case occurred at 0210 UTC on 6 May 1995 (Fig. 3.36, from Johnson et al. 1996). In this situation a mesoscale convective system was moving through east-central Oklahoma with a wake low at the back edge of the northern stratiform region (the southern portion of the system was not captured by the Oklahoma surface mesonetwork). A mesohigh was within the region of heaviest rainfall with a wake low immediately to the rear of the precipitation band. The most intense pressure gradient appeared to "hug" the back edge of the stratiform rain area, consistent with the findings of Johnson and Hamilton (1988), Stumpf et al. (1991), and Loehrer and Johnson (1995). The most intense wake low was at the far southern boundary of the surface network and therefore could not be fully resolved. Nevertheless, the portion that was resolved revealed a pressure gradient exceeding 5 mb $(20\ km)^{-1}$ (a corresponding surface pressure fall of 10 mb in 20 min!). Five-minute average surface winds within this intense gradient were 18.4 m s^{-1} from 092°, with a peak gust of 23.7 m s^{-1}. In some cases, as a result of reduced friction, strong and damaging winds may develop in the vicinity of wake lows that pass over open water areas or smooth terrain (Ely 1982). In addition, the low-level wind shear in the wake low region represents a significant aviation hazard. Recently, Meuse et al. (1996) reported that strong low-level wind shear near the back edge of the trailing stratiform region of a squall line nearly caused an airline crash on 12 April 1996 at the Dallas–Fort Worth International Airport. While the linear theory of Haertel and Johnson (2000) can explain the general structure of the mesohigh–wake low couplets, extreme pressure gradients such as those depicted in Fig. 3.36 are clearly influenced by nonlinear effects (e.g. rapidly descending rear inflow jets).

3.6. Conclusions and outlook

Thirty-five years ago, Byers and Atlas (1963) noted that "The last decade has seen the birth of mesometeorology and with it a vast improvement in visualization of the small-scale circulations which are both the cause and effect of the severe local storm." In the intervening period, there has been considerable progress in identifying many of these processes, principally due to major advances in observing systems (radars, aircraft, sounding systems, mesonets, satellites) and numerical modeling. Although the sheer number of mesoscale processes has made it difficult to treat all topics thoroughly in this review, an attempt has been made to identify the main ones.

However, many questions remain.

- To what extent is the development of severe storms dependent on mesoscale conditions or initiation characteristics? How well can we observe these conditions? How well can we forecast them?

  Over the past two decades, there have been major advances in understanding the basic mechanisms for severe storms through observational studies and idealized numerical simulations. Despite this progress, forecasting severe storms remains a major challenge. Much of the difficulty stems from mesoscale processes inadequately observed and not fully understood. Rapid advances in observing technologies in recent years—for example, wind profilers, surface and airborne Doppler radars, and Raman lidars (measuring humidity profiles)—have greatly enhanced our capability of observing the environment of severe storms. For practical reasons, most past field experiments have focused on developing or mature storms. Perhaps now we have the resources to tackle the convective initiation problem in a major way. Moreover, since mesoscale prediction models have advanced considerably, research resources could be targeted by the use of forecasts. Of course, resources will always be limited, so decisions need to be made about the balance between case

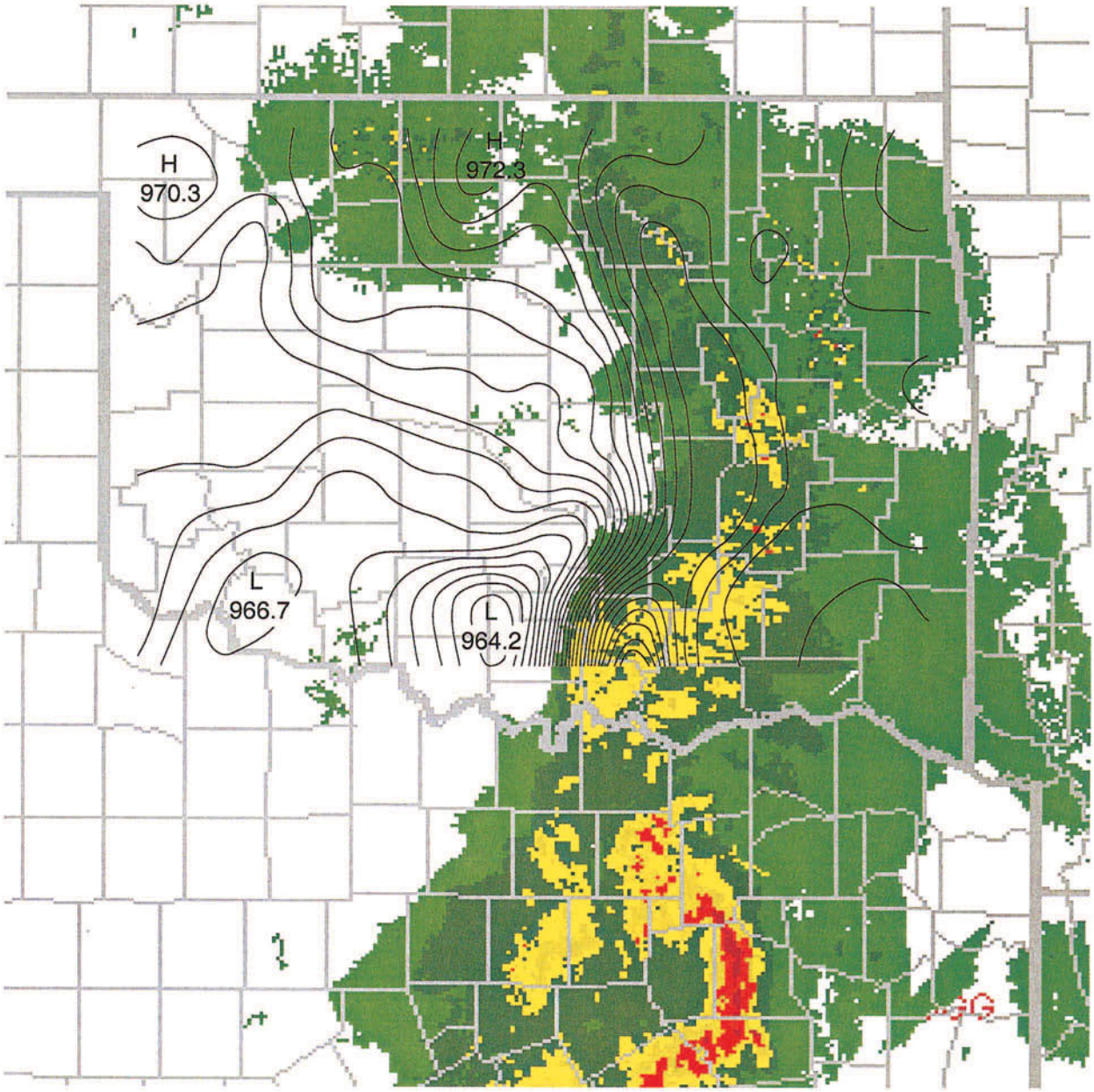

FIG. 3.36. Example of intense mesohigh–wake low couplet. Base-scan radar reflectivity at 0210 UTC 6 May 1995 over Oklahoma (thick state outline). Colors correspond to reflectivity thresholds of 18, 30, 41, 46, and 50 dBZ. Pressure field at 0.5-mb intervals is analyzed at 390 m (the mean station elevation) and is based on time-to-space conversion of 5-min Oklahoma mesonet data. From Johnson et al. (1996).

study and statistical approaches. And an optimum balance between precision and coverage of measurement resources must be determined.

- What are the important triggering mechanisms for different types of severe convective weather and what is their frequency distribution?

  Climatologies of triggering mechanisms for severe weather are virtually nonexistent, largely as a result of inadequate measurements. However, with the recently deployed NWS WSR-88D Doppler radar network, and with other research radars and profilers having sufficient sensitivity to measure boundary layer properties, perhaps some headway could be made on this problem. One approach would be to extend the climatologies of mature-phase severe storms back to the initial stages of development. Also, it would be valuable to survey climatologies of all convection for clues as to why only a small fraction becomes severe.

- How do storms modify their local environment? What processes contribute to the enhancement of convection? To its decay?

  Here again, new measurement technologies will help, but an emphasis on modeling is also suggested. What types of modeling are right or wrong for answering these questions? For example, do storm models need to be run for a longer time, to be less initial condition dependent? Can more sophisticated decompositions of model data, such as into balanced versus unbalanced components, teach us more about the mechanisms at work? Or is complexity of analysis already too great, so that simple robust analyses applied to more cases would be more enlightening?
- In what ways do mesoscale processes (jets, topography, etc.) control the geographical distribution and diurnal variability of severe weather?

  With the advent of the NWS WSR-88D and wind profiler networks, it will be possible within several years to construct meaningful climatologies of severe weather in relation to mesoscale features such as jets, drylines, topography, boundary intersections, and so forth. The mechanisms by which such features control severe storm development will inevitably be exposed by field campaigns and modeling studies.
- What are the main factors in storm severity, propagation, and longevity?

  Many severe storms are unanticipated by forecasters. In addition, there are numerous instances where severe and nonsevere storms develop in the same large-scale environment. How does this happen? Some of the processes are already understood. Numerical simulations by Weisman, Klemp, and others have shown that convective evolution for a given shear profile naturally results in a variety of convective structures, ranging from symmetric splitting storms, preferred right- or left-movers, multicellular development, and so forth. However, in many instances variability can also be attributed to mesoscale effects.

  CAPE and wind shear are obviously first-order factors in storm severity; however, these parameters are ordinarily determined from the synoptic-scale sounding network. A serious challenge is that the growth of storms to severity is often influenced by mesoscale effects, which are not sampled by the operational large-scale network. For example, water vapor, surface conditions, the low-level wind field, and so forth, are known to vary significantly in the mesoscale environment of storms. Cases of differing storm evolution in the same large-scale environment are deserving of thorough study, both from observational and modeling perspectives. The real-time mesoscale modeling now under way in many U.S. universities and research laboratories may be of great help in this matter since in many cases those models are designed to capture regional/mesoscale datasets that otherwise would be lost. Data rejection experiments may be useful in determining the most important factors in storm severity. Of course, in addition to severity, the track, time of formation, and longevity of storms are all important issues and the above approaches should be applied to them too.
- What are the mechanisms for heavy rainfall and flash floods and how can they be better forecast?

  Heavy rainfall is the leading cause of convective weather-related fatalities, yet skillful forecasting of floods remains elusive. Floods generally occur when storms repeatedly form or move over the same area and new cell development is often influenced by complex triggering processes involving interaction of outflow boundaries with terrain or other mesoscale features. Mesoscale models hold some promise for improving flash flood forecasting, but limitations in initialization and data assimilation on the mesoscale will undoubtedly make progress slow. Significant improvements in measuring heavy rainfall from the WSR-88D radar network will necessarily involve the implementation of multiparameter measurements from those radars.
- What factors control the upscale growth of convection? Why do some MCSs develop bow echoes, mesovortices, rear inflows, and so forth, and others not?

  These questions are currently being addressed by modeling studies. As capabilities advance, further modeling studies are inevitable; however, it should be emphasized that many of the processes are sufficiently complex to demand rather sophisticated diagnostic analysis of model results. Major efforts will have to be put into diagnostic analyses and interpretation in light of theoretical considerations.

In summary, while we are beginning to get answers to these questions, much work is yet to be done. The NWS modernization (WSR-88D radars, wind profilers, etc.) will help, but focused field campaigns, such as those anticipated in connection with the U.S. Weather Research Program (USWRP), will be necessary to provide adequate data to study remaining key issues. Advances in theory and numerical modeling will also be essential to make significant strides on these problems.

Acknowledgments. This research has been supported by the National Science Foundation under Grant ATM-9618684 (RJ) and by the National Oceanographic and Atmospheric Administration's Office of Global Programs (BM). The comments of Kerry Emanuel, Mike Fritsch, Dave Parsons, Morris Weis-

man, and Da-Lin Zhang have significantly improved the manuscript.

REFERENCES

Agee, E. M., 1984: Observations from space and thermal convection: A historical perspective. *Bull. Amer. Meteor. Soc.,* **65,** 938–949.

Angevine, W. M., A. W. Grimsdell, L. M. Hartten, and A. C. Delany, 1998: The Flatland boundary layer experiments. *Bull. Amer. Meteor. Soc.,* **79,** 419–431.

Anthes, R. A., 1984: Enhancement of convective precipitation by mesoscale variations in vegetative covering in semiarid regions. *J. Climate Appl. Meteor.,* **23,** 541–554.

Arritt, R. W., T. D. Rink, M. Segal, D. P. Todey, C. A. Clark, M. J. Mitchell, and K. M. Labas, 1997: The Great Plains low-level jet during the warm season of 1993. *Mon. Wea. Rev.,* **125,** 2176–2192.

Asai, T., 1970: Thermal instability of a plane parallel flow with variable vertical shear and unstable stratification. *J. Meteor. Soc. Japan,* **48,** 129–139.

Atkins, N. T., R. M. Wakimoto, and T. M. Weckwerth, 1995: Observations of the sea-breeze front during CaPE. Part II: Dual-Doppler and aircraft analysis. *Mon. Wea. Rev.,* **123,** 944–969.

———, ———, and C. L. Ziegler, 1998: Observations of the finescale structure of a dryline during VORTEX 95. *Mon. Wea. Rev.,* **126,** 525–550.

Atlas, D., 1960: Radar detection of the sea breeze. *J. Meteor.,* **17,** 244–258.

———, R. Tatehira, R. C. Srivastava, W. Marker, and R. E. Carbone, 1969: Precipitation-induced mesoscale wind perturbations in the melting layer. *Quart. J. Roy. Meteor. Soc.,* **95,** 544–560.

Balachandran, N. K., 1980: Gravity waves from thunderstorms. *Mon. Wea. Rev.,* **108,** 804–816.

Balaji, V., and T. L. Clark, 1988: Scale selection in locally forced convective fields and the initiation of deep cumulus. *J. Atmos. Sci.,* **45,** 3188–3211.

Banta, R. M., 1990: The role of mountain flows in making clouds. *Atmospheric Processes over Complex Terrain, Meteor. Monogr.,* No. 45, Amer. Meteor. Soc., 229–283.

Barcilon, A. I., and P. G. Drazin, 1972: Dust devil formation. *Geophys. Fluid Dyn.,* **4,** 147–158.

Barnes, S. L., 1978: Oklahoma thunderstorms on 29–30 April 1970. Part I: Morphology of a tornadic storm. *Mon. Wea. Rev.,* **106,** 673–684.

Bartels, D. L., and R. A. Maddox, 1991: Midlevel cyclonic vortices generated by mesoscale convective systems. *Mon. Wea. Rev.,* **119,** 104–118.

Barth, M. C., and D. B. Parsons, 1996: Microphysical processes associated with intense frontal rainbands and the effect of evaporation and melting on frontal dynamics. *J. Atmos. Sci.,* **53,** 1569–1586.

Beebe, R. G., and F. C. Bates, 1955: A mechanism for assisting in the release of convective instability. *Mon. Wea. Rev.,* **83,** 1–10.

Belair, S., and D.-L. Zhang, 1997: A numerical study of the along-line variability of a frontal squall line during PRE-STORM. *Mon. Wea. Rev.,* **125,** 2544–2561.

Bennetts, D. A., and B. J. Hoskins, 1979: Conditional symmetric instability—A possible explanation for frontal rainbands. *Quart. J. Roy. Meteor. Soc.,* **105,** 945–962.

Bernstein, B. C., and R. H. Johnson, 1994: A dual-Doppler radar study of an OK PRE-STORM heat burst event. *Mon. Wea. Rev.,* **122,** 259–273.

Biggerstaff, M. I., and R. A. Houze Jr., 1991: Kinematic and precipitation structure of the 10–11 June 1985 squall line. *Mon. Wea. Rev.,* **119,** 3034–3065.

Blackadar, A. K., 1957: Boundary-layer wind maxima and their significance for the growth of nocturnal inversions. *Bull. Amer. Meteor. Soc.,* **38,** 283–290.

Blanchard, D. O., and K. W. Howard, 1986: The Denver hailstorm of 13 June 1984. *Bull. Amer. Meteor. Soc.,* **67,** 1123–1131.

———, W. R. Cotton, and J. M. Brown, 1998: Mesoscale circulation growth under conditions of weak inertial instability. *Mon. Wea. Rev.,* **126,** 118–140.

Bluestein, H. B., 1993: *Synoptic-Dynamic Meteorology in Midlatitudes.* Vol. II, Oxford Press, 594 pp.

———, and K. W. Thomas, 1984: Diagnosis of a jet streak in the vicinity of a severe weather outbreak in the Texas panhandle. *Mon. Wea. Rev.,* **112,** 2499–2520.

———, and G. R. Woodall, 1990: Doppler-radar analysis of a low-precipitation (LP) severe storm. *Mon. Wea. Rev.,* **118,** 1640–1664.

———, and S. Parker, 1993: Modes of isolated convective storm formation along the dryline. *Mon. Wea. Rev.,* **121,** 1354–1372.

———, and T. Hutchinson, 1996: Convective-storm initiation and organization near the intersection of a cold front and the dryline. Preprints, *Seventh Conf. on Mesoscale Processes,* Reading, UK, Amer. Meteor. Soc., 41–43.

———, E. W. McCaul Jr., G. P. Byrd, and G. R. Woodall, 1988: Mobile sounding observations of a tornadic storm near the dryline: The Canadian, Texas storm of 7 May 1986. *Mon. Wea. Rev.,* **116,** 1790–1804.

Bonner, W. D., 1966: Case study of thunderstorm activity in relation to the low-level jet. *Mon. Wea. Rev.,* **94,** 167–178.

Booker, D. R., 1963: Modification of convective storms by lee waves. *Severe Local Storms, Meteor. Monogr.,* No. 27, Amer. Meteor. Soc., 129–140.

Bosart, L. F., and F. Sanders, 1981: Johnstown flood of July 1977: A long-lived convective system. *J. Atmos. Sci.,* **38,** 1616–1642.

———, and A. Seimon, 1988: Case study of an unusually intense atmospheric gravity wave. *Mon. Wea. Rev.,* **116,** 1857–1886.

Brady, R. H., and E. J. Szoke, 1989: A case study of nonmesocyclone tornado development in northeast Colorado: Similarities to waterspout formation. *Mon. Wea. Rev.,* **117,** 843–856.

Brandes, E. A., 1978: Mesocyclone evolution and tornadogenesis: Some observations. *Mon. Wea. Rev.,* **106,** 995–1011.

———, 1984a: Relationships between radar-derived thermodynamic variables and tornadogenesis. *Mon. Wea. Rev.,* **112,** 1033–1052.

———, 1984b: Vertical vorticity generation and mesocyclone sustenance in tornadic thunderstorms: The observational evidence. *Mon. Wea. Rev.,* **112,** 2253–2269.

Braun, S. A., and R. A. Houze Jr., 1997: The evolution of the 10–11 June 1985 PRE-STORM squall line: Initiation, development of rear inflow, and dissipation. *Mon. Wea. Rev.,* **125,** 478–504.

Bretherton, C. S., 1993: The nature of adjustment in cumulus cloud fields. *The Representation of Cumulus Convection in Numerical Models,* K. A. Emanuel and D. J. Raymond, Eds., Amer. Meteor. Soc., 63–74.

———, and P. K. Smolarkiewicz, 1989: Gravity waves, compensating subsidence and detrainment around cumulus clouds. *J. Atmos. Sci.,* **46,** 740–759.

Brown, J. M., K. R. Knupp, and F. Caracena, 1982: Destructive winds from shallow, high-based cumulonimbus. Preprints, *12th Conf. on Severe Local Storms,* San Antonio, TX, Amer. Meteor. Soc., 272–275.

Brown, R. A., 1980: Longitudinal instabilities and secondary flows in the planetary boundary layer: A review. *Rev. Geophys. Space Phys.,* **18,** 683–697.

Browning, K. A., and T. W. Harrold, 1970: Air motion and precipitation growth at a cold front. *Quart. J. Roy. Meteor. Soc.,* **96,** 369–389.

———, and C. W. Pardoe, 1973: Structure of low-level jet streams ahead of mid-latitude cold fronts. *Quart. J. Roy. Meteor. Soc.,* **99,** 619–638.

———, and G. A. Monk, 1982: Simple model for the synoptic analysis of cloud fronts. *Quart. J. Roy. Meteor. Soc.,* **108,** 435–452.

———, and Coauthors, 1976: Structure of an evolving hailstorm, Part V: Synthesis and implications for hail growth and hail suppression. *Mon. Wea. Rev.,* **104,** 603–610.

Burgess, D., V. Wood, and R. Brown, 1982: Mesocyclone evolution statistics. Preprints, *12th Conf. on Severe Local Storms,* San Antonio, TX, Amer. Meteor. Soc., 422–424.

Byers, H. R., and H. R. Rodebush, 1948: Causes of thunderstorms of the Florida peninsula. *J. Meteor.,* **5,** 275–280.

———, and R. R. Braham Jr., 1949: *The Thunderstorm.* U.S. Government Printing Office, 287 pp.

———, and D. Atlas, 1963: Severe local storms: In retrospect. *Severe Local Storms, Meteor. Monogr.,* No. 27, Amer. Meteor. Soc., 242–247.

Caracena, F., and J. M. Fritsch, 1983: Focusing mechanisms in the Texas Hill Country flash floods of 1978. *Mon. Wea. Rev.,* **111,** 2319–2332.

———, R. A. Maddox, L. R. Hoxit, and C. F. Chappell, 1979: Mesoanalysis of the Big Thompson storm. *Mon. Wea. Rev.,* **107,** 1–17.

Carbone, R. E., 1982: A severe frontal rainband. Part I: Stormwide hydrodynamic structure. *J. Atmos. Sci.,* **39,** 258–279.

———, 1983: A severe frontal rainband. Part II: Tornado parent vortex circulation. *J. Atmos. Sci.,* **40,** 2639–2654.

———, J. W. Conway, N. A. Crook, and M. W. Moncrieff, 1990: The generation and propagation of a nocturnal squall line. Part I: Observations and implications for mesoscale predictability. *Mon. Wea. Rev.,* **118,** 26–49.

Carlson, T. N., and F. H. Ludlam, 1968: Conditions for the occurrence of severe local storms. *Tellus,* **20,** 203–226.

———, S. G. Benjamin, G. S. Forbes, and Y.-F. Li, 1983: Elevated mixed layers in the regional severe storm environment: Conceptual model and case studies. *Mon. Wea. Rev.,* **111,** 1453–1473.

Carr, F. H., and J. P. Millard, 1985: Composite study of comma clouds and their association with severe weather over the Great Plains. *Mon. Wea. Rev.,* **113,** 370–387.

Carruthers, D. J., and J. C. R. Hunt, 1990: Fluid mechanics of airflow over hills: Turbulence, fluxes, and waves in the boundary layer. *Atmospheric Processes over Complex Terrain, Meteor. Monogr.,* No. 45, Amer. Meteor. Soc., 83–103.

Chang, J.-T., and P. J. Wetzel, 1991: Effects of spatial variations of soil moisture and vegetation on the evolution of a prestorm environment: A numerical case study. *Mon. Wea. Rev.,* **119,** 1368–1390.

Changnon, S. A., R. G. Semonin, and F. A. Huff, 1976: A hypothesis for urban rainfall anomalies. *J. Appl. Meteor.,* **15,** 544–560.

Chappell, C. F., 1986: Quasi-stationary convective events. *Mesoscale Meteorology and Forecasting,* P. S. Ray, Ed., Amer. Meteor. Soc., 289–310.

Charba, J., 1974: Application of the gravity current model to analysis of squall-line gust fronts. *Mon. Wea. Rev.,* **102,** 140–156.

Charney, J. G., 1975: Dynamics of deserts and drought in the Sahel. *Quart. J. Roy. Meteor. Soc.,* **101,** 193–202.

———, and A. Eliassen, 1964: On the growth of the hurricane depression. *J. Atmos. Sci.,* **21,** 68–75.

Chen, S., and W. R. Cotton, 1988: The sensitivity of a simulated extratropical mesoscale convective system to longwave radiation and ice-phase microphysics. *J. Atmos. Sci.,* **45,** 3897–3910.

Christian, T. W., and R. M. Wakimoto, 1989: The relationship between radar reflectivities and clouds associated with horizontal roll convection on 8 August 1982. *Mon. Wea. Rev.,* **117,** 1530–1544.

Christie, D. R., 1992: The morning glory of the Gulf of Carpenteria: A paradigm for nonlinear waves in the lower atmosphere. *Austr. Meteor. Mag.,* **41,** 21–60.

Ciesielski, P. E., D. E. Stevens, R. H. Johnson, and K. R. Dean, 1989: Observational evidence for asymmetric inertial instability. *J. Atmos. Sci.,* **46,** 817–831.

Clarke, R. H., 1972: The morning glory: an atmospheric hydraulic jump. *J. Appl. Meteor.,* **11,** 304–311.

———, 1984: Colliding sea breezes and the creation of internal atmospheric bore waves: two dimensional numerical studies. *Austr. Meteor. Mag.,* **32,** 207–226.

Colby, F. P., Jr., 1984: Convective inhibition as a predictor of convection during AVE-SESAME II. *Mon. Wea. Rev.,* **112,** 2239–2252.

Collins, D. C., and R. Avissar, 1994: An evaluation with the Fourier Amplitude Sensitivity Test (FAST) of which land-surface parameters are of greatest importance in atmospheric modeling. *J. Climate,* **7,** 681–703.

Colman, B. R., 1990: Thunderstorms above frontal surfaces in environments without positive CAPE. Part II: Organization and instability mechanisms. *Mon. Wea. Rev.,* **118,** 1123–1144.

Crook, N. A., 1986: The effect of ambient stratification and moisture on the motion of atmospheric undular bores. *J. Atmos. Sci.,* **43,** 171–181.

———, 1987: Moist convection at a surface cold front. *J. Atmos. Sci.,* **44,** 3469–3494.

———, 1988: Trapping of low-level internal gravity waves. *J. Atmos. Sci.,* **45,** 1533–1541.

———, 1996: Sensitivity of moist convection forced by boundary layer processes to low-level thermodynamic fields. *Mon. Wea. Rev.,* **124,** 1767–1785.

———, and J. D. Tuttle, 1994: Numerical simulations initialized with radar-derived winds. Part II: Forecasts of three gust-front cases. *Mon. Wea. Rev.,* **122,** 1204–1217.

———, T. L. Clark, and M. W. Moncrieff, 1990a: The Denver Cyclone. Part I: Generation in low Froude number flow. *J. Atmos. Sci.,* **47,** 2725–2742.

———, R. E. Carbone, M. W. Moncrieff, and J. W. Conway, 1990b: The generation and propagation of a nocturnal squall line. Part II: Numerical simulations. *Mon. Wea. Rev.,* **118,** 50–65.

Curry, M. J., and R. C. Murty, 1974: Thunderstorm-generated gravity waves. *J. Atmos. Sci.,* **31,** 1402–1408.

Cutrim, E., D. W. Martin, and R. Rabin, 1995: Enhancement of cumulus clouds over deforested lands in Amazonia. *Bull. Amer. Meteor. Soc.,* **76,** 1801–1805.

Danielsen, E. F., 1974: The relationship between severe weather, major duststorms, and rapid large-scale cyclogenesis. Part I. *Subsynoptic Extratropical Weather Systems,* M. Shapiro, Ed., National Center for Atmospheric Research, 215–241.

———, 1982: Statistics of cold cumulonimbus anvils based on enhanced infrared photographs. *Geophys. Res. Lett.,* **9,** 601–604.

Davies-Jones, R. P., 1984: Streamwise vorticity: The origin of updraft rotation in supercell storms. *J. Atmos. Sci.,* **41,** 2991–3006.

———, 1986: Tornado dynamics. *Thunderstorms: A Social and Technological Documentary,* 2d ed., Vol. II, E. Kessler, Ed. University of Oklahoma Press, 197–236.

Davis, C. A., 1997: Mesoscale anticyclonic circulations in the lee of the central Rocky Mountains. *Mon. Wea. Rev.,* **125,** 2838–2855.

———, and M. L. Weisman, 1994: Balanced dynamics of mesoscale vortices produced in simulated convective systems. *J. Atmos. Sci.,* **51,** 2005–2030.

Dempsey, D. P., and R. Rotunno, 1988: Topographic generation of mesoscale vortices in mixed layer models. *J. Atmos. Sci.,* **45,** 2961–2978.

Dinwiddie, F. B., 1959: Waterspout-tornado structure and behavior at Nags Head, N.C., August 12, 1952. *Mon. Wea. Rev.,* **87,** 239–250.

Doswell, C. A., III, 1980: Synoptic-scale environments associated with High Plains severe thunderstorms. *Bull. Amer. Meteor. Soc.,* **61,** 1388–1400.

———, 1987: The distinction between large-scale and mesoscale contribution to severe convection: A case study example. *Wea. Forecasting,* **2,** 3–16.

Doviak, R. J., and R. Ge, 1984: An atmospheric solitary gust observed with a Doppler radar, a tall tower and a surface network. *J. Atmos. Sci.,* **41,** 2559–2573.

Droegemeier, K. K., and R. B. Wilhelmson, 1985: Three-dimensional numerical modeling of convection produced by interacting outflows. Part II: Variations in vertical wind shear. *J. Atmos. Sci.,* **42,** 2404–2414.

Drosdowsky, W., and G. J. Holland, 1987: North Australian cloud lines. *Mon. Wea. Rev.,* **115,** 2645–2659.

Dudhia, J., 1989: Numerical study of convection observed during the Winter Monsoon Experiment using a mesoscale two-dimensional model. *J. Atmos. Sci.,* **46,** 3077–3107.

Ely, G. F., 1982: Case study of a significant thunderstorm wake depression along the Texas coast: May 29–30 1981. NOAA Tech. Memo NWS SR-105, 64 pp.

Emanuel, K. A., 1979: Inertial instability and mesoscale convective systems. Part I: Linear theory of inertial instability in rotating viscous fluid. *J. Atmos. Sci.,* **36,** 2425–2449.

———, 1980: Forced and free mesoscale motions in the atmosphere. *CIMMS Symp. Collection of Lecture Notes on Dynamics of Mesometeorological Disturbances*, Norman, OK, University of Oklahoma/NOAA, 189–259.

———, 1983: The Lagrangian parcel dynamics of moist symmetric instability. *J. Atmos. Sci.,* **40,** 2368–2376.

———, 1985: Frontal circulations in the presence of small moist symmetric stability. *J. Atmos. Sci.,* **42,** 1062–1071.

———, 1986: Overview and definition of mesoscale meteorology. *Mesoscale Meteorology and Forecasting,* P. S. Ray, Ed., Amer. Meteor. Soc., 1–17.

———, 1994: *Atmospheric Convection.* Oxford Press, 580 pp.

Esbensen, S., 1978: Bulk thermodynamic effects and properties of small tropical cumuli. *J. Atmos. Sci.,* **35,** 826–837.

Etling, D., and R. A. Brown, 1993: Roll vortices in the planetary boundary layer: a review. *Bound.-Layer Meteor.,* **65,** 215–248.

Fankhauser, J. C., N. A. Crook, J. Tuttle, and C. G. Wade, 1995: Initiation of deep convection along boundary-layer convergence lines in a semitropical environment. *Mon. Wea. Rev.,* **123,** 291–313.

Fovell, R., and Y. Ogura, 1988: Numerical simulation of a midlatitude squall line in two dimensions. *J. Atmos. Sci.,* **45,** 3846–3879.

———, and ———, 1989: Effect of vertical wind shear on numerically simulated multicell storm structure. *J. Atmos. Sci.,* **46,** 3144–3176.

———, D. Durran, and J. R. Holton, 1992: Numerical simulations of convectively generated stratospheric gravity waves. *J. Atmos. Sci.,* **49,** 1427–1442.

Fritsch, J. M., and R. A. Maddox, 1981: Convectively driven mesoscale pressure systems aloft. Part I: Observations. *J. Appl. Meteor.,* **20,** 9–19.

———, and D. M. Rodgers, 1981: Ft. Collins hailstorm: An example of the short-term forecast enigma. *Bull. Amer. Meteor. Soc.,* **62,** 1560–1569.

———, J. Kapolka, and P. A. Hirschberg, 1992: The effects of subcloud-layer diabatic processes on cold air damming. *J. Atmos. Sci.,* **49,** 49–70.

———, J. D. Murphy, and J. S. Kain, 1994: Warm core vortex amplication over land. *J. Atmos. Sci.,* **51,** 1780–1807.

Fujita, T. T., 1955: Results of detailed synoptic studies of squall lines. *Tellus,* **7,** 405–436.

———, 1958: Structure and movement of a dry front. *Bull. Amer. Meteor. Soc.,* **39,** 574–582.

———, 1963: Analytical mesometeorology: A review. *Severe Local Storms, Meteor. Monogr.,* No. 27, Amer. Meteor. Soc., 77–125.

———, 1978: Manual of downburst identification for project NIMROD. SMRP Research Paper 156, University of Chicago, 42 pp.

———, 1981: Tornadoes and downbursts in the context of generalized planetary scales. *J. Atmos. Sci.,* **38,** 1511–1534.

———, and F. Caracena, 1977: Analysis of three weather-related aircraft accidents. *Bull. Amer. Meteor. Soc.,* **58,** 1164–1181.

Fulton, R., D. S. Zrnić, and R. J. Doviak, 1990: Initiation of a solitary wave family in the demise of a nocturnal thunderstorm density current. *J. Atmos. Sci.,* **47,** 319–337.

Gentry, R. C., and P. L. Moore, 1954: Relation of local and general wind interaction near the sea coast to time and location of air-mass showers. *J. Meteor.,* **11,** 507–511.

Gill, A. E., 1982: *Atmosphere-Ocean Dynamics.* Academic Press, 662 pp.

Gilmore, M. S., and L. J. Wicker, 1998: The influence of midtropospheric dryness on supercell morphology and evolution. *Mon. Wea. Rev.,* **126,** 943–958.

Golden, J. H., 1973: Some statistical aspects of waterspout formation. *Weatherwise,* **26,** 108–117.

———, 1974: Scale-interaction implications for the waterspout life cycle. II. *J. Appl. Meteor.,* **13,** 693–709.

———, 1978: Picture of the month: Jet aircraft flying through a Denver tornado? *Mon. Wea. Rev.,* **106,** 574–578.

Grady, R.L., and J. Verlinde, 1997: Triple-Doppler analysis of a discretely propagating, long-lived, High Plains squall line. *J. Atmos. Sci.,* **54,** 2729–2748.

Gray, W. M., and R. W. Jacobson, Jr., 1977: Diurnal variation of deep cumulus convection. *Mon. Wea. Rev.,* **105,** 1171–1188.

Graziano, T. M., and T. N. Carlson, 1987: A statistical evaluation of lid strength on deep convection. *Wea. Forecasting,* **2,** 127–139.

Gurka, J. J., 1976: Satellite and surface observations of strong wind zones accompanying thunderstorms. *Mon. Wea. Rev.,* **104,** 1484–1493.

Haase, S. P., and R. K. Smith, 1984: Morning glory wave clouds in Oklahoma: A case study. *Mon. Wea. Rev.,* **112,** 2078–2089.

Haertel, P. T., and R. H. Johnson, 2000: The linear dynamics of squall-line mesohighs and wake lows. *J. Atmos. Sci.,* **57,** 93–107.

Hagemeyer, B. C., 1984: An investigation of summertime convection over the Upper Current River Valley of Southwest Missouri. NOAA Tech. Memo. NWS CR-71, 35 pp.

Hane, C. E., H. B. Bluestein, T. M. Crawford, M. E. Baldwin, and R. M. Rabin, 1997: Severe thunderstorm development in relation to along-dryline variability: A case study. *Mon. Wea. Rev.,* **125,** 231–251.

Hauf, T., 1993: Aircraft observation of convection waves over southern Germany—A case study. *Mon. Wea. Rev.,* **121,** 3282–3290.

Hertenstein, R. F. A., and W. H. Schubert, 1991: Potential vorticity anomalies associated with squall lines. *Mon. Wea. Rev.,* **116,** 1663–1672.

Heymsfield, G. M., and R. Fulton, 1994: Passive microwave and visible/infrared structure of mesoscale precipitation systems. *Meteor. Atmos. Phys.,* **54,** 123–139.

Holton, J. R., 1967: The diurnal boundary-layer wind oscillation above sloping terrain. *Tellus,* **19,** 199–205.

Houze, R. A., Jr., 1993: *Cloud Dynamics.* Academic Press, 573 pp.

———, 1997: Stratiform precipitation in regions of convection: A meteorological paradox? *Bull. Amer. Meteor. Soc.,* **78,** 2179–2196.

———, S. G. Geotis, F. D. Marks, and A. K. West, 1981: Winter monsoon convection in the vicinity of north Borneo. Part I:

Structure and time variation of the clouds and precipitation. *Mon. Wea. Rev.*, **108,** 1595–1614.
———, S. A. Rutledge, M. I. Biggerstaff, and B. F. Smull, 1989: Interpretation of Doppler weather radar displays of midlatitude mesoscale convective systems. *Bull. Amer. Meteor. Soc.*, **70,** 608–619.
———, B. F. Smull, and P. Dodge, 1990: Mesoscale organization of springtime rainstorms in Oklahoma. *Mon. Wea. Rev.*, **118,** 613–654.
———, W. Schmid, R. G. Fovell, and H.-H. Schiesser, 1993: Hailstorms in Switzerland: Left movers, right movers, and false hooks. *Mon. Wea. Rev.*, **121,** 3345–3370.
Hoxit, L. R., C. F. Chappell, and J. M. Fritsch, 1976: Formation of mesolows or pressure troughs in advance of cumulonimbus clouds. *Mon. Wea. Rev.*, **104,** 1419–1428.
Hsu, S. A., 1969: Mesoscale structure of the Texas coast sea breeze. Rep. 16, Atmospheric Science Group, University of Texas, 237 pp.
Hutchinson, T. A., and H. B. Bluestein, 1998: Prefrontal wind-shift lines in the Plains of the United States. *Mon. Wea. Rev.*, **126,** 141–166.
Jascourt, S. D., S. S. Lindstrom, C. J. Seman, and D. D. Houghton, 1988: Observation of banded convective development in the presence of weak symmetric stability. *Mon. Wea. Rev.*, **116,** 175–191.
Johns, R. H., 1984: Synoptic climatology of northwest flow severe weather outbreaks. Part II: Meteorological parameters and synoptic patterns. *Mon. Wea. Rev.*, **112,** 449–464.
———, 1993: Meteorological conditions associated with bow echo development in convective storms. *Wea. Forecasting,* **8,** 294–299.
———, and W. D. Hirt, 1985: The derecho of 19–20 July 1983: A case study. *Natl. Wea. Dig.*, **10,** 17–32.
———, and ———, 1987: Derechos: Widespread convectively induced windstorms. *Wea. Forecasting,* **2,** 32–49.
———, and C. A. Doswell III, 1992: Severe local storms forecasting. *Wea. Forecasting,* **7,** 588–612.
Johnson, B. C., 1983: The heat burst of 29 May 1976. *Mon. Wea. Rev.*, **111,** 1776–1792.
Johnson, R. H., and P. J. Hamilton, 1988: The relationship of surface pressure features to the precipitation and air flow structure of an intense midlatitude squall line. *Mon. Wea. Rev.*, **116,** 1444–1472.
———, and D. L. Bartels, 1992: Circulations associated with a mature-to-decaying midlatitude mesoscale convective system. Part II: Upper-level features. *Mon. Wea. Rev.*, **120,** 1301–1320.
———, S. Chen, and J. J. Toth, 1989: Circulations associated with a mature-to-decaying midlatitude mesoscale convective system. Part I: Surface features—Heat bursts and mesolow development. *Mon. Wea. Rev.*, **117,** 942–959.
———, B. D. Miner, and P. E. Ciesielski, 1995: Circulations between mesoscale convective systems along a cold front. *Mon. Wea. Rev.*, **123,** 585–599.
———, E. R. Hilgendorf, and K. C. Crawford, 1996: Study of midwestern mesoscale convective systems using new operational networks. Preprints, *18th Conf. on Severe Local Storms,* San Francisco, CA, Amer. Meteor. Soc., 308–312.
Karyampudi, V. M., S. E. Koch, C. Chen, J. W. Rottman, and M. L. Kaplan, 1995: The influence of the Rocky Mountains on the 13–14 April 1986 severe weather outbreak. Part II: Evolution of a prefrontal bore and its role in triggering a squall line. *Mon. Wea. Rev.*, **123,** 1423–1446.
Keenan, T. D., B. R. Morton, Y. S. Zhang, and K. Nyguen, 1990: Some characteristics of thunderstorms over Bathurst and Melville Islands near Darwin, Australia. *Quart. J. Roy. Meteor. Soc.*, **116,** 1153–1172.
———, B. Ferrier, and J. Simpson, 1993: Development and structure of a maritime continent thunderstorm. *Meteor. Atmos. Phys.*, **53,** 185–222.
Keyser, D., and M. A. Shapiro, 1986: A review of the structure and dynamics of upper-level frontal zones. *Mon. Wea. Rev.*, **114,** 452–499.
King, P., and D. M. L. Sills, 1998: The 1987 ELBOW Project: An experiment to study the effects of lake breezes on weather in southern Ontario. Preprints, *19th Conf. on Severe Local Storms,* Minneapolis, MN, Amer. Meteor. Soc., 317–320.
Kingsmill, D. E., 1995: Convection initiation associated with a sea-breeze front, a gust front, and their collision. *Mon. Wea. Rev.*, **123,** 2913–2933.
Klemp, J. B., 1987: Dynamics of tornadic thunderstorms. *Ann. Rev. Fluid Mech.*, **19,** 369–402.
———, and R. Rotunno, 1983: A study of the tornadic region within a supercell thunderstorm. *J. Atmos. Sci.*, **40,** 359–377.
Klimowski, B. A., 1994: Initiation and development of rear inflow within the 28–29 June 1989 North Dakota mesoconvective system. *Mon. Wea. Rev.*, **122,** 765–779.
Knox, J. A., 1997: Possible mechanisms of clear-air turbulence in strongly anticyclonic flows. *Mon. Wea. Rev.*, **125,** 1251–1259.
Koch, S. E., and J. McCarthy, 1982: The evolution of a Oklahoma dryline. Part II: Boundary-layer forcing of mesoconvective systems. *J. Atmos. Sci.*, **39,** 237–257.
———, and P. B. Dorian, 1988: A mesoscale gravity wave event observed during CCOPE. Part III: Wave environment and probable source mechanisms. *Mon. Wea. Rev.*, **116,** 2570–2592.
———, and R. E. Golus, 1988: A mesoscale gravity wave event observed during CCOPE. Part I: Multiscale statistical analysis of wave characteristics. *Mon. Wea. Rev.*, **116,** 2527–2544.
———, and L. M. Siedlarz, 1999: Mesoscale gravity waves and their environment in the central United States during STORM-FEST. *Mon. Wea. Rev.*, **127,** 2854–2879.
———, R. E. Golus, and P. B. Dorian, 1988: A mesoscale gravity wave event observed during CCOPE. Part II: Interactions between mesoscale convective systems and antecedent waves. *Mon. Wea. Rev.*, **116,** 2545–2569.
———, F. Einaudi, P. B. Dorian, S. Lang, and G. M. Heymsfield, 1993: Mesoscale gravity-wave event observed during CCOPE. Part IV: Stability analysis and Doppler-derived wave vertical structure. *Mon. Wea. Rev.*, **121,** 2483–2510.
Kocin, P. J., L. W. Uccellini, and R. A. Petersen, 1986: Rapid evolution of a jet streak circulation in a pre-convective environment. *Meteor. Atmos. Phys.*, **35,** 103–138.
Kuettner, J. P., 1959: The band structure of the atmosphere. *Tellus,* **2,** 267–294.
Kuettner, J. P., 1971: Cloud bands in the earth's atmosphere: Observations and theory. *Tellus,* **23,** 404–426.
Kuo, H. L., 1963: Perturbations of plane Couette flow in stratified fluid and origin of cloud streets. *Phys. Fluids,* **6,** 195–211.
———, L. Cheng, and R. A. Anthes, 1984: Mesoscale analyses of the Sichuan Flood catastrophe, 11–15 July 1981. *Mon. Wea. Rev.*, **114,** 1984–2003.
———, ———, and J.-W. Bao, 1988: Numerical simulation of the 1981 Sichuan Flood. Part I: Evolution of a mesoscale southwest vortex. *Mon. Wea. Rev.*, **116,** 2481–2504.
Lafore, J.-P., and M. W. Moncrieff, 1989: A numerical investigation of the organization and interaction of the convective and stratiform regions of tropical squall lines. *J. Atmos. Sci.*, **46,** 521–544.
Lanicci, J. M., T. N. Carlson, and T. T. Warner, 1987: Sensibility of the Great Plains severe storm environment to soil-moisture distribution. *Mon. Wea. Rev.*, **115,** 2660–2673.
Lee, B. D., and R. B. Wilhelmson, 1997: The numerical simulation of non-supercell tornadogenesis. Part I: Initiation and evolution of pretornadic misocyclone circulations along a dry outflow boundary. *J. Atmos. Sci.*, **54,** 32–60.
———, R. D. Farley, and M. R. Hjelmfelt, 1991: A numerical case study of convection initiation along colliding convergence boundaries in northeast Colorado. *J. Atmos. Sci.*, **48,** 2350–2366.

Lemon, L. R., and C. A. Doswell III, 1979: Severe thunderstorm evolution and meso-cyclone structure as related to tornadogenesis. *Mon. Wea. Rev.*, **107,** 1184–1197.

LeMone, M. A., 1973: The structure and dynamics of horizontal roll vortices in the planetary boundary layer. *J. Atmos. Sci.*, **30,** 1077–1091.

Lilly, D. K., 1966: On the instability of Ekman boundary flow. *J. Atmos. Sci.*, **23,** 481–494.

———, 1979: The dynamical structure and evolution of thunderstorms and squall lines. *Ann. Rev. Earth Planet. Sci.*, **7,** 117–161.

Lindzen, R. S., 1974: Wave-CISK in the tropics. *J. Atmos. Sci.*, **31,** 156–179.

———, and K.-K. Tung, 1976: Banded convective activity and ducted gravity waves. *Mon. Wea. Rev.*, **104,** 1602–1617.

Locatelli, J. D., J. E. Martin, J. A. Castle, and P. V. Hobbs, 1995: Structure and evolution of winter cyclones in the central United States and their effects on the distribution of precipitation. Part III: The development of a squall line associated with weak cold frontogenesis aloft. *J. Atmos. Sci.*, **123,** 2641–2662.

———, M. T. Stoelinga, R. D. Schwartz, and P. V. Hobbs, 1997: Surface convergence induced by cold fronts aloft and prefrontal surges. *Mon. Wea. Rev.*, **125,** 2808–2820.

Loehrer, S. M., and R. H. Johnson, 1995: Surface pressure and precipitation life cycle characteristics of PRE-STORM mesoscale convective systems. *Mon. Wea. Rev.*, **123,** 600–621.

Ludlam, F. H., 1963: Severe local storms—a review. *Severe Local Storms, Meteor. Monogr.*, No. 27, Amer. Meteor. Soc., 1–30.

Lynn, B. H., W.-K. Tao, and P. J. Wetzel, 1998: A study of landscape-generated deep moist convection. *Mon. Wea. Rev.*, **126,** 928–942.

Lyons, W. A., and J. F. Chandik, 1971: Thunderstorms and the lake breeze front. Preprints, *Seventh Conf. on Severe Local Storms,* Kansas City, MO, Amer. Meteor. Soc., 46–54.

Maddox, R. A., 1976: An evaluation of tornado proximity wind and stability data. *Mon. Wea. Rev.*, **104,** 133–142.

———, 1980: Mesoscale convective complexes. *Bull. Amer. Meteor. Soc.*, **61,** 1374–1387.

———, 1983: Large-scale meteorological conditions associated with midlatitude, mesoscale convective complexes. *Mon. Wea. Rev.*, **111,** 1475–1493.

———, and C. A. Doswell, 1982: Examination of jet stream configurations, 500-mb vorticity advection, and low-level thermal advection patterns during extended periods of intense convection. *Mon. Wea. Rev.*, **110,** 184–197.

———, L. R. Hoxit, C. F. Chappell, and F. Caracena, 1978: Comparison of meteorological aspects of the Big Thompson and Rapid City flash floods. *Mon. Wea. Rev.*, **106,** 375–389.

———, F. Canova, and L. R. Hoxit, 1980a: Meteorological characteristics of flash flood events over the western United States. *Mon. Wea. Rev.*, **108,** 1866–1877.

———, L. R. Hoxit, and C. F. Chappell, 1980b: A study of tornadic thunderstorm interactions with thermal boundaries. *Mon. Wea. Rev.*, **108,** 322–336.

———, D. J. Perkey, and J. M. Fritsch, 1981: Evolution of upper tropospheric features during the development of a mesoscale convective complex. *J. Atmos. Sci.*, **38,** 1664–1674.

Mahoney, W. P., 1988: Gust front characteristics and the kinematics associated with interacting thunderstorm outflows. *Mon. Wea. Rev.*, **116,** 1474–1491.

Mapes, B. E., 1993: Gregarious tropical convection. *J. Atmos. Sci.*, **50,** 2026–2037.

———, 1998: The large-scale part of a mesoscale convective system circulations: A linear vertical spectral band model. *J. Meteor. Soc. Japan,* **76,** 29–55.

———, and R. A. Houze Jr., 1995: Diabatic divergence profiles in western Pacific mesoscale convective systems. *J. Atmos. Sci.*, **52,** 1807–1828.

Markowski, P. M., E. N. Rasmussen, J. M. Straka, and D. C. Dowell, 1998: Observations of low-level baroclinity generated by anvil shadows. *Mon. Wea. Rev.*, **126,** 2942–2958.

Mass, C. F., 1981: Topographically forced convergence in western Washington State. *Mon. Wea. Rev.*, **109,** 1335–1347.

———, and D. P. Dempsey, 1985: One-level, mesoscale model for diagnosing surface winds in mountainous and coastal regions. *Mon. Wea. Rev.*, **113,** 1211–1227.

McAnelly, R. L., J. E. Nachamkin, W. R. Cotton, and M. E. Nicholls, 1997: Upscale evolution of MCSs: Doppler radar analysis and analytical investigation. *Mon. Wea. Rev.*, **125,** 1083–1110.

McCarthy, J., and S. E. Koch, 1982: The evolution of an Oklahoma dryline. Part I: A mesoscale and subsynoptic-scale analysis. *J. Atmos. Sci.*, **39,** 225–236.

McGinley, J. A., 1986: Nowcasting mesoscale phenomena. *Mesoscale Meteorology and Forecasting,* P. S. Ray, Ed., Amer. Meteor. Soc., 657–688.

McNider, R. T., and R. A. Pielke, 1981: Diurnal boundary layer development over sloping terrain. *J. Atmos. Sci.*, **38,** 2198–2212.

———, J. A. Song, and S. Q. Kidder, 1995: Assimilation of GOES-derived solar insolation into a mesoscale model for studies of cloud shading effects. *Int. J. Remote Sensing,* **16,** 2207–2231.

Means, L. L., 1952: On thunderstorm forecasting in the central United States. *Mon. Wea. Rev.*, **80,** 165–189.

Meuse, C., L. Galusha, M. Isaminger, M. Moore, D. Rhoda, F. Robasky, and M. Wolfson, 1996: Analysis of the 12 April 1996 wind shear incident at DFW airport. Preprints, *Workshop on Wind Shear and Wind Shear Alert Systems,* Oklahoma City, OK, Amer. Meteor. Soc., 23–33.

Miles, J. W., and L. N. Howard, 1964: Note on a heterogeneous shear flow. *J. Fluid Mech.*, **20,** 331–336.

Miller, D. A., and F. Sanders, 1980: Mesoscale conditions for the severe convection of 3 April 1974 in the east-central United States. *J. Atmos. Sci.*, **37,** 1041–1055.

Miller, R. C., 1972: Notes on Analysis and Severe-Storm Forecasting Procedures of the Air Force Global Weather Central. Tech. Rep. 200 (rev. 1975), U.S. Air Force, Air Weather Service, 190 pp.

Mitchell, M. J., R. W. Arritt, and K. Labas, 1995: A climatology of the warm season Great Plains low-level jet using wind profiler observations. *Wea. Forecasting,* **10,** 576–591.

Modahl, A. C., 1979: Low-level wind and moisture variations preceding and following hailstorms in northeast Colorado. *Mon. Wea. Rev.*, **107,** 442–450.

Moncrieff, M. W., and J. S. A. Green, 1972: The propagation and transfer properties of steady convective overturning in shear. *Quart. J. Roy. Meteor. Soc.*, **98,** 336–352.

———, and M. J. Miller, 1976: The dynamics and simulation of tropical cumulonimbus and squall lines. *Quart. J. Roy. Meteor. Soc.*, **102,** 373–394.

Moore, J. T., and G. E. VanKnowe, 1992: The effect of jet-streak curvature on kinematic fields. *Mon. Wea. Rev.*, **120,** 2429–2441.

Mueller, C. K., and R. E. Carbone, 1987: Dynamics of a thunderstorm outflow. *J. Atmos. Sci.*, **44,** 1879–1898.

Namias, J., and P. F. Clapp, 1949: Confluence theory of the high tropospheric jet stream. *J. Meteor.*, **6,** 330–336.

Neumann, J., 1951: Land breezes and nocturnal thunderstorms. *J. Meteor.*, **8,** 60–67.

Newton, C. W., 1950: Structure and mechanisms of the prefrontal squall line. *J. Meteor.*, **7,** 210–222.

———, 1963: Dynamics of severe convective storms. *Severe Local Storms, Meteor. Monogr.*, No. 27, Amer. Meteor. Soc., 33–58.

———, and H. R. Newton, 1959: Dynamical interactions between large convective clouds and environment with vertical shear. *J. Meteor.*, **16,** 483–496.

Nicholls, M. E., R. A. Pielke, and W. R. Cotton, 1991: Thermally forced gravity waves in an atmosphere at rest. *J. Atmos. Sci.,* **48,** 1869–1884.

Nieman, P. J., and R. M. Wakimoto, 1999: The interaction of a Pacific cold front with shallow air masses east of the Rocky Mountains. *Mon. Wea. Rev.,* **127,** 2102–2127.

Ogura, Y., 1963: A review of numerical modeling research on small-scale convection in the atmosphere. *Severe Local Storms, Meteor. Monogr.,* No. 27, Amer. Meteor. Soc., 65–76.

———, and Y. L. Chen, 1977: A life history of an intense mesoscale convective storm in Oklahoma. *J. Atmos. Sci.,* **34,** 1458–1476.

———, and M.-T. Liou, 1980: The structure of a midlatitude squall line: A case study. *J. Atmos. Sci.,* **37,** 553–567.

———, and D. Portis, 1982: Structure of the cold front observed in SESAME-AVE III and its comparison with the Hoskins-Bretherton frontogenesis model. *J. Atmos. Sci.,* **39,** 2773–2792.

Ookouchi, Y., M. Segal, R. C. Kessler, and R. A. Pielke, 1984: Evaluation of soil moisture effects on the generation and modification of mesoscale circulations. *Mon. Wea. Rev.,* **112,** 2281–2292.

Ooyama, K. V., 1982: Conceptual evolution of the theory and modeling of the tropical cyclone. *J. Meteor. Soc. Japan,* **60,** 369–380.

Orlanski, I., 1975: A rational subdivision of scales for atmospheric processes. *Bull. Amer. Meteor. Soc.,* **56,** 527–530.

Paegle, J., 1978: A linearized analysis of diurnal boundary layer convergence over the topography of the United States. *Mon. Wea. Rev.,* **106,** 492–502.

———, K. C. Mo, and J. Nogues-Paegle, 1996: Dependence of simulated precipitation on surface evaporation during the 1993 United States summer floods. *Mon. Wea. Rev.,* **124,** 345–361.

Pandya, R. E., and D. R. Durran, 1996: The influence of convectively generated thermal forcing on the mesoscale circulation around squall lines. *J. Atmos. Sci.,* **53,** 2924–2951.

———, ———, and C. Bretherton, 1993: Comments on "Thermally forced gravity waves in an atmosphere at rest." *J. Atmos. Sci.,* **50,** 4097–4101.

Parish, T. R., 1982: Barrier winds along the Sierra Nevada Mountains. *J. Appl. Meteor.,* **21,** 925–930.

Parsons, D. B., 1992: An explanation for intense frontal updrafts and narrow cold-frontal rainbands. *J. Atmos. Sci.,* **49,** 1810–1825.

———, C. G. Mohr, and T. Gal-Chen, 1987: Severe frontal rainband. Part III: Derived thermodynamic structure. *J. Atmos. Sci.,* **44,** 1615–1631.

———, M. A. Shapiro, R. M. Hardesty, R. J. Zamora, and J. M. Intreri, 1991: The finescale structure of a west Texas dryline. *Mon. Wea. Rev.,* **119,** 1242–1258.

Pedgley, D. E., 1962: A meso-synoptic analysis of the thunderstorms on 28 August 1958. U.K. Met Office, Geophys. Mem. 106, 74 pp.

Perry, K. D., and P. V. Hobbs, 1996: Influences of isolated cumulus clouds on the humidity of their surroundings. *J. Atmos. Sci.,* **53,** 159–174.

Petersen, W. A., L. D. Carey, S. A. Rutledge, J. C. Knievel, N. J. Doesken, R. H. Johnson, T. B. McKee, T. H. Vonder Haar, and J. F. Weaver, 1999: Mesoscale and radar observations of the Fort Collins flash flood of 28 July 1997. *Bull. Amer. Meteor. Soc.,* **80,** 191–216.

Pielke, R. A., 1974: A three-dimensional numerical model of the sea breezes over south Florida. *Mon. Wea. Rev.,* **102,** 115–139.

———, and M. Segal, 1986: Mesoscale circulations forced by differential terrain heating. *Mesoscale Meteorology and Forecasting,* P. S. Ray, Ed., Amer. Meteor. Soc., 516–548.

Pothecary, I. J. W., 1954: Short-period variations in surface pressure and wind. *Quart. J. Roy. Meteor. Soc.,* **80,** 395–401.

Preston-Whyte, R. A., 1970: Land breezes and rainfall on the Natal coast. *S. Afr. Geogr. J.,* **52,** 38–43.

Proctor, F. H., 1989: Numerical simulation of an isolated microburst. Part II: Sensitivity experiments. *J. Atmos. Sci.,* **46,** 2143–2165.

Przybylinski, R. W., 1995: The bow echo: Observations, numerical simulations, and severe weather detection methods. *Wea. Forecasting,* **10,** 203–218.

———, and D. M. DeCaire, 1985: Radar signatures associated with the derecho, a type of mesoscale convective system. Preprints, *13th Conf. on Severe Local Storms,* Tulsa, OK, Amer. Meteor. Soc., 270–273.

Purdom, J. F. W., 1973: Meso-highs and satellite imagery. *Mon. Wea. Rev.,* **101,** 180–181.

———, 1982: Subjective interpretations of geostationary satellite data for nowcasting. *Nowcasting,* K. Browning, Ed., Academic Press, 149–166.

Rabin, R. M., S. Stadler, P. J. Wetzel, D. J. Stensrud, and M. Gregory, 1990: Observed effects of landscape variability on convective clouds. *Bull. Amer. Meteor. Soc.,* **71,** 272–280.

Ralph, F. M., M. Crochet, and S. V. Venkateswaran, 1993: Observations of a mesoscale ducted gravity wave. *J. Atmos. Sci.,* **50,** 3277–3291.

Ramage, C. S., 1971: *Monsoon Meteorology.* Academic Press, New York, 296 pp.

Raymond, D. J., 1975: A model for predicting the movement of continuously propagating convective storms. *J. Atmos. Sci.,* **32,** 1308–1317.

———, 1976: Wave-CISK and convective mesosystems. *J. Atmos. Sci.,* **33,** 2392–2398.

———, 1978: Instability of the low-level jet and severe storm formation. *J. Atmos. Sci.,* **35,** 2274–2280.

———, 1987: A forced gravity wave model of self-organizing convection. *J. Atmos. Sci.,* **44,** 3528–3543.

Rhea, J. O., 1966: A study of thunderstorm formation along dry lines. *J. Appl. Meteor.,* **5,** 58–63.

Rochette, S. M., and J. T. Moore, 1996: Initiation of an elevated mesoscale convective system associated with heavy rainfall. *Wea. Forecasting,* **11,** 443–457.

Rotunno, R., 1981: On the evolution of thunderstorm rotation. *Mon. Wea. Rev.* **109,** 577–586.

———, 1984: Investigation of a three-dimensional asymmetric vortex. *J. Atmos. Sci.,* **41,** 283–298.

———, and J. B. Klemp, 1982: The influence of shear-induced pressure gradient on thunderstorm motion. *Mon. Wea. Rev.,* **110,** 136–151.

———, and ———, 1985: On the rotation and propagation of simulated supercell thunderstorms. *J. Atmos. Sci.,* **42,** 271–292.

———, ———, and M. L. Weisman, 1988: A theory for strong, long-lived squall lines. *J. Atmos. Sci.,* **45,** 463–485.

Rutledge, S. A., 1989: A severe frontal rainband. Part IV: Precipitation mechanisms, diabatic processes and rainband maintenance. *J. Atmos. Sci.,* **46,** 3570–3594.

———, and R. A. Houze Jr., 1987: Diagnostic modeling study of the trailing stratiform region of a midlatitude squall line. *J. Atmos. Sci.,* **44,** 2640–2656.

Sanders, F., and D. O. Blanchard, 1993: The origin of a severe thunderstorm in Kansas on 10 May 1985. *Mon. Wea. Rev.,* **121,** 133–149.

Sawyer, J. S., 1946: Cooling by rain as the cause of the pressure rise in convective squalls. *Quart. J. Roy. Meteor. Soc.,* **72,** 168.

Schaefer, J. T., 1974a: A simulative model of dryline motion. *J. Atmos. Sci.,* **31,** 956–964.

———, 1974b: Life cycle of the dryline. *J. Appl. Meteor.,* **13,** 444–449.

———, 1986: The dryline. *Mesoscale Meteorology and Forecasting,* P. S. Ray, Ed., Amer. Meteor. Soc., 549–572.

Schlesinger, R. E., 1980: A three-dimensional numerical model of an isolated deep thunderstorm. Part II: Dynamics of updraft splitting and mesovortex couplet evolution. *J. Atmos. Sci.,* **37,** 395–420.

Schmid, W., and M. Lehre, 1998: Drainage flow: A key factor for prediction of severe storms near mountain chains? Preprints, *19th Conf. on Severe Local Storms,* Minneapolis, MN, Amer. Meteor. Soc., 22–25.

Schmidt, J. M., and W. R. Cotton, 1989: High Plains squall line associated with severe surface winds. *J. Atmos. Sci.,* **46,** 281–302.

———, and ———, 1990: Interactions between upper and lower tropospheric gravity waves on squall line structure and maintenance. *J. Atmos. Sci.,* **47,** 1205–1222.

Schubert, W. H., S. R. Fulton, and R. F. A. Hertenstein, 1989: Balanced atmospheric response to squall lines. *J. Atmos. Sci.,* **46,** 2478–2483.

———, M. T. Montgomery, R. K. Taft, T. A. Guinn, S. R. Fulton, J. P. Kossin, and J. P. Edwards, 1999: Polygonal eyewalls, asymmetric eye contraction, and potential vorticity mixing in hurricanes. *J. Atmos. Sci.,* **56,** 1197–1223.

Schultz, D. M., and P. N. Schumacher, 1999: The use and misuse of conditional symmetric instability. *Mon. Wea. Rev.,* **127,** 2709–2732.

Segal, M., and R. W. Arritt, 1992: Nonclassical mesoscale circulations caused by surface sensible heat-flux gradients. *Bull. Amer. Meteor. Soc.,* **73,** 1593–1604.

———, W. E. Schreiber, G. Kallos, J. R. Garratt, A. Rodi, J. Weaver, and R. A. Pielke, 1989: The impact of crop areas in northeast Colorado on midsummer mesoscale thermal circulations. *Mon. Wea. Rev.,* **117,** 809–825.

———, R. W. Arritt, C. Clark, R. Rabin, and J. Brown, 1995: Scaling evaluation of the effect of surface characteristics on potential for deep convection over uniform terrain. *Mon. Wea. Rev.,* **123,** 383–400.

Seman, C. J., 1994: A numerical study of nonlinear nonhydrostatic conditional symmetric instability in a convectively unstable atmosphere. *J. Atmos. Sci.,* **51,** 1352–1371.

Shapiro, M. A., 1981: Frontogenesis and geostrophically forced secondary circulations in the vicinity of jet stream-frontal zone systems. *J. Atmos. Sci.,* **38,** 954–973.

———, 1982: Mesoscale weather systems of the central United States. *The National STORM Program,* UCAR, Boulder, CO, 3-1–3-77.

———, 1985: Frontal hydraulic head: A microscale (approximately 1-km) triggering mechanism for mesoconvective weather systems. *Mon. Wea. Rev.,* **113,** 1166–1183.

———, and P. J. Kennedy, 1981: Research aircraft measurements of jet stream geostrophic and ageostrophic winds. *J. Atmos. Sci.,* **38,** 2642–2652.

Shreffler, J. H., and F. S. Binkowski, 1981: Observations of pressure jump lines in the Midwest, 10–12 August 1976. *Mon. Wea. Rev.,* **109,** 1713–1725.

Simpson, J. E., 1969: A comparison between laboratory and atmospheric density currents. *Quart. J. Roy. Meteor. Soc.,* **95,** 758–765.

Simpson, J., B. R. Morton, M. C. McCumber, and R. S. Penc, 1986: Observations and mechanisms of GATE waterspouts. *J. Atmos. Sci.,* **43,** 753–782.

———, T. D. Keenan, B. Ferrier, R. H. Simpson, and G. J. Holland, 1993: Cumulus mergers in the Maritime Continent region. *Meteor. Atmos. Phys.,* **51,** 73–99.

———, 1987: *Gravity Currents.* Ellis Horwood Limited, 244 pp.

Skamarock, W. C., M. L. Weisman, and J. B. Klemp, 1994: Three-dimensional evolution of simulated long-lived squall lines. *J. Atmos. Sci.,* **51,** 2563–2584.

Smith, R. B., 1982: Synoptic observations and theory of orographically disturbed wind and pressure. *J. Atmos. Sci.,* **39,** 60–70.

———, 1989: Comments on "Low Froude number flow past three-dimensional obstacles. Part I: Baroclinically generated lee vortices." *J. Atmos. Sci.,* **46,** 3611–3613.

Smith, R. K., 1988: Travelling waves and bores in the lower atmosphere: The "Morning Glory" and related phenomena. *Earth-Sci. Rev.,* **25,** 267–290.

———, and M. A. Page, 1985: Morning glory wind surges and the Gulf of Carpentaria cloud line of 25–26 Oct. 1984. *Austr. Met. Mag.,* **33,** 185–194.

Smolarkiewicz, P. K., and R. Rotunno, 1989: Low Froude number flow past three-dimensional obstacles. Part I: Baroclinically generated lee vortices. *J. Atmos. Sci.,* **46,** 1154–1164.

Smull, B. F., and R. A. Houze Jr., 1987: Rear inflow in squall lines with trailing stratiform precipitation. *Mon. Wea. Rev.,* **115,** 2869–2889.

Sortais, J.-L., J.-P. Cammas, X. D. Yu, E. Richard, and R. Rosset, 1993: A case study of coupling between low- and upper-level jet-front systems: Investigation of dynamical and diabatic processes. *Mon. Wea. Rev.,* **121,** 2239–2253.

Srivastava, R. C., 1985: Simple model of evaporatively driven downdraft: application to microburst downdraft. *J. Atmos. Sci.,* **42,** 1004–1023.

———, 1987: Model of intense downdrafts driven by the melting and evaporation of precipitation. *J. Atmos. Sci.,* **44,** 1752–1773.

Stensrud, D. J., and R. A. Maddox, 1988: Opposing mesoscale circulations: A case study. *Wea. Forecasting,* **3,** 189–204.

———, ———, and C. L. Ziegler, 1991: A sublimation-initiated mesoscale downdraft and its relation to the wind field below a precipitating anvil cloud. *Mon. Wea. Rev.,* **119,** 2124–2139.

Stull, R. B., 1985: Fair-weather cumulus cloud classification scheme for mixed-layer studies. *J. Climate Appl. Meteor.,* **24,** 49–56.

Stumpf, G. J., R. H. Johnson, and B. F. Smull, 1991: The wake low in a midlatitude mesoscale convective system having complex organization. *Mon. Wea. Rev.,* **119,** 134–158.

Sun, W.-Y., and Y. Ogura, 1979: Boundary-layer forcing as a possible trigger to a squall-line formation. *J. Atmos. Sci.,* **36,** 235–253.

Szoke, E. J., and R. Brady, 1989: Forecasting implications of the 26 July 1985 northeastern Colorado thunderstorm case. *Mon. Wea. Rev.,* **117,** 1834–1860.

———, M. L. Weisman, J. M. Brown, F. Caracena, and T. W. Schlatter, 1984: A subsynoptic analysis of the Denver tornadoes of 3 June 1981. *Mon. Wea. Rev.,* **112,** 790–808.

Tao, S., and Y.-H. Ding, 1981: Observational evidence of the influence of the Qinghai-Xizang (Tibet) Plateau on the occurrence of heavy rain and severe convective storms in China. *Bull. Amer. Meteor. Soc.,* **62,** 23–30.

Tao, W.-K., J. Simpson, C.-H. Sui, B. Ferrier, S. Lang, J. Scala, M.-D. Chou, and K. Pickering, 1993: Heating, moisture, and water budgets of tropical and midlatitude squall lines: Comparisons and sensitivity to longwave radiation. *J. Atmos. Sci.,* **50,** 673–690.

Tepper, M., 1950: A proposed mechanism of squall lines: The pressure jump line. *J. Meteor.,* **7,** 21–29.

———, 1951: On the desiccation of a cloud bank by a propagated pressure wave. *Mon. Wea. Rev.,* **79,** 61–70.

Thorpe, A. J., M. J. Miller, and M. W. Moncrieff, 1982: Two-dimensional convection in nonconstant shear: a model of midlatitude squall lines. *Quart. J. Roy. Meteor. Soc.,* **108,** 739–762.

———, H. Volkert, D. Heimann, 1993: Potential vorticity of flow along the Alps. *J. Atmos. Sci.,* **50,** 1573–1591.

Toth, J. J., and R. H. Johnson, 1985: Summer surface flow characteristics over northeast Colorado. *Mon. Wea. Rev.,* **113,** 1458–1469.

Trier, S. B., and D. B. Parsons, 1993: Evolution of environmental conditions preceding the development of a nocturnal mesoscale convective complex. *Mon. Wea. Rev.,* **121,** 1078–1098.

———, ———, and J. H. E. Clark, 1991: Environment and evolution of a cold-frontal mesoscale convective system. *Mon. Wea. Rev.,* **119,** 2429–2455.

Tripoli, G. J., and W. R. Cotton, 1989a: Numerical study of an observed orogenic mesoscale convective system. Part I: Simulated genesis and comparison with observations. *Mon. Wea. Rev.,* **117,** 283–304.

———, and ———, 1989b: Numerical study of an observed orogenic mesoscale convective system. Part II: Analysis of governing dynamics. *Mon. Wea. Rev.*, **117,** 305–328.

Uccellini, L. W., 1975: A case study of apparent gravity wave initiation of severe convective storms. *Mon. Wea. Rev.*, **103,** 497–513.

———, 1990: Processes contributing to the rapid development of extratropical cyclones. *Extratropical Cyclones: The Erik Palmén Memorial Volume,* C. W. Newton and E. O. Holopainen, Eds., Amer. Meteor. Soc., 81–105.

———, and D. R. Johnson, 1979: The coupling of upper- and lower-tropospheric jet streaks and implications for the development of severe convective storms. *Mon. Wea. Rev.*, **107,** 682–703.

Ulanski, S. L., and G. M. Heymsfield, 1986: Meso-β perturbations of the wind field by thunderstorm cells. *Mon. Wea. Rev.*, **114,** 780–787.

Velasco, I., and J. M. Fritsch, 1987: Mesoscale convective complexes in the Americas. *J. Geophys. Res.*, **92,** 9591–9613.

Wakimoto, R. M., 1985: Forecasting dry microburst activity over the High Plains. *Mon. Wea. Rev.*, **113,** 1131–1143.

———, and J. W. Wilson, 1989: Non-supercell tornadoes. *Mon. Wea. Rev.*, **117,** 1113–1140.

———, and J. K. Lew, 1993: Observations of a Florida waterspout during CaPE. *Wea. Forecasting,* **8,** 412–423.

———, and N. T. Atkins, 1994: Observations of the sea-breeze front during CaPE. Part I: Single-Doppler, satellite, and cloud-photogrammetry analysis. *Mon. Wea. Rev.*, **122,** 1092–1114.

———, and P. G. Black, 1994: Damage survey of Hurricane Andrew and its relationship to the eyewall. *Bull. Amer. Meteor. Soc.*, **75,** 189–200.

———, and C. Liu, 1998: The Garden City, Kansas, storm during VORTEX 95. Part II: The wall cloud and tornado. *Mon. Wea. Rev.*, **126,** 393–408.

Wallace, J. M., 1975: Diurnal variations in precipitation and thunderstorm frequency over the conterminous United States. *Mon. Wea. Rev.*, **103,** 406–419.

Watanabe, H., and Y. Ogura, 1987: Effects of orographically forced upstream lifting on mesoscale heavy precipitation: A case study. *J. Atmos. Sci.*, **44,** 661–675.

Weckwerth, T. M., and R. M. Wakimoto, 1992: The initiation and organization of convective cells atop a cold-air outflow boundary. *Mon. Wea. Rev.*, **120,** 2169–2187.

———, J. W. Wilson, and R. M. Wakimoto, 1996: Thermodynamic variability within the convective boundary layer due to horizontal convective rolls. *Mon. Wea. Rev.*, **124,** 769–784.

Weisman, M. L., 1992: The role of convectively generated rear-inflow jets in the evolution of long-lived mesoconvective systems. *J. Atmos. Sci.*, **49,** 1826–1847.

———, 1993: The genesis of severe, long-lived bow echoes. *J. Atmos. Sci.*, **50,** 645–670.

———, and J. B. Klemp, 1982: The dependence of numerically simulated convective storms on vertical wind shear and buoyancy. *Mon. Wea. Rev.*, **110,** 504–520.

———, and ———, 1984: The structure and classification of numerically simulated convective storms in directionally varying wind shears. *Mon. Wea. Rev.*, **112,** 2479–2498.

———, and ———, 1986: Characteristics of isolated convective storms. *Mesoscale Meteorology and Forecasting,* P. S. Ray, Ed., Amer. Meteor. Soc., 331–358.

———, and C. A. Davis, 1998: Mechanisms for the generation of mesoscale vortices within quasi-linear convective systems. *J. Atmos. Sci.*, **55,** 2603–2622.

Wetzel, P. J., 1973: Moisture sources and flow patterns during the northeast Colorado hail season. Master's thesis, Dept. of Atmos. Sci., Colorado State University, 90 pp.

Whiteman, C. D., B. Xindi, and S. Zhong, 1997: Low-level jet climatology from enhanced rawinsonde observations at a site in the southern Great Plains. *J. Appl. Meteor.*, **36,** 1363–1376.

Wilczak, J. M., and J. W. Glendening, 1988: Observations and mixed-layer modeling of a terrain-induced mesoscale gyre: The Denver cyclone. *Mon. Wea. Rev.*, **116,** 2688–2711.

———, and T. W. Christian, 1990: Case study of an orographically induced mesoscale vortex (Denver cyclone). *Mon. Wea. Rev.*, **118,** 1082–1102.

Williams, D. T., 1963: The thunderstorm wake of May 4, 1961. Natl. Severe Storms Project Rep. 18, U.S. Dept. of Commerce, Washington, DC, 23 pp. [NTIS PB-168223.]

Williams, M., and R. A. Houze Jr., 1987: Satellite-observed characteristics of winter monsoon cloud clusters. *Mon. Wea. Rev.*, **115,** 505–519.

Wilson, J. W., and W. E. Schreiber, 1986: Initiation of convective storms at radar-observed boundary-layer convergence lines. *Mon. Wea. Rev.*, **114,** 2516–2536.

———, G. B. Foote, N. A. Crook, J. C. Fankhauser, C. G. Wade, J. D. Tuttle, C. K. Mueller, and S. K. Krueger, 1992: The role of boundary-layer convergence zones and horizontal rolls in the initiation of thunderstorms: A case study. *Mon. Wea. Rev.*, **120,** 1785–1815.

Xu, Q., 1986: Conditional symmetric instability and mesoscale rainbands. *Quart. J. Roy. Meteor. Soc.*, **112,** 315–334.

Yan, H., and R. A. Anthes, 1988: The effect of variations in surface moisture on mesoscale circulations. *Mon. Wea. Rev.*, **116,** 192–208.

Yanai, M., C. Li, and Z. Song, 1992: Seasonal heating of the Tibetan Plateau and its effects on the evolution of the Asian summer monsoon. *J. Meteor. Soc. Japan,* **70,** 189–221.

Zhang, D.-L., 1992: The formation of a cooling-induced mesovortex in the trailing stratiform region of a midlatitude squall line. *Mon. Wea. Rev.*, **120,** 2763–2785.

———, and J. M. Fritsch, 1986: Numerical simulation of the meso-beta-scale structure and evolution of the 1977 Johnstown flood. Part I: Model description and verification. *J. Atmos. Sci.*, **43,** 1913–1943.

———, and ———, 1988: Numerical investigation of a convectively generated, inertially stable, extratropical warm-core mesovortex over land. Part I: Structure and evolution. *Mon. Wea. Rev.*, **116,** 2660–2687.

———, and K. Gao, 1989: Numerical simulation of an intense squall line during 10–11 June 1985 PRE-STORM. Part II: Rear inflow, surface pressure perturbations and stratiform precipitation. *Mon. Wea. Rev.*, **117,** 2067–2094.

———, and H.-R. Cho, 1992: The development of negative moist potential vorticity in the stratiform region of a simulated squall line. *Mon. Wea. Rev.*, **120,** 1322–1341.

Ziegler, C. L., and C. E. Hane, 1993: An observational study of the dryline. *Mon. Wea. Rev.*, **121,** 1134–1151.

———, W. J. Martin, R. A. Pielke, and R. L. Walko, 1995: A modeling study of the dryline. *J. Atmos. Sci.*, **52,** 263–285.

Zipser, E. J., 1977: Mesoscale and convective-scale downdrafts as distinct components of squall-line circulation. *Mon. Wea. Rev.*, **105,** 1568–1589.

Ziv, B., and N. Paldor, 1999: The divergence fields associated with time-dependent jet streams. *J. Atmos. Sci.*, **56,** 1843–1857.